Operational Control and Analysis of a Hybrid AC/DC Microgrid

by

Hasan Alsiraji

A thesis
presented to the University of Waterloo
in fulfillment of the
thesis requirement for the degree of
Doctor of Philosophy
in
Electrical and Computer Engineering

Waterloo, Ontario, Canada, 2018

Author's Declaration

I hereby declare that I am the sole author of this thesis. This is a true copy of the thesis, including any required final revisions, as accepted by my examiners.

I understand that my thesis may be made electronically available to the public.

Abstract

In light of the growing demand for electrical power around the globe, the need to increase electrical power generation in order to diminish total carbon emissions has led to the installation of renewable resources to replace traditional generators. Most of today's microgrids are AC microgrids, whose advantages and shortcomings with respect to control techniques and stability assessment have been demonstrated through extensive studies reported in the literature. These considerations have led to the recent proposal and investigation of DC microgrids, accompanied by the introduction of the hybrid AC/DC microgrid as a means of combining the advantages and benefits of both types of microgrid. However, since a hybrid microgrid is viewed as a weak system with low inertia, controlling and assessing the performance of a hybrid microgrid constitutes a high-priority issue that requires further investigation. The lack of inertia of power electronics converters, especially in an islanded hybrid microgrid, poses a threat to stability and control. For these reasons, effective stability analysis has become a necessity with respect to the implementation of hybrid microgrids.

Because of these challenges, the emulation of synchronous machine (SM) inertia and damping is now viewed as necessary for enhancing the effect of a VSC on an active distribution system and for facilitating its participation in voltage and frequency support. Improving the stability and performance of a hybrid microgrid therefore requires the introduction of a form of inertia into a hybrid microgrid. This research first proposes the incorporation of a novel form of virtual inertia into a hybrid microgrid using virtual synchronous machine (VSM) control of the intertying converter (IC) controller. The second proposal of this research is to employ the VSM control to establish autonomous control of the IC.

A first research component, a novel control strategy for the Intertying converter in hybrid AC/DC microgrid has been proposed to ensure the benefit of a virtual synchronous machine (VSM) control algorithm in the hybrid AC/DC microgrid. The VSM controller application in hybrid AC/DC microgrid is capable to enable an IC converter to support the AC-side voltage and frequency as well as the DC-side voltage. The proposed control application of the VSM is chosen based on a comprehensive assessment of VSM control algorithms that are exist in the literature. Moreover, proposing an autonomous operation control of the VSM intertying converter based on dual droop characteristics which is quite different compared to using only current controller. The autonomous operation of the intertying converter based on dual droop control is modified and proposed to be capable to feed the

VSM controller (swing equation) to ensure accurate power exchange management between the AC and DC sub-subsystems.

The most important portion for the hybrid microgrid system is the stability study due to that fact that the behavior of the system when it is subjected to a temporary disturbance is the main concern. In hybrid microgrid, the disturbances take place continuously because of the load changing endlessly. Satisfying the hybrid microgrid operation during the disturbances conditions must be achieved in order to supply the demand. Therefore, the second part of the research introduces a generic small-signal state space model of the hybrid AC/DC microgrid system, and built to carry out the stability analysis. The development of the small-signal state-space model for the entire hybrid AC/DC microgrid was developed to investigate the overall system stability under different operating points.

The final part of this thesis reveals three serious issues of operating hybrid AC/DC microgrid; some of these issues are temporary take a place based on the system operating conditions. In hybrid AC/DC microgrid, an Intertying converter (IC) becomes harmonics voltage source due to the antiparallel diodes and the shunt capacitor at its DC side. The nonlinearity behavior of ICs introduces another operation issue that is circulating current in case of parallel ICs. Reconnecting an IC after abnormal operation condition or schedule maintenance requires an extra challenging synchronization control due the variation of the AC subgrid voltages and frequency; which is the third issue. This part proposes a solution for all these issues by developing a new control strategy that combines the VSM control concept with a dual based droop control. The developed VSM controller on the IC solves these issues.

The test system used in this research, which is simulated in a PSCAD/EMTDC environment, consisted of simulated voltage source converters with two AC voltage levels; while the stability analysis is conducted in MATLAB environment.

Acknowledgements

First and foremost, all my thankfulness is to Allah who helped and guided me to carry out this work. I would like to thank Prof- Ramadan El-Shatshat for his valuable suggestions, support, encouragement, and patience during my PhD program.

Moreover, I would like to thank to Professor Mohamed E. El-Hawary, Professor Kankar Bhattacharya, Professor Sagar Naik, Professor Gordon Savage, and Professor Magdy Salama for being committee members of my thesis.

Also, I would like to express my thanks to all the members of my research group. Much appreciation goes to my friends in the University of Waterloo for their friendship.

I am especially grateful to my family for their patience, prayers, understanding, and for believing in me. They have given me much care, love and support throughout the research. I would also like to thank my wife Fatoon for her true endless love and honest support inspired me to work hard.

Dedication

This thesis is dedicated:

To my lovely grandmother,

To my lovely parents,

To brothers,

To only sister,

To my lovely wife,

To my expected baby.

Table of Contents

List of Figures

List of Tables

List of Acronyms

AC	Alternative Current
ANSI	American National Standards Institute
d-	Direct
DC	Direct Current
DG	Distributed Generation
DPC	Direct Power Control
EMTDC	Electromagnetic Transients Including DC
ES	Energy Storage
HVDC	High-Voltage Direct Current
IC	Intertying Converter
IEEE	Institute Of Electrical And Electronics Engineers
KCL	Kirchhoff's Current Law
Kd	Virtual Damping Coefficient
KVL	Kirchhoff's Voltage Law
L-L	Line To Line
LPF	Low Pass Filter
mac	Active Power AC Droop Coefficient
mp	Active Power Droop Coefficient
MPC	Model Predictive Control
MV	Medium Voltage
NEMA	The National Electrical Manufacturers Association
nq	Reactive Power Droop Coefficient
PCC	Point Common Coupling
PI	Proportional Integral
PLL	Phase Lock Loop
PRC	Proportional Resonance Control
PSCAD	Power System Computer Aided Design
PV	Photovoltaics
PVUR	Phase Voltage Unbalance Rate
PWM	Pulse Width Modulation
q-	Quadrature
RES	Renewable Energy Sources
SM	Synchronous Machines

SRF	Synchronous Reference Frame
THD	Total Harmonic Distortion
VC	Vector Control
VSC	Voltage Source Converter
VSG	Virtual Synchronous Generator
VSM	Virtual Synchronous Machine

List of Symbols

C_{dc}	Shunt capacitor at DC side
C_f	Shunt capacitor at AC side for VSC
C_f'	Shunt DC filter capacitor
D_d	Damping coefficient
E_a	Induced back emf phase a
E_b	Induced back emf phase b
E_c	Induced back emf phase c
I_1	Fundamental AC voltage
$I_{a(i)}$	Phase (a) current of the inverter
$I_{b(i)}$	Phase (b) current of the inverter
$I_{c(i)}$	Phase (c) current of the inverter
I_{cir}^{cross}	Cross circulating-current
I_{cir}^{zero}	Zero sequence circulating-current
I_k	Harmonic AC current for order k
K_{ic}	Integrator current controller gain
K_{iv}	Integrator voltage controller gain
K_{pc}	Proportional current controller gain
K_{pv}	Proportional voltage controller gain
L_f	Converter inductance filter
L_o	AC line inductance
L_o'	DC line inductance
L_s	Stator winding inductance
L_v	Virtual controller loop inductance
$P_{AC,DG}(i)$	Active AC power of distributed generator i
$P_{AC\ load}$	Active AC load power
$P_{DC,DG}(i)$	Active DC power of distributed generator i
$P_{DC\ load}$	Active DC load power
P_{IC}^{ac}	Reference power desire from intertying converter via AC sub-grid
P_{IC}^{dc}	Reference power desire from intertying converter via DC sub-grid

P_{IC}^{ref}	Reference power desire from intertying converter
P_{ele}	Electrical power
P_{mech}	Mechanical power
R_f	AC/DC converter resistance filter
R_f'	DC/DC converter resistance filter
R_o	AC line resistance
R_o'	DC line resistance
R_s	Stator winding resistance
R_v	Virtual controller loop resistance
T_s	Transformation matrix
T_v^{-1}	Voltage inverse transformation matrix
V_1	Fundamental AC voltage
V_{LLh}	Line to line voltage
V_{PCC}	Voltage at point common coupling
V_{conv}	AC converter's voltage
V_{dc}^{inv}	DC converter's voltage
V_{dc}^{max}	Maximum allowable range of DC sub-system voltage
V_{dc}^{meas}	Instantaneous measured DC sub-system voltage
V_{dc}^{min}	Minimum allowable range of DC sub-system voltage
V_f	Excitation voltage
V_g	AC grid voltages
V_g'	DC grid voltages
V_{in}	Dc converter's voltage
V_k	Harmonic AC voltage for order k
i_c	Capacitor's current
i_{conv}	Converter's current
i_{line}	Line current
i_{load}	Load current
i_o	Filtered converter's AC current
i_o	Output filtered converter's current

i_o'	Filtered converter's dc current
i^{ref}	Reference controller current
m_p^{ac}	Active AC power droop coefficient
m_p^{dc}	Active DC power droop coefficient
v_a	Stator winding phase a voltage
v_b	Stator winding phase b voltage
v_c	Stator winding phase c voltage
v^{inv}	Operational AC voltage for a converter
v_o	Output filtered voltage of the AC converter voltage
v_o'	Output filtered voltage of the DC converter voltage
v^{ref}	Voltage controller reference
θ_{vsm}	Virtual synchronous machine rotation angle
ω_{ac}^{meas}	Instantaneous measured DC sub-system angular frequency
ω_{com}	AC sub-system common frequency
ω_f	Cutoff frequency for low pass filter
ω_g	Grid angular speed frequency
ω^{inv}	Operational angular speed frequency for a converter
ω^{max}	Maximum allowable range of the system angular speed frequency
ω^{min}	Minimum allowable range of the system angular speed frequency
ω_{vsm}	Virtual synchronous machine angular speed frequency
$\mathcal{M}\text{Ap}_{inv}$	Mapping inverter matrix
$\mathcal{M}\text{Ap}_{line}$	Mapping line matrix
$\mathcal{M}\text{Ap}_{load}$	Mapping load matrix
A	State matrix that contains of the system parameters and characteristics
B	Matrix that contains of the system inputs.
C	Matrix that contains of the system output.
D	Matrix that contains of the system feedforward
J	Machine's inertia
$Vabe$	The difference between line voltage Vab and the average of total line voltages
$Vbce$	The difference between line voltage Vbc and the average of total line voltages
$Vcae$	The difference between line voltage Vca and the average of total line voltages

il	Input reference to current controller of DC/DC converter
θ	AC sub-system rotation angle
γ	Extra state variable for current controller
δ	Angle between an inverter reference frame and the common reference frame
φ	Extra state variable for voltage controller
ω	Angular speed frequency

Chapter 1

Introduction

To meet the increased demand for electrical power and address environmental concerns, increasing levels of renewable energy sources (RESs) are being integrated into traditional AC distribution systems because of their potential to diminish the need for energy derived from fossil fuels and to decrease greenhouse gas emissions. A traditional distribution system is based solely on a unidirectional power flow from the grid (utility) to the customers (load) throughout distribution network. However, the installation of distributed generation (DG) on the load side (close to customers) has altered this characteristic because DG units are capable of meeting local load demands, which makes the distribution system to become an active system that can be disconnected from the grid (utility) and function in islanded operation mode.

Interconnecting DGs into classical AC distribution systems usually can be done by using power electronics converters interfacing either an AC/DC or DC/DC converters; which depends on the system types. However, each type of connection has its own advantages and disadvantages. Roughly, comparing the AC connection option with the DC connection option is that for short distances between the renewable source and AC systems, the AC connection option is more reasonable due to the fact that there is not much reactive power flowing because of less capacitance in the transmission lines[1], [2]. Also, the skin effect would be less in distribution system compare to the transmission level. On the other hand, implementing DC distribution system is promising option due to the absence of frequency stability issue as well as the reactive power issues.

Microgrids, known in the literature as active distribution systems [3], have become a widely accepted option for distribution power systems over the past decade. Recently, the concept of microgrids – either AC or DC systems – has become an extensively established in practical for the accommodation of the large-scale integration of renewable energy sources (RESs) into distribution systems. To take advantage of the benefits offered by both AC and DC microgrid systems, the concept of combining both types of microgrid is forming a hybrid microgrid; which has been introduced [4].

A hybrid AC/DC microgrid includes the interconnection of an AC and a DC microgrid via a voltage source converter (VSC) that names an intertying converter (IC). Hybrid AC/DC microgrids have two operating modes: grid-connected mode and isolated mode; which is similar to AC and DC microgrid. Maintaining the frequency for the AC microgrid and the DC voltage for the DC microgrid to be within an acceptable standard range for both sub-grids is the most important issue associated with hybrid microgrids,

particularly for isolated hybrid AC/DC microgrids. The high penetration of RESs affects the system's DC voltage and frequency and, hence, its stability [5]. The intertying of AC and DC sub-grids via the intertying converter (IC) ensures stability of the hybrid AC/DC microgrid via bidirectional power sharing between sub-systems; thus, intertying converter (IC) control is the primary means of ensuring stable operation of the entire hybrid AC/DC microgrid.

An existing AC power grid infrastructure can be used with an AC microgrid, while a DC microgrid facilitates the minimization of conversion stages with an accompanying reduction in implementation costs and power losses [6], [7]. The desirability of both sets of advantages have led to the introduction of combined AC and DC microgrid systems as hybrid microgrids [4], [8]–[10], an example of which is illustrated in Figure 1-1.
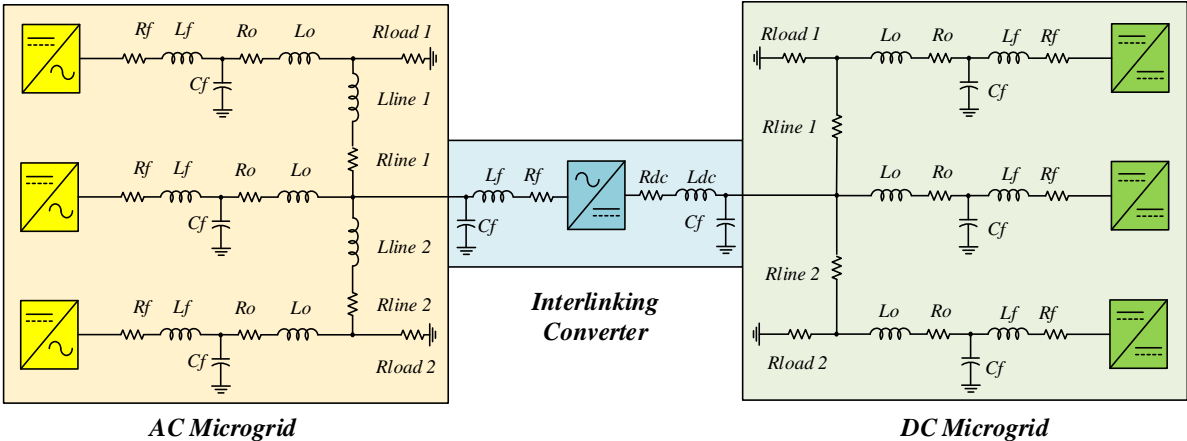
Figure 1-1: Hybrid Microgrid Structure.

Numerous benefits can be derived from the implementation of microgrids. First, they enhance the overall reliability of the system because they can operate autonomously when no main utility grid is present [11], a type of operation that provides a means of avoiding the possibility of load shading. For instance, microgrid contains of sensors that provide a freedom to the system operators to operate the system independently from the main grid when it is necessary. Secondly, a microgrid can engage in voltage support of the main grid during peak loads [12]. A third advantage is the energy efficiency provided by a microgrid, because environmental factors such as temperature mean that local generation will entail much lower losses than generating large amounts of power from a thermal generator [13]. A microgrid is also associated with a reduced environmental impact because of its smaller global carbon footprint [14], a positive feature that is driving the increased penetration of renewable resources.

Microgrids concept leads the distribution is to be more resilient compared to conventional distribution system.

1.1 Research Motivation

High levels of renewable energy source (RES) penetration can create stability problems and affect system dynamics [15]–[18]. Due to their numerous benefits and superior performance, voltage source converters (VSCs) have become a practical way of providing an interface with renewable resources that are characterized by either variable frequencies or direct current, such as wind, photovoltaics (PV), and fuel cells. However, unlike synchronous machines (SMs), VSCs that interface with RESs lack the inertia needed to support and participate in the frequency and voltage control of an AC system and are hence unable to contribute to the enhancement of system stability. In fact, lack of inertia constitutes the foremost challenge related to the microgrid concept. A microgrid is applied primarily in a distribution system, where unbalanced AC voltages commonly occur [19], constituting a second, but nonetheless equally important challenge. The control technique commonly implemented in microgrids is based on a droop strategy to mimic the governor of the synchronous generator [20]; however, this technique lacks precise power flow control [2], and the small bandwidth involved in droop-based control has a negative effect on microgrid stability. A final challenge is the fact that the load changing that occurs with a microgrid causes disturbances that could, in turn, create stability issues, especially in islanded operation mode.

A variety of microgrid power generation sources, such as PV, fuel cells, energy storage, and wind, require power electronics conversion stages. For example, power produced by a PV panel, energy storage, and fuel cells is generated as DC value and must be inverted to AC via a DC-AC converter to enable it to be interconnected into an AC microgrid. The power electronics interfacing stages that are clearly required in an AC microgrid increase the costs of implementation [21], resulting in the introduction of DC microgrids [6] as a means of decreasing these stages [7]. Although, as mentioned, each type of microgrid (either AC or DC) offers specific advantages [22] that have led to the recent proposal and examination of hybrid microgrids, including studies of their use from a control perspective [8]–[10], [23]–[26], issues remain with respect to the multistage power electronics interfacing in a DC microgrid. Both DC and AC microgrids are also associated with energy losses [7] and expensive implementation [21]. For these reasons, any microgrid research must include investigation of all three categories: AC, DC, and hybrid [21].

A hybrid microgrid has two different operating modes: grid-connected and islanded. In islanded mode, in particular, the lack of frequency support to the AC sub-system and the absence of voltage support to the DC sub-system make the stability of a hybrid microgrid the most important issue to be addressed. An extremely critical factor in system stability is the power sharing between the AC and DC sub-systems because of the bidirectional power flow involved. Since microgrids are generally considered to be weak systems, they are subject to changes in generation or loading conditions that can cause large frequency deviations and create further instability problems [27]. In [28], the authors demonstrated that increasing AC microgrid loading moves the dominant system poles to an unstable region. Therefore, the stability in a hybrid microgrid is dependent not only on the AC sub-system but also on the DC sub-system due to the power exchange thought out an IC.

The hybrid microgrid concept requires further in-depth study that includes exploration of control operation, power sharing, and stability. Researchers have proposed and examined the autonomous power sharing operation of a hybrid microgrid based on droop control both for all DGs and for the intertying converter (IC) [23], [29], [30]. It is clear that the IC is the most important factor in hybrid microgrid operation and stability because of its bidirectional power flow feature. Supplying or absorbing power via the IC affects the dynamics and performance of both the AC and DC sub-systems and could lead to stability issues for the whole hybrid system due to the lack of inertia in the VSC interface. Therefore, considering only one IC decreases the system reliability as well as affects the AC sub-system dynamics' as can be seen based on [23],[30]. Introducing multiple ICs increases the system reliability[31], but the AC sub-system dynamics and performance become worst and more sensitive to power exchange. Due to the pervious issues, the idea of including an energy storage (ES) to achieve smooth power exchange between sub-system is proposed [25], but it is clearly be noted that the implementation cost of the ES and the operation issue are raised[32]. Also, additional area for subsequent investigation for hybrid microgrid will be power sharing.

Based on previous issues and overcoming on the challenges earlier declared above, a hybrid ac/dc microgrid concept below a smart grid paradigm requires a sufficient control and stability analysis evaluation. Therefore, there is a need for:

- Improving the system dynamic and its performance.
- Smoothing energy exchange among the AC and DC sub-grids.
- Efficient coordination control of AC/DC sub-grids.

4

- Improving synchronization for reconnecting a converter after abnormal operating conditions or schedule maintenance.

- Enhancing power quality.

- Sufficient system inertia as a microgrid is considered a weak system.

1.2 Research Objectives:

The literature review revealed a number of gaps and issues that should be investigated in order to improve the performance of a hybrid microgrid and to increase its reliability. The thesis research goal is the development of new solutions for hybrid AC/DC microgrids that incorporate the SM concept as a new strategy for efficiently controlling and operating hybrid microgrids in isolated modes. Emulation of SM inertia and damping is necessary for mitigating the effect of the VSC on a hybrid ac/dc microgrid and enabling the VSC to participate in voltage and frequency support. Consideration of the inclusion of a virtual synchronous machine (VSM) control algorithm in the IC in a hybrid microgrid is a novel idea not previously reported in the literature. The development of such an algorithm will be the first contribution of the research presented in this thesis. Then, it is necessary after implementation of the VSM in a hybrid ac/dc microgrid IC to ensure the bidirectional power flow between subsystems. Due the VSM control concept is a slightly different compare to the controller that is exist in the literature, an autonomous power control should be capable to be implemented on VSM control algorithm to allow bidirectional power flow between sub-systems. Moreover a small-signal dynamic model of the hybrid microgrid must be created as a means of evaluating the stability of the hybrid ac/dc microgrid into which the proposed VSM control strategy has been incorporated. These are the goals of this thesis, and they can be divided into two specific objectives related to the device level and the system level. The device level objective is focused on the development of a robust and efficient primary control structure for microgrid VSCs. The system level objective is centred on the development of a comprehensive framework for the power management of hybrid ac/dc microgrids in a manner that ensures reliable and autonomous hybrid microgrid operation in isolated mode. The proposed solutions address the technical problems associated with the steady-state and transient operation of hybrid microgrids. Details of the specific objectives can be summarized as follows:

- Investigate and examine a variety of VSM models to determine the most efficient model for implementation on a hybrid microgrid IC. The literature includes references to several differently structured control algorithms. However, synchronous machine inertia and damping characteristics must be mimicked, which makes the cost and simplicity of implementation important from an

economic perspective. This objective presents a comprehensive comparison of VSM control algorithms, and the most significant factors should be investigated. This task presents the viability of VSM algorithms during the kind of abnormal operation that might raise instability issues with respect to practical operation issues such as short circuit, unbalanced AC voltage, and total harmonic distortion.

- Develop a VSM control algorithm for controlling the IC. The proposed controller should enable an IC converter to support the AC-side voltage and frequency as well as the DC-side voltage and ensure bidirectional power flow between the AC and DC sub-systems through the IC converter. This task examine the benefit of a virtual synchronous machine (VSM) control algorithm that emulates the properties of traditional synchronous machines in the hybrid ac/dc microgrid. Therefore, this objective presents a novel control of the intertying converter based VSM. The most significant factor investigated in this stage is based on the power exchange from the AC into DC side, and vice versa using simple representation of AC and DC microgrid as shown in the figure 1.2 below.
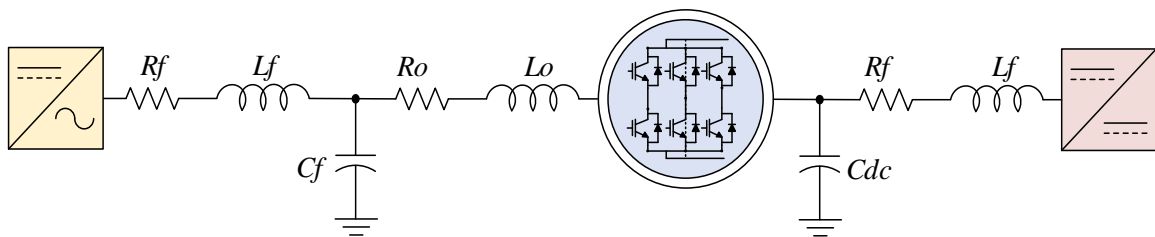
Figure 1-2: Simple Representation of Hybrid AC/DC System

- Develop an autonomous operation control of the VSM intertying converter based on dual droop characteristics which is quite different to conventional droop. This is determined by measuring the DC voltage level and AC sub-grid's frequency at its AC and DC sides instantaneously. Therefore, the input reference consists of a summation of AC droop associated with AC sub-grid frequency, and DC droop associated with DC sub-grid DC voltage that should feed the VSM controller. This task must ensure the power sharing flow between the AC and DC sub-systems in the case of a shortage of active power in each of the sub-system, and provide support for both microgrids during disturbances.

- Develop mathematical and fully detailed simulation models in PSCAD/EMTDC environment for a hybrid ac/dc microgrid based on IEEE Standard 399 configuration [33] to ensure the proposed

controller should enable an IC converter to support the AC-side voltage and frequency as well as the DC-side voltage and ensure bidirectional power flow between the AC and DC sub-systems through the IC converter.

- Develop the dynamic model for the hybrid AC/DC microgrid is the most important component of the control design and stability assessment. The main benefit of the small-signal modelling is to present further investigation of the hybrid microgrid once the eigenvalues and the stable region are determined. Particularly, the small-signal model of hybrid microgrid presents the system stability and also the effect of the system parameters changing such as PI controller coefficients. Therefore, it becomes necessary for studying the small-signal model to find the large-signal dynamic model of the hybrid microgrid first; which is represented using nonlinear differential equations. This task should evaluate the system stability during different mode of the IC operation, which are namely: a rectification mode of the IC (during power exchange from AC into DC sub-system) and an inversion mode of the IC (during power exchange from DC into AC sub-system).

- Examine the impact of the ICs' behaviour during power exchange from AC/DC sub-system which is identical to nonlinear load. Therefore, the parallel ICs degrades the AC voltage of the entire AC sub-system. As a result, circulating current between parallel ICs will raise and exist even in islanded operation mode with droop control concept, so this issue must be solved in order of achieving sufficient operation performance of the system. Furthermore, reconnecting an IC after abnormal operating conditions or schedule maintenance is another issue should be included in this task due to the requirement of synchronization control. In fact, these issues have not been investigated yet in hybrid AC/DC microgrid application in the literature.

1.3 Thesis Outline

The organization of this thesis consists of seven chapters as follows:

- Chapter 2 presents an overview of the background topics significant to the research containing VSC control strategies, recent work on hybrid AC/DC microgrid, and VSM control concept.

- Chapter 3 presents a comprehensive evaluation of several VSM control concept in order to determine the most efficient control algorithm performance during normal and abnormal operation conditions such as step load changing, short circuit, and unbalance AC voltage.

7

- Chapter 4 presents a novel control strategy application for the hybrid AC/DC intertying converter (IC). The proposed control application is based on VSM including a modified dual droop control characteristics to ensure autonomous bidirectional power sharing between sub-systems. Moreover, this chapter compares the proposed controller application with the controller that exists in the literature.

- Chapter 5 presents modelling hybrid AC/DC microgrid based on small-signal state space model, and the stability analysis is evaluated using the aid of developing the small-signal state space model.

- Chapter 6 reveals some operation issues of hybrid AC/DC microgrid that is associated with the existence of parallel IC. Therefore, proposing VSM control application remedies these operation serious issues.

- Chapter 7 summarizes and highlights the main contributions in the thesis, and it offers recommendations for future research work and directions.

Chapter 2
Background and Literature Review

Using virtual synchronous machine (VSM) control in the hybrid microgrid is a novel control application concept. Therefore, the literature review is divided into three main sections. The first section introduces the background of voltage source converter (VSC) control concept. The second section reviews the previous work on hybrid microgrid, while the third section focuses on the proper and efficient control algorithm of the VSM.

2.1 VSC Control Strategies

The control strategy of VSC mainly depends on a phase voltage difference between the two points on the AC side filter of the VSC. Therefore, the value of the phase voltage determines the direction of power flow either from DC to AC side or AC to DC side. On the other hand, the reactive power can be controlled via varying the voltage magnitude of the AC voltage, because the reactive power moves from a high voltage point into a low potential voltage point. To clarify the active and reactive power control concepts of VSC, Figure 2.1 shows AC side filter of VSC.
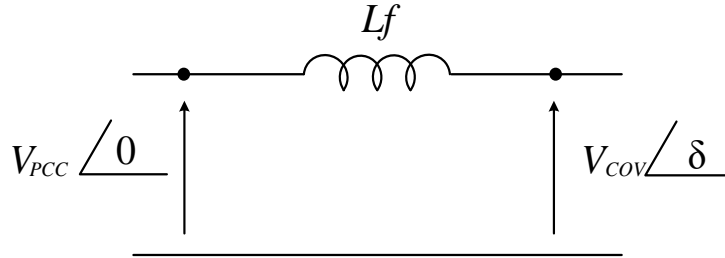
Figure 2-1: AC Line Inductance.

Based on Figure 2.1, the active and reactive power equations are shown [34]:

$$P = \frac{|V_{PCC}| \times |V_{conv}|}{\omega L} \cdot \sin \delta \tag{2.1}$$

$$Q = \frac{|V_{PCC}|^2}{\omega L} - \frac{|V_{PCC}| \times |V_{conv}|}{\omega L} \cdot \cos \delta \tag{2.2}$$

It is obvious that the active power flow mainly depends on the phase voltage angle as written in equation (2.1). However, the main factor that dominates the reactive power is the voltage magnitude; which is represented in equation (2.2). Based on the literature there are more than three strategies to control

the active and reactive power of VSC: direct power control (DPC), proportional resonance control, model predictive control (MPC), and vector control which is the most commonly used. These control strategies are known in the literature as the primary control which is necessary to form the voltages and currents to control the VSC.

2.1.1 Direct Power Control (DPC)

As this strategy does not depend on a PWM technique, a VSC will be fired (pulsated) based on the instantaneous difference between the desired and predicted power [35]. In other words, this strategy has not have fix switching frequency which means that there are more harmonics production. Moreover, there are no inner current control loops to decouple a reactive power from an active power. The controls of the active and reactive powers are correlated; thus, deviation in the value of the active power will immediately affect the reactive power.

2.1.2 Proportional Resonance Control (PRC)

The PRC strategy has the superior advantage of zero steady state error, and it is easily designed and tuned. Moreover, there is no need for decoupled terms in order to separate the active and reactive powers. However, the fatal disadvantage of this strategy is that it is very sensitive to the frequency variation [36], [37] which is a common situation in the islanded microgrid. It is obvious that this control strategy is not suitable for use in microgrid applications.

2.1.3 Model Predictive Control (MPC)

MPC is a control concept based on solving a minimization optimization problem that can control the VSC. The objective function this optimization control problem is known as a cost function; which is formed by the difference between the desired value of the control target and the predicted future value[38]. This control technique offers decouple independent control for an active and a reactive power. However, due to an online solution of this objective function, the switching frequency is not fix. This method suffers from non-deterministic harmonics production; which is hard to be filtered and similar to the DPC harmonics issue.

2.1.4 Vector Control (VC)

This control strategy is used mostly for VSC, specifically in microgrid applications [9], [10], [23], [26], [39] due to the fact that it produces less voltage harmonics than a DPC. Moreover, this strategy allows independent control of reactive power and active power [2]. The real values of the voltage and

10

current in abc frames transform into DC vector components using Park transformations, which are represented in a d-q frame. These vectors have a small margin of error that can be corrected using a proportional-integral controller (PI). This method will be considered in this dissertation.

2.1.4.1 Vector Control Design of VSC

Controlling a VSC requires two stages of controllers: the inner controller and the outer controller. The inner controller's inputs are fed from the outer controllers that are responsible to provide currents references based on the desired control employed such as the active and reactive power control or AC voltage control. The inner control loops prevent overloading during electrical problems and evaluate the voltage drop value at the AC side. In order to design, implement, and tune the inner and outer controllers, the dynamic model of the VSC must be derived.

2.1.4.2 Mathematical Model of VSC Interfacing DG Unit into AC Microgrid

Deriving the dynamic model for the VSC is the most important point associated with control design and stability assessment. The general representation of a VSC that interfaces a DG unit into an AC microgrid is shown in Figure 2.2.
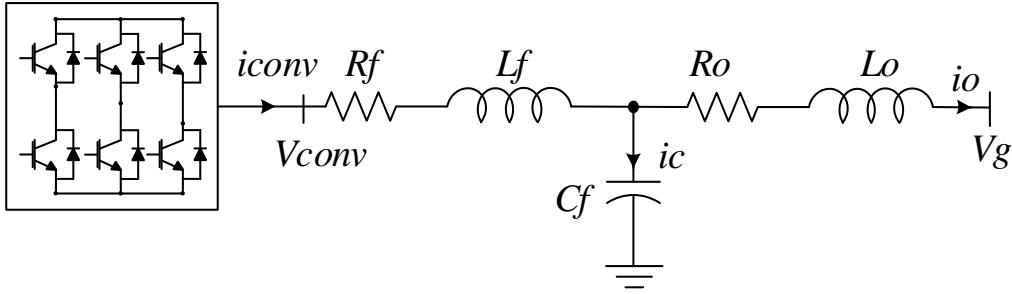
Figure 2-2: Schematic Single Line of VSC

Applying KVL at the AC side in Figure 2.2 gives an equivalent differential equation of a voltage drop across the inductance and the resistance in terms of the d-q frame after considering Park transformation. Also via KCL, the differential equation of the voltage across the shunt capacitor can be determined. Therefore, the dynamic model equations of the voltages and current for LCL electrical circuit known as large signal model can be written in d-q frame as follows: **{for further details see appendix}**

$$Lf \frac{diconv_d}{dt} = Vconv_d - Vo_d - Rf.iconv_d + \omega.Lf.iconv_q \tag{2.3}$$

11

$$Lf\frac{diconv_q}{dt} = Vconv_q - Vo_q - Rf.iconv_q - \omega.Lf.iconv_d \tag{2.4}$$

$$Cf\frac{dvo_d}{dt} = \omega.Cf.vo_q + iconv_d - io_d \tag{2.5}$$

$$Cf\frac{dvo_q}{dt} = -\omega.Cf.vo_d + iconv_q - io_q \tag{2.6}$$

$$Lo\frac{dio_d}{dt} = Vo_d - Vg_d - Ro.io_d + \omega.Lo.io_q \tag{2.7}$$

$$Lo\frac{dio_q}{dt} = Vo_q - Vg_q - Ro.io_q - \omega.Lo.io_d \tag{2.8}$$

Where ω in equation (2.3)-(2.8) is the angular speed of the rotation of the d-q frame that is found from Park transformation. The LC filter and coupling components of the VSC are represented by $Rf, Lf,$ and Cf, for the filter, while the coupling components to the AC microgrid are represented via Ro and Lo.

2.1.4.3 VSC Controller Structure

This subsection will discuss the controller loops of the VSC in detail. The controller loops of the VSC consist of three different stages in case of islanded operation mode: current controller loops, voltage controller loops, and power droop controller loops.

2.1.4.3.1 VSC Current Controller

Due to the small margin of error while using the vector control, the current controller loops of equations (2.3) and (2.4) can be arranged to include the proportional integral (PI) transfer function. Designing the inner current controller includes eliminating an inductance crossing term in the controller loop effect by a feed-forward. Involving PI controllers into equations (2.3) and (2.4) has an advantage, as the dominant poles of the VSC can be cancelled by the zeroes of the PI controllers. Thus the current loops controller of the VSC is achieved from these equations. Accordingly, the nonlinear term can be achieved by tracking i_d^{ref} and i_q^{ref} in the inner control loops with instantaneous values of $iconv_d$ and $iconv_q$ as written in equations (2.9) and (2.10).

$$Lf\frac{diconv_d}{dt} = \left(K_{pc} + \frac{K_{ic}}{s}\right) \times \left(i^{ref}{}_d - iconv_d\right) \tag{2.9}$$

$$Lf\frac{diconv_q}{dt} = \left(K_{pc} + \frac{K_{ic}}{s}\right) \times \left(i^{ref}{}_q - iconv_q\right) \tag{2.10}$$

Substituting equations (2.9) and (2.10) with equations (2.3) and (2.4) respectively allows implementation of the inner current controller loops of the VSC as depicted in Figure 2.3. The main current controller loops equations of VSC become:

$$\left(K_{pc} + \frac{K_{ic}}{s}\right) \times \left(i^{ref}{}_d - iconv_d\right) = Vconv_d - Vo_d - Rf.iconv_d + \omega.Lf.iconv_q \tag{2.11}$$

$$\left(K_{pc} + \frac{K_{ic}}{s}\right) \times \left(i^{ref}{}_q - iconv_q\right) = Vconv_q - Vo_q - Rf.iconv_q - \omega.Lf.iconv_d \tag{2.12}$$

Generally, the resistance term in the current controller is neglected due to the fact that it is small and does not have an effect on the VSC dynamic, especially in power applications [40]. Moreover, the feed forward voltage is used to minimize the slow dynamic response of cascade loops controllers [41] and to achieve fully decoupled d-q components [42].
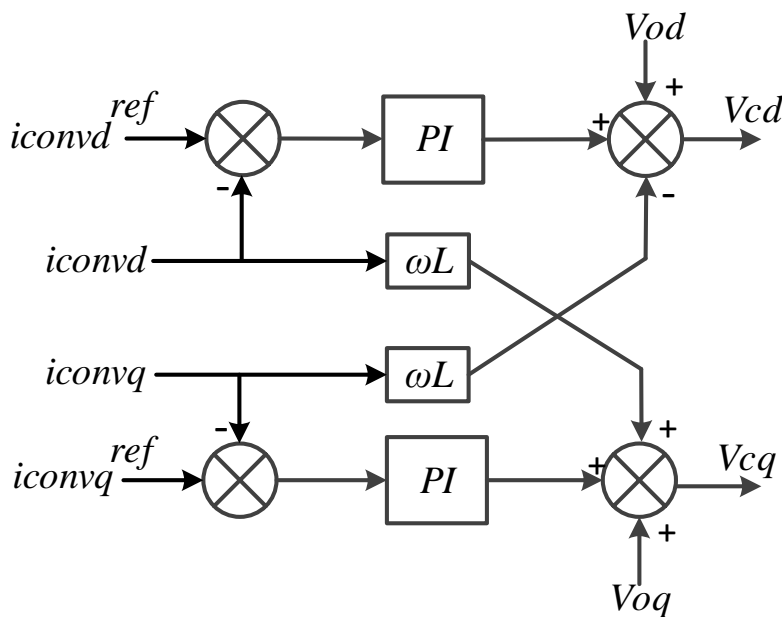
Figure 2-3: Block Diagram of Current Controller Loops

2.1.4.3.2 VSC Voltage Controller

Designing the voltage controller follows the same procedure as the current controller. The voltage controller eliminates a capacitance crossing term in the controller loop effect by a feed-forward. By including PI controllers into equations (2.5) and (2.6), the nonlinear term can be achieved by tracking v_d^{ref}

13

and v_q^{ref} in the voltage control loops with instantaneous values of vo_d and vo_q as written in (2.13) and (2.14). The feed-forward in the voltage controller loops is the output converter current [43].

$$Cf\frac{dvo_d}{dt} = \left(K_{pv} + \frac{K_{iv}}{s}\right) \times \left(vo^{ref}{}_d - vo_d\right) \tag{2.13}$$

$$Cf\frac{dvo_q}{dt} = \left(K_{pv} + \frac{K_{iv}}{s}\right) \times \left(vo^{ref}{}_q - vo_q\right) \tag{2.14}$$

Substituting equations (2.13) and (2.14) with equations (2.5) and (2.6) respectively allows implementation of the voltage control loops of the VSC as shown in Figure 2.4. Generally the feed-forward in the voltage controller loops is multiplied by a gain of less than 0.8 in order to expand the bandwidth of the controller loops [44].

$$\left(K_{pv} + \frac{K_{iv}}{s}\right) \times \left(vo^{ref}{}_d - vo_d\right) = \omega.Cf.vo_q + iconv_d - io_d \tag{2.15}$$

$$\left(K_{pv} + \frac{K_{iv}}{s}\right) \times \left(vo^{ref}{}_q - vo_q\right) = -\omega.Cf.vo_d + iconv_q - io_q \tag{2.16}$$
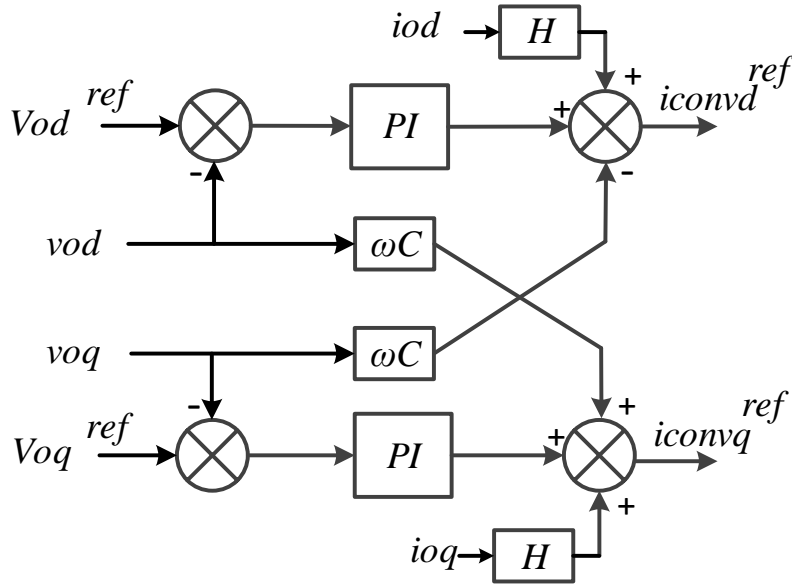
Figure 2-4: Block Diagram of Voltage Controller Loop for VSC

2.1.4.3.3 VSC Power Controller

The power control of the VSC connected to microgrid should be based on droop control in order to mimic the governor behaviour of synchronous generator [20]. The active and reactive powers can be

14

calculated using the instantaneous output voltages and currents in d-q frame as shown in equations (2.17) and (2.18) respectively. Due to the effect of switching on the calculated instantaneous voltages and currents, the calculated powers should pass through a low pass filter (LPF) to determine the instantaneous value which matches the fundamental system frequency [43], [45]. Moreover, the power control bandwidth is the smallest compared to voltage and current control; therefore, the cut-off frequency of the LPF based on the literature is equal to 10% of the fundamental system frequency [20], [45], [46].

$$p = \frac{3}{2}\left((vo_d * io_d) + (vo_q * io_q)\right) \qquad (2.17)$$

$$q = \frac{3}{2}\left((vo_d * io_q) - (vo_q * io_d)\right) \qquad (2.18)$$

Including the LPFs into equations (2.17) and (2.18) results in rewriting the instantaneous active and reactive powers as follows:

$$P = \left(\frac{\omega_f}{s + \omega_f}\right)\left(\frac{3}{2}\left((vo_d * io_d) + (vo_q * io_q)\right)\right) \qquad (2.19)$$

$$Q = \left(\frac{\omega_f}{s + \omega_f}\right)\left(\frac{3}{2}\left((vo_d * io_q) - (vo_q * io_d)\right)\right) \qquad (2.20)$$

Finding the instantaneous filtered active and reactive powers as shown in equations (2.19) and (2.20) facilitates the development of the droop control for the VSC. Figure 2.5 shows the droop characteristics for controlling the VSC active and reactive power that should be implemented into the VSC controller in order to emulate the governor behaviour.
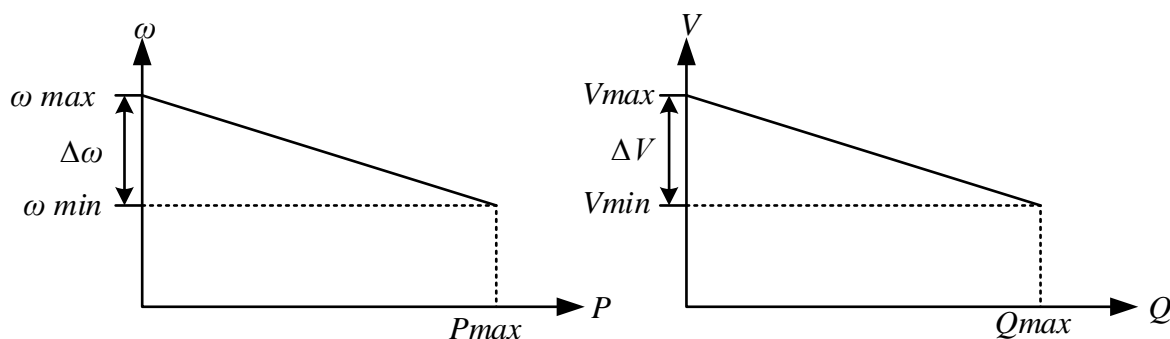
Figure 2-5: Droop Characteristics for Active and Reactive Powers.

The linear relationships of the droop graphs for both active and reactive powers can be written as shown below in equations (2.21) and (2.22):

$$\omega_{ref} = \omega^{inv} - \left(\frac{\omega_{max} - \omega_{min}}{P_{max}}\right) * P = \omega^{inv} - m_p * P \tag{2.21}$$

$$v_{ref} = v^{inv} - \left(\frac{v_{max} - v_{min}}{Q_{max}}\right) * Q = v^{inv} - n_q * Q \tag{2.22}$$

Where w^{inv} and v^{inv} are the outputs frequency and voltages magnitude at no load condition. The allowable range of maximum and minimum voltage and frequency of the VSC are notated via V_{max}, V_{min}, w_{max}, and w_{min}, respectively. These limits are determined by IEEE standard for interconnecting distributed resources with electric power systems[47]. The rated powers of the VSC are notated by P_{max} and Q_{max} based on power capability limits [48]. It is shown that the outputs of the power controllers are angular speed and the voltage magnitude; however, it is necessary to find out the phase angle in order to transform all voltages and current quantities in d-q frame. Therefore, by integrating the angular speed that is achieved from active power droop, the phase angle will be determined. In order to clarify the determination of the angular speed and the phase angle, the power control implementation is depicted in Figure 2.6.
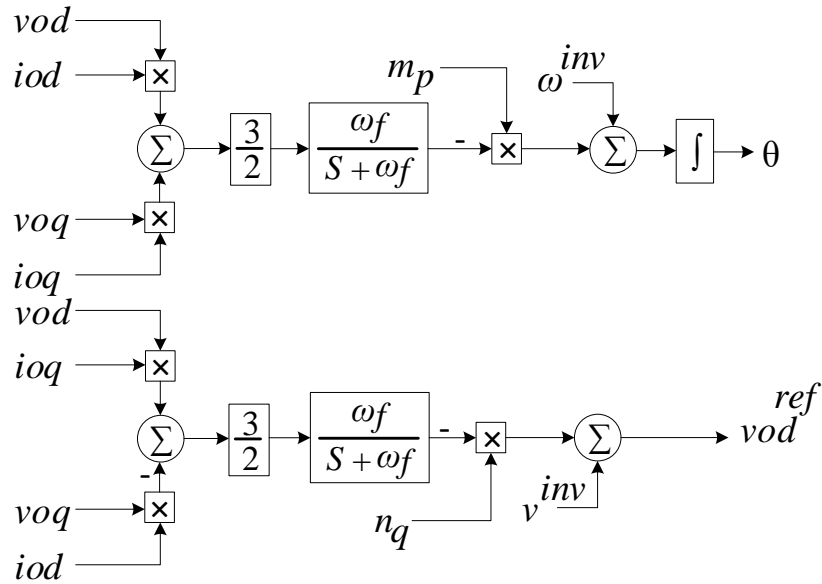
Figure 2-6: Power Controller for VSC.

2.1.4.4 Mathematical Model of Half-Bridge DC-to-DC Interfacing DG Unit into DC Microgrid

The general representation of the DC-to-DC converter that is interfacing a DG unit into DC microgrid is shown in Figure 2.7. In fact, it is similar to the AC microgrid, but the main difference is the converter circuit structure which is a half-bridge DC-to-DC converter, and the LC filter and the DC line are represented in single line circuit.
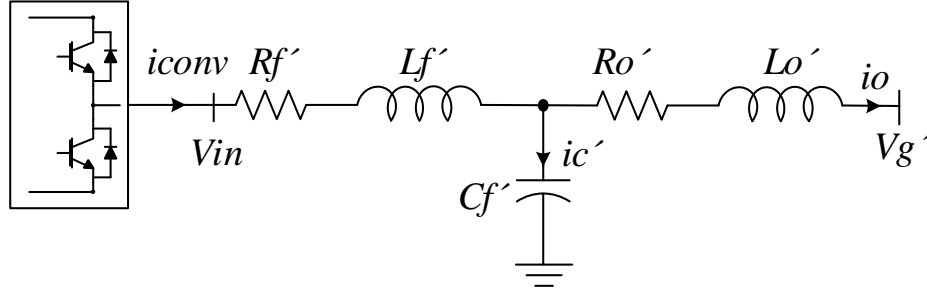
Figure 2-7: Half-Bridge DC-to-DC Converter.

Applying KVL at the filter side and the DC line in Figure 2.7 gives an equivalent differential equation of a voltage drop across the inductance and the resistance. Also via KCL, the voltage across the shunt capacitor can be determined. Therefore, the dynamic equations of the voltages and currents known as large signal model for DC-DC converter including the DC line can be written as follows:

$$Lf' \frac{dil'}{dt} = Vin - Vo' - Rf'.il \tag{2.23}$$

$$Lo' \frac{dio'}{dt} = Vo' - Vg' - Ro'.io \tag{2.24}$$

$$Cf' \frac{dvo'}{dt} = il - io' \tag{2.25}$$

The DC filter components of the half-bridge are represented by $Rf', Lf',$ and Cf', while the coupling components to the DC microgrid are represented via Ro' and Lo'.

2.1.4.4.1 Half-Bridge DC-to-DC Converter Controller Structure

The half-bridge DC-to-DC converter controllers are similar the VSC that is interfaced a DG unit into an AC microgrid, which consists of current, voltage, and power droop controller. However, there is no need to use Park transformation due to the fact that the control quantities are already constant as DC

17

values. The following subsections will discuss the controller loops of the half-bridge DC-to-DC converter in detail.

2.1.4.4.2 Half-Bridge DC-to-DC Converter Current Controller

According to equation (2.23), developing the current controller including the PI can be considered by substituting the nonlinear term by the PI transfer function to track il^{ref} with instantaneous value of il as written in equation (2.26):

$$Lf'\frac{dil'}{dt} = \left(K_{pc} + \frac{K_{ic}}{s}\right)(il^{ref} - il) \tag{2.26}$$

Due to no coupled control components in the DC control quantities, there is no need for a feed-forward in the half-bridge DC-to-DC converter current controller loop. Figure 2.8 shows the current controller loop for the half-bridge DC-to-DC converter.
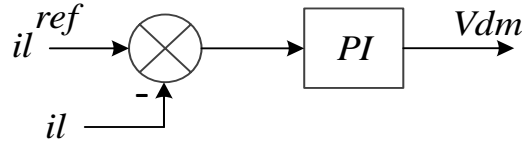
Figure 2-8: Current Controller for Half-Bridge DC-to-DC Converter.

2.1.4.4.3 Half-Bridge DC-to-DC Converter Voltage Controller

The output control quantities of the voltage controller are the input reference to the current controller. Referring to equation (2.25), the nonlinear capacitor voltage term can be replaced by PI transfer function, and is written in equation (2.27) by tracking the DC capacitor voltage. Nevertheless, using the output current as feed-forward in the voltage controller improves the dynamic response during the load transient [49], as depicted in Figure 2.9.

$$Cf'\frac{dvo'}{dt} = \left(K_{pv} + \frac{K_{iv}}{s}\right)(vo^{ref} - vo) \tag{2.27}$$
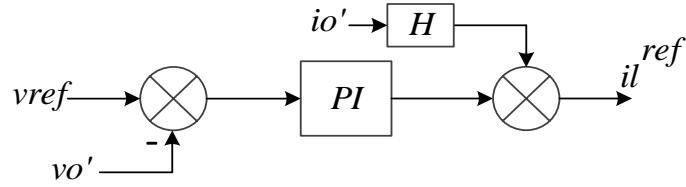
Figure 2-9: Voltage Controller for Half-Bridge DC-to-DC Converter.

2.1.4.4.4 Half-Bridge DC-to-DC Converter Power Controller

In a DC microgrid, the droop characteristic depends on either DC voltage versus active power [50] or the DC current versus DC voltage [51]; accordingly, the droop characteristics based on DC voltage versus active power are considered in this thesis, as depicted in Figure 2.10.
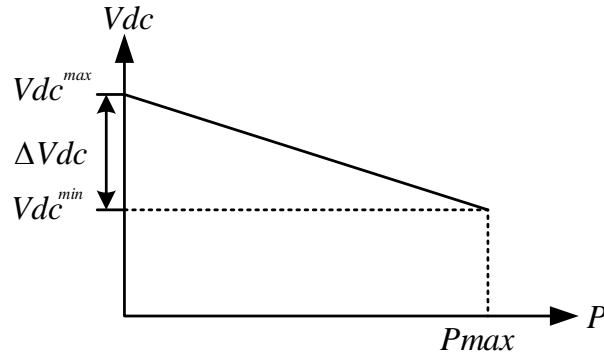
Figure 2-10: Droop Characteristics for Active Power in DC Microgrid.

The linear relationship of the droop graph for active power verses DC voltage can be written as shown in equation (2.28):

$$Vdc_{ref} = Vdc^{inv} - \left(\frac{Vdc_{max} - Vdc_{min}}{P_{max}}\right) * P = Vdc^{inv} - K_p * P \tag{2.28}$$

Where Vdc^{inv} is the output DC voltages at no load condition.

The maximum and the minimum voltages are based on the allowable range of the DC voltage as notated by Vdc$_{max}$ and Vdc$_{min}$. The rated power of the VSC is notated by P$_{max}$. Due to measuring the instantaneous values of outputs DC voltage and current in order to determine the required reference, the LPF is required to eliminate the switching frequency effect. As shown in Figure 2.11, the power controller of the half-bridge DC-to-DC converter is presented.

19
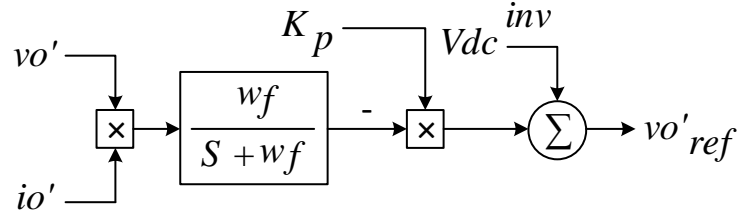
Figure 2-11: Power Controller for Half-Bridge DC-to-DC Converter.

2.2 Small-signal Modeling

This section reviews the small-signal-model of AC microgrid presented by Pogaku [20] as well as the small-signal model of the DC microgrid published in [52]. Small-signal dynamic model analysis is commonly used to analyse the dynamic performance of the microgrid and to design the control DG units [53]. The advantage of the small-signal modelling is to provide further investigation of the system once the eigenvalues are determined such as the relationships between the system parameters and the stable region. In other words, the small-signal model not only shows whether the system is stable or not, but it can also show the changing effect in either the system parameters such as lines resistances and inductances or the controller parameters such as PI coefficients [20]. In order to develop the small-signal dynamic model for an electrical system such as a microgrid, it is first necessary to identify the large signal model that is represented via nonlinear differential equations that are presented previously in form of the following equations:

$$\frac{dx}{dt} = f(x(t), u(t)) \tag{2.29}$$

$$y = g(x(t), u(t)) \tag{2.30}$$

Where equation (2.29) is a state equation in which $x(t)$ represents the state vector, and $u(t)$ represents the input vector. Equation (2.30) is known as output equation. These equations can be written in standard form of the state space representation. Nevertheless, the nonlinear differential equations must be linearized around the operating points in order to study the stability of the system. Therefore, the small-signal model representation of equations (2.29) and (2.30) become the following:

$$\frac{d\Delta x}{dt} = A.\Delta x + B.\Delta u \tag{2.31}$$

$$\Delta y = C.\Delta x + D.\Delta u \tag{2.32}$$

Where:

A is a state matrix that contains of the system parameters and characteristics.

B is a matrix that contains of the system inputs.

C is a matrix that contains of the system output.

D is a matrix that contains of the system feedforward.

2.3 Hybrid Microgrids

Due to its recent proposal, more investigation is needed into the limitation of controlling hybrid microgrid and analysing its stability [4], [7]–[10], [23], [25], [54]. The complexity of controlling hybrid microgrid is primarily based on numerous control objectives that must be handled via sub-grids and IC as well. These control objectives are namely sufficient power sharing in AC and DC sub-grids, voltage and frequency stability, and power exchange among the sub-grids [21].

The autonomous power control of hybrid microgrid with only one IC was proposed in [8]. The authors presented the droop principle for the sub-grids as well as for the IC. In this method, the input reference to the IC is based on combining AC and DC droop characteristics. In other words, the droop characteristics should apply to both AC and DC sides for the IC. In the DC side, the droop characteristics depend on DC voltage and DC power, while in the AC side, the droop characteristics depend on the AC power and frequency as shown in Figure 2.12. Therefore, because of the bidirectional power flow of the IC the droop characteristics should be merged by summing them with respect to reference input sign to ensure bidirectional power flow. The implementation characteristics of a droop controller to control an active power of the IC are shown in equations (2.33) and (2.34). In general, conventional droop can be simplified as a linear relationship as shown in Fig. 2.

$$P_{ref} = \left\{ P_{meas} - \left(\frac{\omega^{max} - \omega^{min}}{P_{max}} \right) \times V_{dc_{meas}} , for\ DC - to - AC\ power\ flow \right. \tag{2.33}$$

$$V_{dc_{ref}} = \left\{ V_{dc_{meas}} + \left(\frac{v_{dc}^{max} - v_{dc}^{min}}{P_{max}} \right) \times P_{meas} , for\ AC - to - DC\ power\ flow \right. \tag{2.34}$$

21
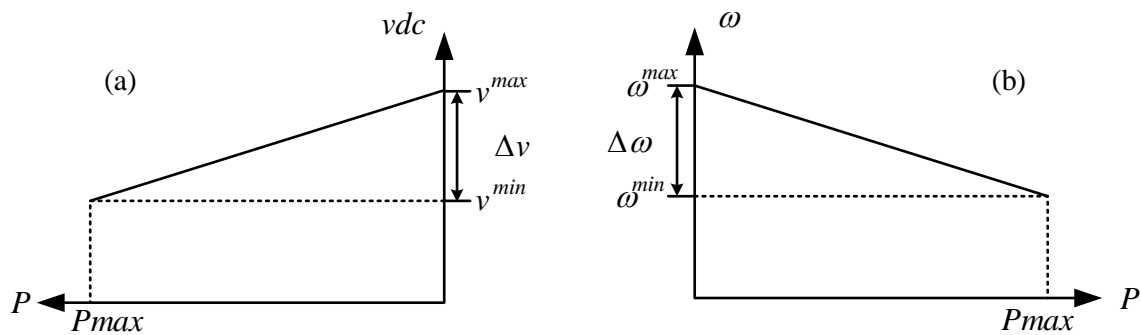
Figure 2-12: Droop Characteristics: (A) DC Voltage versus Active Power, (B) Frequency versus Active Power.

The topology of hybrid microgrid with just one IC decreases the reliability of hybrid microgrid; therefore, multiple ICs were proposed in order to achieve high system reliability [30]. Multiple ICs provide high system reliability, as proposed in [30]; however, the effect of both sub-grids' dynamics are increased, especially in islanded operation mode due to the variation of the AC and DC voltage and the AC system frequency. The autonomous control scheme for multiple ICs was introduced as normalized DC voltage versus the frequency [28]. Nevertheless, operating multiple ICs via applying normalized droop does not provide an accurate operation of the parallel ICs [21]. The reason behind this issue is the circulating current.

Due to the system dynamics sensitivity in hybrid microgrid during power exchange between the sub-grids, the authors in [6] proposed using energy storage to achieve smooth energy exchange. It is clear that this proposed solution is costly and has certain operation issues such as lifetime characteristics [31]. The other associated issues of considering the energy storage are: cooling system for supper conducting bearing, low energy density, charging and discharging ability, and thermal losses [38]. This method suffers from imprecise power sharing, particularly for the ICs due to the droop control concept, and the existence of both zero sequence and cross circulating currents.

The authors of [32] proposed a centralized power management control for hybrid microgrid. The proposed centralized control was investigated for grid-connected mode. This control method requires communication infrastructure and more sensors to measure the load demand in the AC and DC sub-grids. Moreover, this method has not been validated with droop-based control, which is important in the case of islanded mode.

In [30], the centralized power management of hybrid microgrid was introduced for islanded operation mode. The purpose of this centralized power management control is to avoid the false operation of the hybrid microgrid in the case of changing the droop coefficient.

Also, the hybrid microgrid dynamics are affected during power exchange between both sub-grids which could potentially lead to stability issues due to the lack of inertia and load-dependent voltage [12], [11], [33], and [34].

2.4 Virtual Synchronous Machine (VSM)

The high penetration of renewable resources causes the electrical system to be unstable due to the lack of inertia in converters compared to traditional synchronous machines (SMs). The benefit of the synchronous machine inertia in an electrical system is that it stabilizes the grid frequency [32] by supplying energy for a short time period [55]; thus, synchronous machines support and participate in the AC system's frequency and voltage control. Moreover, the majority of the renewable resources (such as wind, PV, and fuel cell) are interconnected via voltage source converter (VSC). VSC is commonly used in microgrid and HVDC applications and does not have either an inertia or behave as a traditional SM.

This issue can be addressed through the application of the concept of virtual synchronous machine (VSM) controllers, which combine VSC and SM characteristics. The VSM control algorithm of a power electronics converter is a control feature that can be added to a converter controller to enable it to behave as an SM [56]. The algorithm allows the incorporation of virtual inertia and damping behaviour into the loop controllers of an interfacing converter [57], [56], [58], [59], and [60]. Thus, the VSC has no physical mass of inertia as in the case of practical SMs; i.e., it does not have limited inertia or constant damping values. Instead, only the converter power response mimics the inertia response of a real SM as illustrated in Figure 2.13.

VSC   SM   *VSM:SM's behaviour*
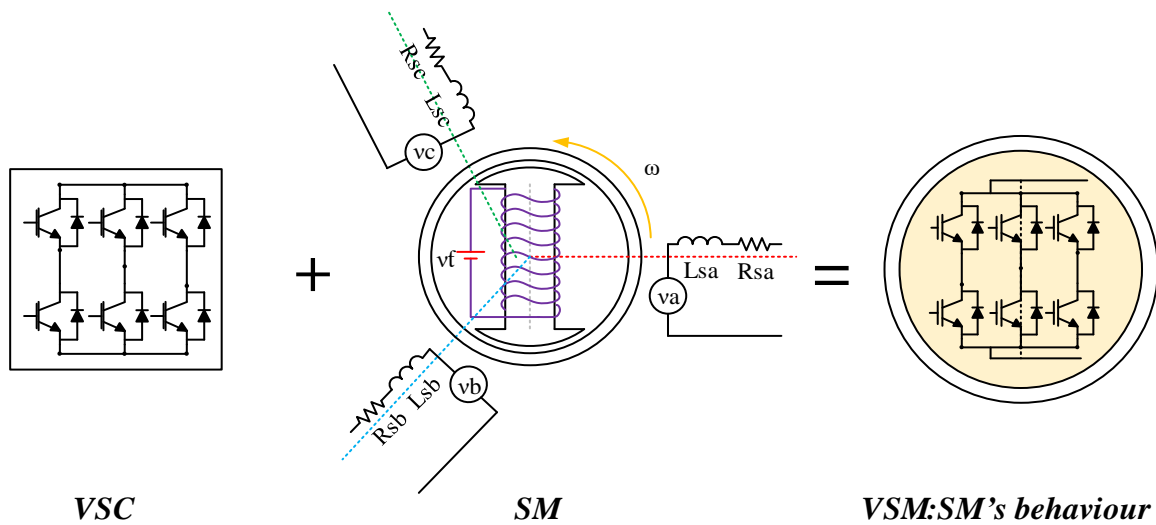
Figure 2-13: Mixing of Power Electronics Converter Technology with Synchronous Machine Characteristics.

VSM control algorithms, which can be implemented through a slight modification to the VSC controller, are categorized as either high-order or low-order VSM control algorithms. Although both types of VSM algorithms provide active and reactive power control, each has a specific control frame, as will be discussed in Chapter 3[61].

A number of VSM control algorithms have been developed to enable a VSC to mimic the behaviour of an SM. In [58], the implementation of virtual inertia in the converter controller loops with a storage unit was introduced as a virtual synchronous generator (VSG). The authors of [16] presented a different VSM concept named VISMA as represented by a hysteresis current-controlled SM model for controlling a three-phase inverter. The control of a VSG that emulates SM transient as well as steady state characteristics was further investigated in [57], [59], and [62], while a VISIM algorithm was adopted by the authors of [16], [18], [63], [64], and [65]. As an alternative, synchronverters were employed in the work reported by [66], [67], and [68], and a theoretical review of these control algorithms was provided in [56] and [69].

These types of VSMs can be classified either in terms of their output references [69] or their topologies [56]. The majority of the studies related to VSM control algorithms that are described in the literature have been focused on the development and implementation of VSMs [56], [69]. In [17], the dynamic characteristics of VSGs were compared with droop control under normal operating conditions.

The authors of [70] examined the inertial dynamics of a VSG used with doubly fed induction generator- (DFIG) based wind turbines by including a short circuit in the AC-side system which is remote from the converter. A VSG for grid-connected DFIG-based wind turbines was studied with respect to different damping coefficients and varied short circuit ratios (SCRs) [71]. In other work [68], the performance of a multi-terminal direct current (MTDC) was evaluated under single-fault conditions with a VSM-based synchronverter. The most VSM control concept algorithms are classified based on the control order as pictured in Figure 2.14.
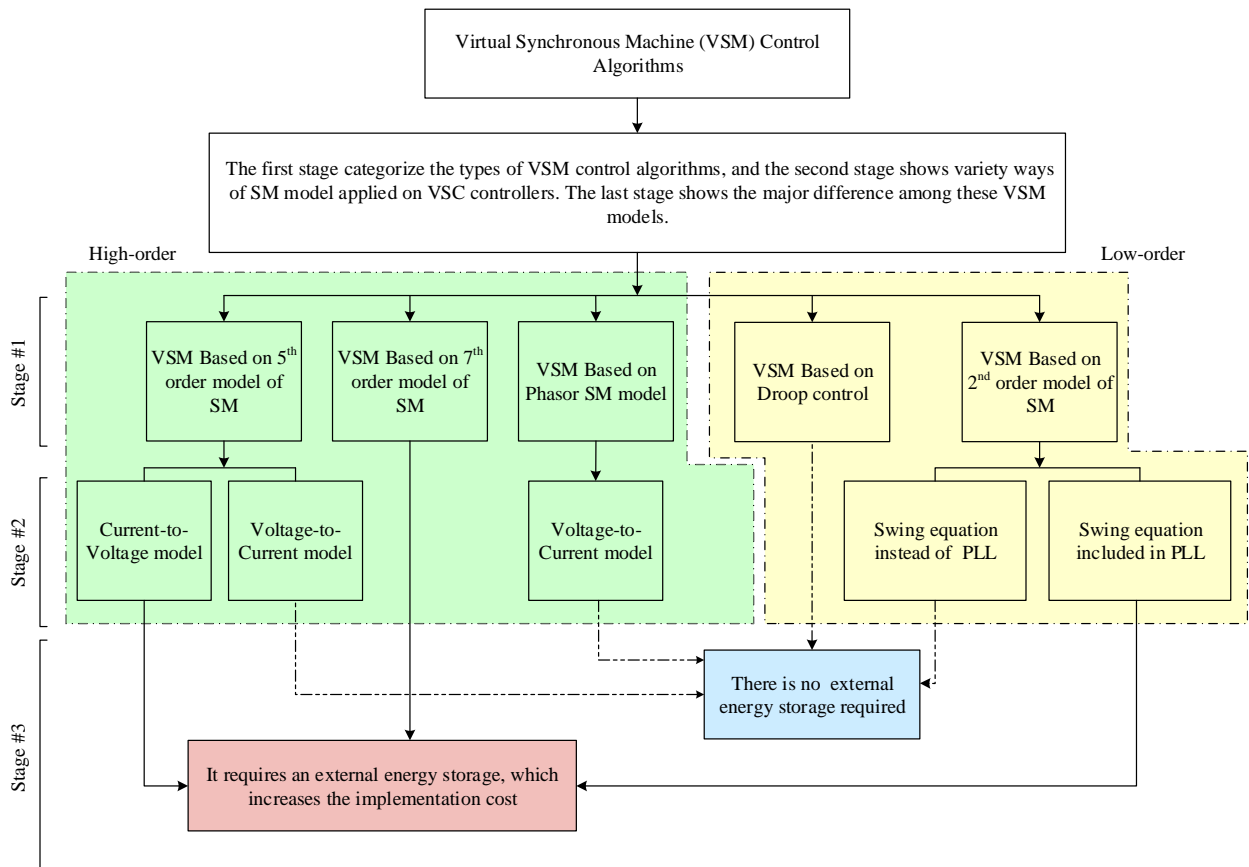
Figure 2-14: Classification of VSM Based on Model's Order.

Indeed, the process of choosing an appropriate VSM control algorithm (low or high-order) to implement is critical, complex, and requires further investigation. Only limited comparative studies of VSM algorithms are available [72],[18]. The authors of [72], [43] studied the equivalent of a VSM for

conventional frequency droop control and compared it with VSC droop control in order to demonstrate similar behaviour during load step changes. Another study focused on the difference between the implementation of two types of high-order SM models with respect to implementation simplicity and the behaviour of the converter with balanced AC voltages [18].

All of these previous studies involved the investigation and comparison of VSM controllers based on an ideal voltage source. An important element of determining the most appropriate algorithm is therefore examining and comparing the dynamic characteristics and behaviour of VSM control algorithms and their performance during abnormal conditions that commonly occur in distribution systems, such as short circuits and unbalanced AC voltages.

Chapter 3

Comprehensive assessment of virtual synchronous machine based voltage source converter controllers [1]

3.1 Introduction

The majority of the previous works of VSM control concept in the literature were focused on the implementation of VSM, but, they did not carried out the serious issues as an unbalance AC voltage and short circuit situation. This chapter presents a comprehensive examination and assessment of VSM control algorithms in order to establish suitable choices of VSM control algorithms for implementation and use in a variety of applications. Therefore, this chapter reveals the serious issue with implementing the high order model in the practical real system; which might lead to unstable operation especially in AC microgrid application. The study presented in this chapter also entailed an investigation of the equivalence of a low-order VSM control algorithm with a high-order VSM control algorithm under normal and abnormal conditions, such as unbalanced AC voltages and short circuits. A comparison of the dynamic and performance behaviour of VSM control in grid-connected mode for different operating scenarios is provided. However, since conventional frequency droop control provides behaviour equivalent to that of a VSM [72], consideration of both algorithms in this study was unnecessary because conventional frequency droop control lacks an inertia coefficient in the control loops, which means zero inertia [72]. Also, in grid connected mode of operation, the droop control concept cannot be implemented due to the fixed system's frequency.in other words, the variation of system's frequency does not exist. The system discussed in this chapter is based on a full detailed switching VSC model in order to evaluate the VSM controllers during short circuit conditions, which was simulated in a PSCAD/EMTDC environment.

This chapter is organized as follows: Section (3.2) provides a brief overview of VSM control algorithms and their categorization, Section (3.3) presents the simulation results and analysis, and the final section offers conclusions of this chapter.

_____

3.2 Virtual Synchronous Machine Types

The nature of renewable energy source is not deterministic, so the power will fluctuate; therefore, the voltage level and the system's frequency can be affected [55]. Solving this issue can be done via adding an extra inertia to the system [56]. Therefore, the operation of several synchronous machines is a hint of combining power electronics with the behaviour of the synchronous machines to be emulated [65].

There are enormous applications for VSM control concept. Using the second order VSM model for smart grid application was studied to show the seamless transition between grid connected mode and islanded mode[73]. Moreover, applying the VSM based on high order model was investigated for parallel inverter in AC Microgrid[74]; however, this model does not provide the converter either overloading or overcurrent protection. In grid connected DFIG-based wind turbines was studied with high order VSM including currents limitation[71], but the model mainly depends on measuring the instantaneous voltages. Therefore, in case of unbalance voltages and short circuit conditions did not investigated yet; which will affect the system stability. The power distribution system with high penetrations of converters was studied with including the VSM control concept to improve system performance[75]. Nevertheless, the VSM control concept can be implemented for single-phase bidirectional battery charger for providing vehicle-to-grid services[76]. In HVDC application connected to weak AC system using the VSM control concept offers frequency support to the weak AC system with low inertia [77]. Moreover, in AC microgrid application, the transition from islanded mode to grid connected mode presents large transients in voltages and currents that reflects high transient in power might hit the stability boundaries of the microgrid. Using the concept of VSM control provides smooth transition of the AC microgrid operation[78].

Due to the existence of several VSM control algorithms for VSC, they can be classified into two categories which are high-order and low-order VSM. Also, the VSM models can be divided based on the requirement of an extra component such as energy storage; therefore, Figure 2.13 in the previous chapter summarizes the differences of VSM models at different stages, and they were found in the literature. Therefore, the choice of the VSM models to be assessed and studied is based on the fact that there is no need of an extra component as shown in Figure 2.13 in the light blue box. However, the VSM based on phasor SM is not considered due to a serious problem when its implemented in d-q frame that is the model become unsteady state in case of unbalanced load [64]. Moreover, the droop control does not have yet virtual inertia unless by includes a low pass filter (LPF) to filter out the active power, but still the virtual damping does not exist with the LPF. It is clear that without (LPF) the droop control has zero inertia[72].

28

3.2.1 High-order VSM Model

Mimicking the behaviour of SM inertia on VSC control algorithm can be achieved via introducing virtual inertia and damping characteristics into VSC control using the mathematical model of SM [56]-[62]. Subsequently, the idea of implementing a virtual inertia to the converter controller loops with storage unit is introduced as virtual synchronous generator (VSG)[57], which requires an extra storage unit. Also, the author of [16] presented another concept of virtual synchronous machine (VISMA) which is represented as hysteresis current controlled of the high-order of traditional synchronous machine model to control the three-phase inverter. Moreover, in [18], the authors presented and investigated the behaviours of two high-order models of VSM based on current-to-voltage and voltage-to-current of SM model, so they used different switching techniques which are a PWM controller and a hysteresis controller respectively.

The high-order model of the synchronous machine is used to calculate the reference values. It is worthwhile to notice that the mathematical model of SM consists of mechanical and electrical parts. The mechanical part is responsible for generating the angular speed and a positive phase voltage angle which is known as swing equation (3.1). The electrical part is the stator winding equations which are energized by the phase angle to generate either the current or voltage references to the controller. The interaction between the mechanical and electrical parts is simplified as shown in Figure 3.1.
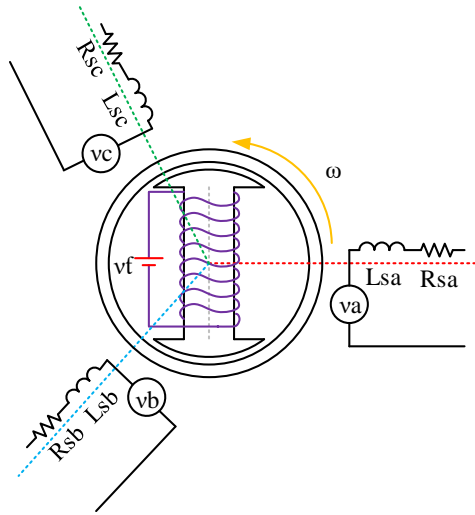
Figure 3-1: Simplified Synchronous Machine Model.

The equations (3.1)-(3.5) are based on a SM simplified model which is retrieved from[16].

29

$$J.\omega\frac{d\Delta\omega}{dt} = P_{mech} - P_{ele} - f(t) D_d \tag{3.1}$$

$$\theta = \int \omega.dt \tag{3.2}$$

$$E_a - v_a = R_{sa}.I_a + L_{sa}.\frac{di_a}{dt} \tag{3.3}$$

$$E_b - v_b = R_{sb}.I_b + L_{sb}.\frac{di_b}{dt} \tag{3.4}$$

$$E_c - v_c = R_{sc}.I_c + L_{sc}.\frac{di_c}{dt} \tag{3.5}$$

In equations (3.3)-(3.5): where E_a, E_b, and E_c are the voltages at PCC which are measured values; v_a, v_b, and v_c are the induced back EMFs; the symbols R_s and L_s represent the stator resistances and the stator inductances respectively. In (3.1), the machine's inertia is donated by J; the mechanical input power is donated by P_{mech}, and the electrical power is represented P_{ele}. The damping coefficient is donated by D_d. The $f(t)$ is the phase compensation term. In equation (3.2), the angular speed donated by ω and a positive phase voltage angle represented by θ.

The high-order VSM control algorithm has two configurations. In[16], the first configuration is presented in detail which is a voltage-to-current model, and it mainly depends on measuring AC voltage at PCC. In contrast to [66], a current-to-voltage model was presented and studied [18], but without energy storage. A comparison between both high-order control algorithms of VISMA was studied in [18] under normal operation conditions with different switching techniques. The control structure of using this model depends on these equations, so this control strategy of can be done using a hysteresis current control technique or PWM control technique[18]. Therefore, the voltage-to-current model provides the reference current values to control the VSC as shown in Figure 3.2, while the reference voltage values are provided by current-to-voltage model and can be seen in Figure 3.3.
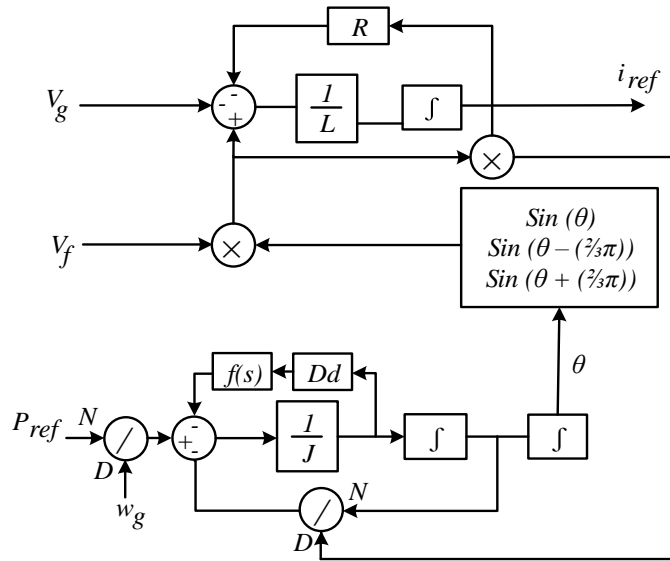
(N = Numerator , D = Denominator)

Figure 3-2: Block Diagram of Simplified High-Order SM Model Represents Voltage-to-Current model.
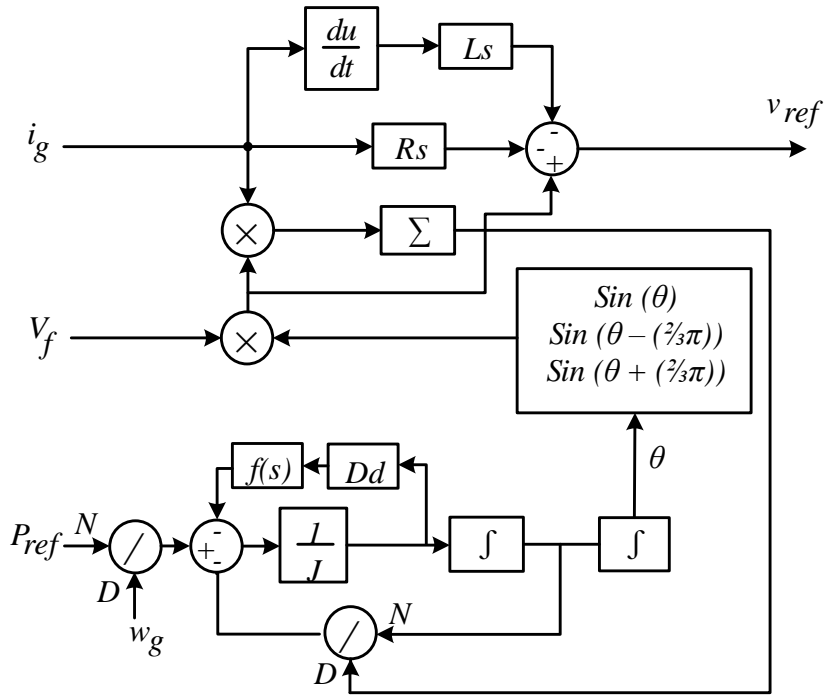
Figure 3-3: Block Diagram of Simplified High-Order SM Model Represents Current-to-Voltage model.

31

Where V_g and i_g are the voltages at PCC and the output converter's currents; the excitation voltage of the SM is donated by V_f. the symbol ω_g represents the grid angular speed, and the P_{ref} is the command reference. The V_{ref} and i_{ref} are the output of the SM which are used as input signals to the converter controllers.

3.2.2 Low-order VSM Model

The high-order VSM control algorithm described above provides the same properties as SM does. However, the low-order VSM control algorithm is equivalent to the conventional droop mechanism; which mainly depends on swing equation[69],[72]as shown in Figure 3.4.
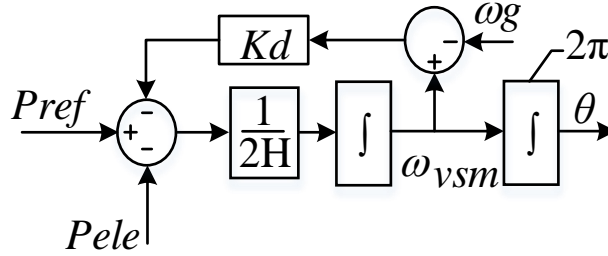
Figure 3-4: Control block implementation of Swing Equation for Low order VSM model.

As the main target of introducing VSM is to mimic the SM behaviour, the emulation of SM's inertia and damping can be captured using just the swing equation. Therefore, the general form of the swing equation for SM based on Newton's law is written in term of torque parameters as shown in equation (3.6)[79], and also it can be written based on active power in case of implementing the VSM control by Multiplying equation (3.6) by the rotor synchronous speed ω_{VSM} as shown in equation (7) [43].

$$J\frac{d^2\delta}{dt^2} + D_d\frac{d\delta}{dt} = \tau_m - \tau_{ele} \tag{3.6}$$

$$J.\omega_{VSM}.\frac{d^2\delta}{dt^2} + D\omega_{VSM}\frac{d\delta}{dt} = P_m - P_{ele} \tag{3.7}$$

According to [1], the derivative term of the rotor angle $d\delta/dt = \Delta\omega = \omega_{vsm} - \omega_g$ is the rotor speed deviation in electrical radians per second; thus it is more convenient to replace the second-order differential equation term in equation (3.7) by two first-order equations as the following:

$$J.\,\omega_{VSM}\frac{d\Delta\omega}{dt} = P_{mech} - P_{ele} - (\omega_{vsm} - \omega_g)\,D_d \qquad (8)$$

$$\frac{d\delta}{dt} = \Delta\omega_{VSM} \qquad (9)$$

The phase angle and angular speed are used to convert the voltages and the currents in d-q vector control frame[72].Where the inertia is donated by J; the mechanical input power is donated by P_{mech} which is the reference power command, and the electrical power is represented P_{ele}. The damping coefficient is donated by D_d. The symbol ω_{vsw} represents the synchronous speed that is generated by the swing equation while ω_g is the estimated grid angular frequency via PLL.

The VSM can be implemented on an inverter with a classical cascaded voltage and current control loops. Even though, the VSM based on the swing power equation is simple, the required behaviour of the inertia and damping is available. The outcomes of the swing equation are a phase voltage angle θ and angular speed ω.

The cascaded controller loops of the VSC voltage source converter consist of two stages: the inner and the outer controller[43],[46] and Figure 3.5 shows the cascaded control structure of VSC[2]. This control strategy is used mostly for VSC applications due to the fact that it produces less voltage harmonics[1]. Also, this strategy allows independent control of a reactive and an active power[43], [46].
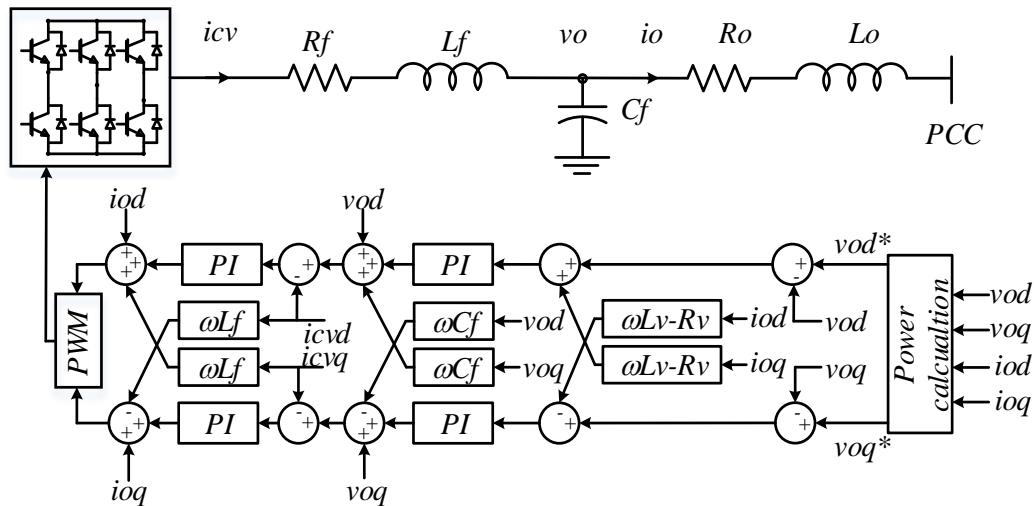
Figure 3-5: Control block implementation of Cascaded Voltage and Current Controllers including Virtual Impendence.

33

The main difference between the high and low-order VSM control algorithm is the controlled loops structure of the VSC. Even though, the high-order and low-order VSM provides independently an active and a reactive power control, each of these algorithms has a specific control frame. Hence, there is no doubt that both high-order and low-order VSM algorithms emulate and mimic the SM inertia and damping due to the existence of the swing power equation in their control structure. Still it is not clear which type of these is the most efficient choice. For this reason, this chapter presents a comprehensive study between high-order and low-order VSM control algorithms in order to achieve clear guidance for choosing the appropriate VSM algorithm.

3.3 Simulation results and analysis

The system model used in this study consists of a fully detailed switching VSC model, and whose parameters are set out in Table I. A detailed VSM-based controller was built in PSCAD/EMTDC environment. The reason for building a fully detailed system was to study and compare static and dynamic properties during normal and abnormal operation, such as that which occurs with sudden load changes, unbalanced AC voltages, and short circuits. The two VSM control approaches proposed in [16] and [46], [72] were considered. The study presented here was concentrated on four important factors: the amount of active power, the virtual inertia generated, the system frequencies, and the value of the virtual damping. The comparison of the two VSM algorithms was based on their dynamic properties, the total voltage and the current harmonic distortion, sudden load changes, and unbalanced AC voltages. Moreover, the switching control techniques for both high-order and low-order VSM are based on PWM switching concept.

Table 3-1: VSC System Parameters.

Quantity	Value	Unit
Converter rated power	20	kVA
AC Voltage (L-L) r.ms	208	V
AC side resistance	0.15	Ω
AC side inductance	2	mH
AC side capacitance	45	μF
Switching frequency	2	kHz
System frequency	60	Hz
DC voltage	450	V
Virtual inertias	0.05& 0.025	kg. m^2

3.3.1 Case 1: Dynamic Properties of VSM Algorithms during Load Changes

This case investigates the similarity between the low- and high-order based VSM controllers. The results shown in Figure 3.6 and Figure 3.7 sequentially have indicated that both VSM models have almost symmetrical and identical behaviours in terms of dynamic properties. However, it remains unclear as to which type of VSM control is the most efficient choice. In other words, using VSM, for example, in distribution system applications might lead to unstable operation in the case of unbalanced AC voltages; which is commonly occurred in distribution system. In this case, both VSM algorithms exhibited similar power and frequency response behaviours for the same inertia values ($J = 0.05$ and $J = 0.025$ kg.m^2). The damping coefficients for the VSM control algorithms are unequal because the low-order VSM is dependent on just the swing equation expressed while the virtual stator resistances and inductances in the high-order VSM affect the damping coefficient.
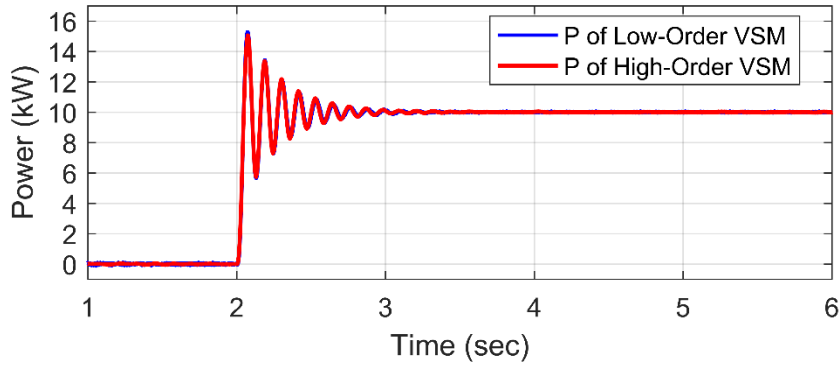
Figure 3-6: Dynamic Properties of VSM Algorithms of Power response for both VSMs with virtual inertia = 0.05 kg.m^2.
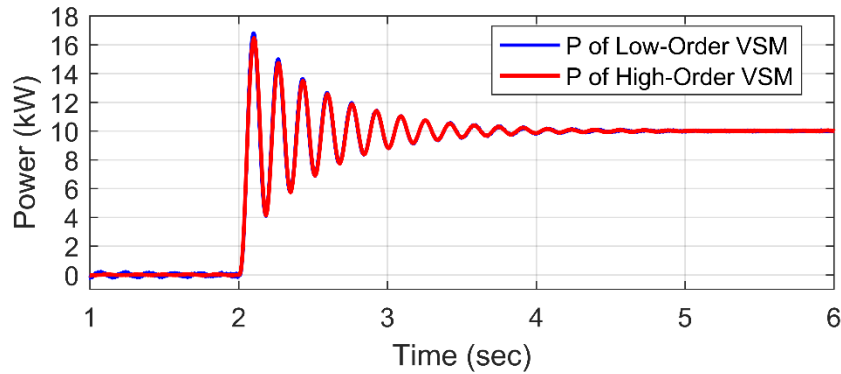
Figure 3-7: Dynamic Properties of VSM Algorithms of Power response for both VSMs with virtual inertia = 0.025 kg.m^2.

Both algorithms exhibit similar response behaviours for $J = 0.05$ and $J = 0.025$ kg.m^2 as displayed in Figure 3.6 and Figure 3.7, respectively. It is clear that the power oscillated once command of the active power took place at t = 2 sec due the small damping coefficient. These figures show that both VSM algorithms mimicked the behaviour of a real synchronous generator.

Figure 3.8 and Figure 3.9 display the system frequency response due to sudden load changes. Although virtual inertia is replicated in the VSC controller through the use of both algorithms, the implementation of the low-order VSM is preferable due to its superior design and simplicity of implementation.
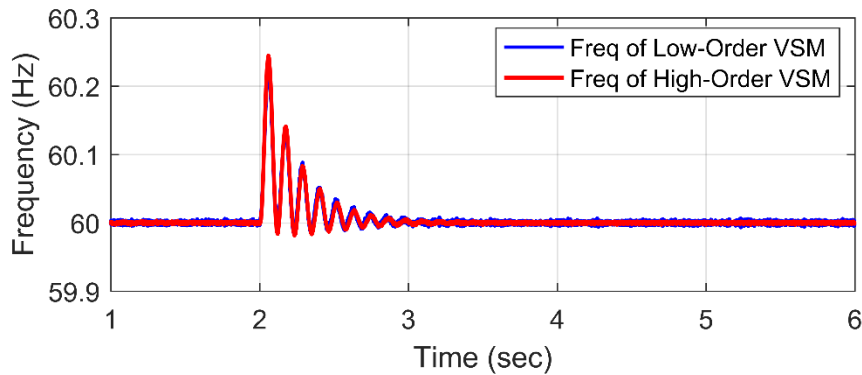
Figure 3-8: Dynamic Properties of VSM Algorithms of Effect of 0.05 kg.m^2 of virtual inertia on the system frequency.
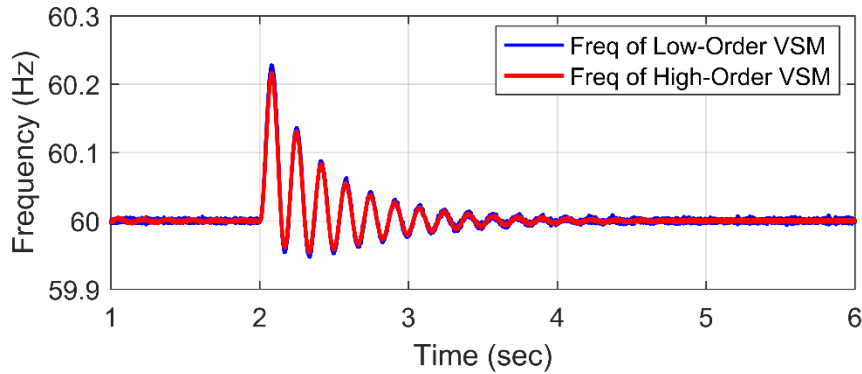
Figure 3-9: Dynamic Properties of VSM Algorithms of Effect of 0.025 kg.m^2 of virtual inertia on the system frequency.

The effect of the virtual inertia and virtual damping coefficient when the system frequency change in case of island AC microgrid in response to the $J = 0.05$ kg.m^2 and $J = 0.025$ inertia values is shown in Figure 3.10 and Figure 3.11, respectively. At t = 3 sec, the system frequency decreased within an allowable range: 0.3 %. The response of both VSMs based on the virtual inertia was almost symmetrical. The low-order VSM is also an equivalent to the SM frequency droop mechanism, so this algorithm mimics real practical SM characteristics. In fact, no doubt exists that both VSM algorithms provide similar properties with almost equal levels of accuracy when the frequency deviations associated with the high-order algorithm are considered. Therefore, it is clear that increasing the virtual inertia helps to support the grid with more active power.
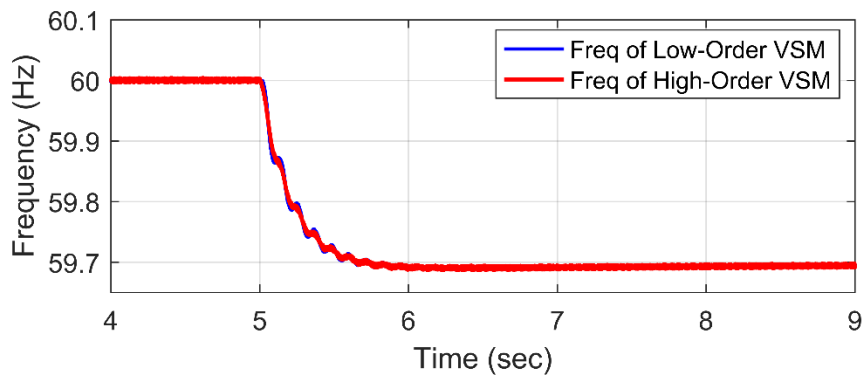
Figure 3-10: Dynamic Properties of VSM Algorithms of Effect of virtual inertia on the drop in system frequency for J = 0.05kg.m^2.
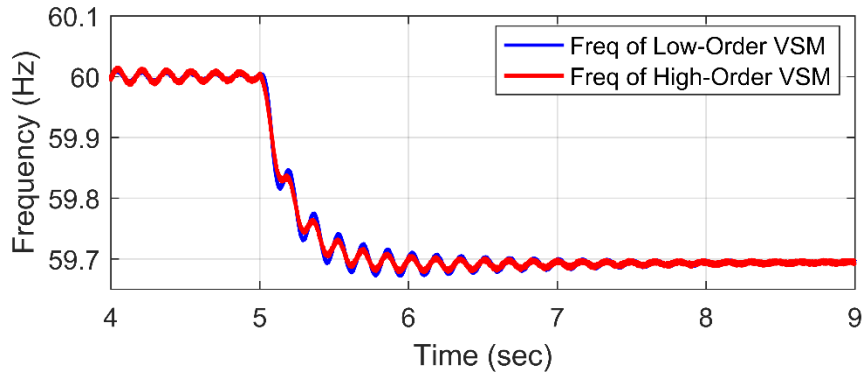
Figure 3-11: Dynamic Properties of VSM Algorithms of Effect of virtual inertia on the drop in system frequency for $J = 0.025$kg.m^2.

3.3.2 Case 2: Total Harmonic Distortion at the PCC

This case demonstrates the efficiency of the VSM control algorithms in terms of power quality. The results in Case 1 do not show any differences between the high and low order VSM performances. Therefore, the purpose of this case is to compare the efficiency of VSM control algorithms based on the total harmonics distortion. This case shows the advantage of using the low-order VSM over the high-order VSM control algorithm. Although this section of the study has not been carried out previously in literature, it is necessary from a power quality perspective to improve the system's quality and performance.

For this case, the voltage and current harmonics distortion at the PCC were measured in order to compare the control algorithms from a power quality point of view. As clearly shown in Figure 3.12, the low-order VSM control algorithm generated more voltage harmonics than the high-order VSM algorithm, but in low-order model the voltage harmonics is almost equal to 2.8% compared to the high-order model; which is almost fixed.
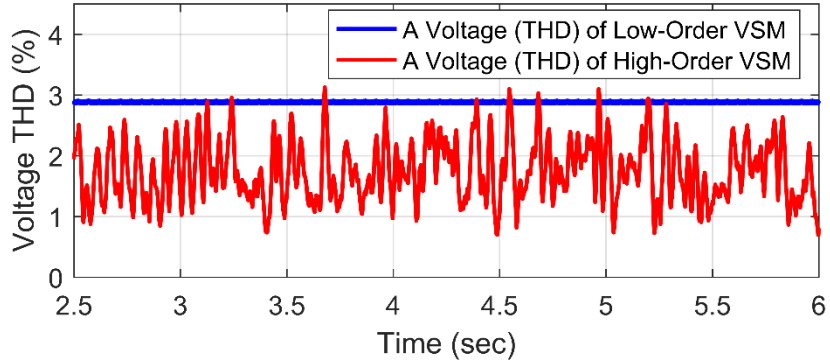
Figure 3-12: Total Harmonic Distortion at the PCC Voltage harmonics distortion (THD).

Based on the previous figure, the total harmonics voltage distortion using the high-order VSM algorithm was fluctuating around 2%. It is clear that the high-order model produces non-characteristic harmonics compared to the low-order model. On the other hand, the total harmonics current distortion using the low-order VSM algorithm was roughly 0.55 %, but in the high-order VSM algorithm, it was about 0.9 % as shown in Figure 3.13. The high-order VSM algorithm thus spread the harmonics over the entire voltage and current spectrum. In contrast, the low-order VSM has specific harmonics in voltage and current as well, but they can be easily filtered due to their deterministic pattern.
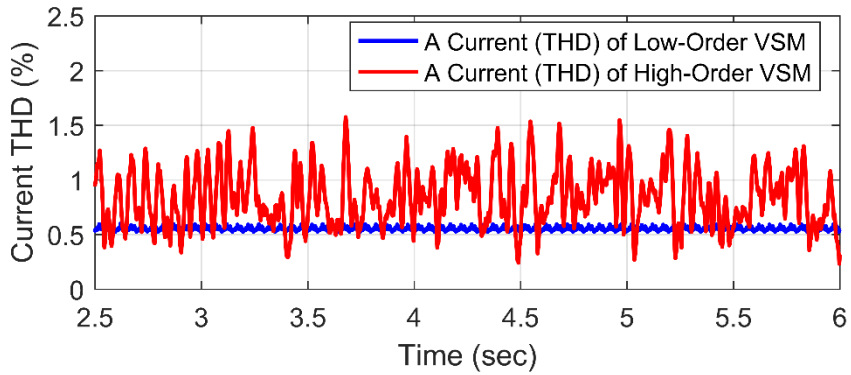
Figure 3-13: Total Harmonic Distortion at the PCC Current harmonics distortion (THD).

The harmonics order and the output voltage can be determined from equation (3.10) and equation (3.11), respectively [80]. The total voltage and current harmonics distortions can be calculated using equation (3.12) and equation (3.13), respectively [81].

$$h_{order} = 6k \pm 1 \qquad \forall\, k = 1,2,\cdots \tag{3.10}$$

39

$$V_{LLh} = \frac{V_{LL1}}{h} \tag{3.11}$$

$$V_{THD}(\%) = \frac{\sqrt{\sum_{k=2}^{\infty} V_k^2}}{V_1} \times 100 \tag{3.12}$$

$$I_{THD}(\%) = \frac{\sqrt{\sum_{k=2}^{\infty} I_k^2}}{I_1} \times 100 \tag{3.13}$$

Where h_{order} represents the characteristic and non- characteristic harmonics distortion. The V_{THD} and I_{THD} represent the total harmonics distortion for voltage and current. The symbol k represent an individual harmonic order.

3.3.3 Case 3: Comparison of Short Circuit Performance

Both controller algorithms were investigated in case of the three-phase to ground short circuits that take place in the middle of the line that connects the PCC to the main grid for durations of 0.1 sec, or about five cycles. For this case, the dynamic responses of the active power for both controllers are indicated in Figure 3.14 and Figure 3.15, respectively. It can be seen that for a short circuit applied at t = 6 sec, the power of both VSM models decreased almost to zero and that they delivered quite similar levels of dynamic performance. However, the output power that is measured from the converter side of both VSM control algorithms do not reach the zero due to the existence of the virtual inertia and damping behaviours in controller loops.
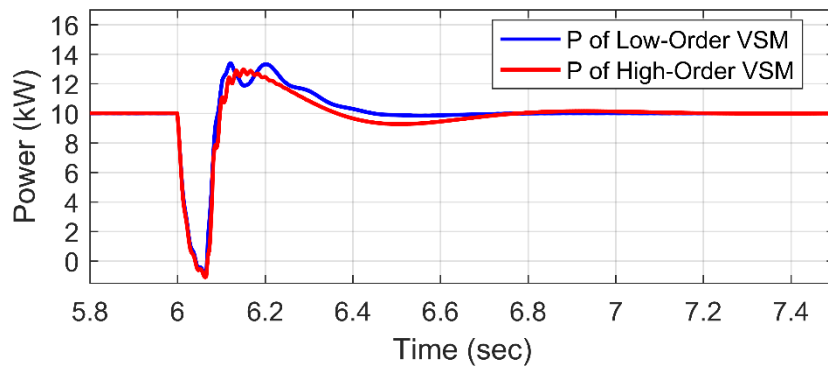
Figure 3-14: Short Circuit Performance Active power behavior of both VSMs under a three-phase-to-ground fault from Grid Side.
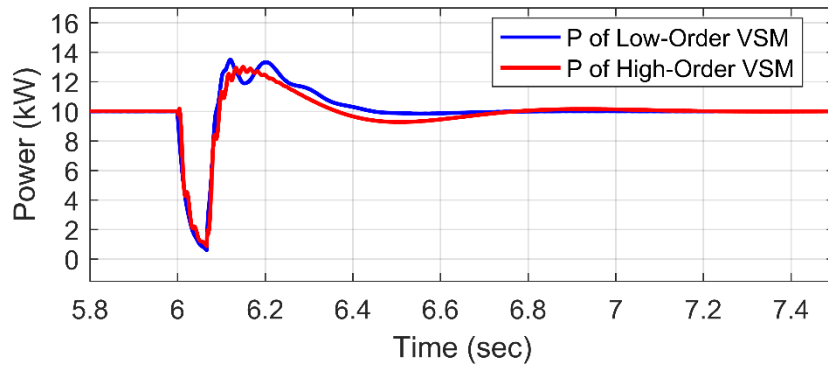
Figure 3-15: Short Circuit Performance Active power behavior of both VSMs under a three-phase-to-ground fault from Converter Side.

In fact, the three-phase short circuit is not enough to compare the VSM models with each other because based on Figure 3.2 the high-order VSM model it mainly depends on the instantaneous measured voltage at the PCC. Therefore, it is necessary to investigate the performance of both VSM models under either two-phase-to-ground or single-phase-to-ground short circuit in order to show a fair comparison. For this reason, the two-phase-to-ground is carried out in this case to reveal the issue of unstable operation that is correlated with high-order model of VSM. As shown in Figure 3.16 the two-phase-to-ground short circuit takes place at t=6 sec. Hence the power of the high-order VSM model supplied almost 40% of its reference power, and it has a quite large oscillatory behavior compared to the low-order model. On the other hand, the low-order model is supplying approximately 50% of the reference value as shown in Figure 3.16.
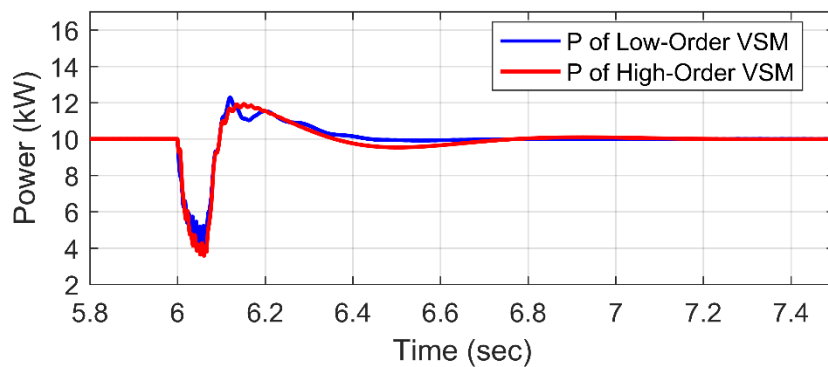
Figure 3-16: Short Circuit Performance shows Active power behavior of both VSMs under a two-phase-to-ground fault.

41

It can clearly be seen that during the two-phase-to-ground short circuit low-order VSM model shows better performance over the high-order model under the short circuits study. Indeed, this case shows the undesirable performance of the high-order VSM model compared to the low-order VSM model during the two-phase-to-ground short circuit study.

Results in this case indicate that, the low-order VSM model shows better transient performance. The control structure of low-order VSM, however, offers limited options to protect the converter from overcurrent issues, which is a very complex process in the case of high-order VSM model implementation. Also the control structure of low-order VSM offers limited options to protect the converter from overcurrent issues; which is very complex in case of high-order VSM model implementation.

3.3.4 Case 4: Unbalanced AC Voltage

The VSM control algorithms were compared under unbalanced AC voltages because of the common occurrence of these voltages [19]. The standards permit a small window of deviation in unbalanced AC voltages. For example, operating an electrical distribution system with a voltage unbalanced by more than 5 % is not endorsed by ANSI/NEMA [82] nor by IEEE standards. In the case examined in this study, the phase voltage unbalance rate (PVUR) was calculated according to equation (3.14), which is based on the IEEE definition [83].

$$PVUR\ \% = \frac{82 \times \sqrt{V_{abe}^2 + V_{bce}^2 + V_{cae}^2}}{V_{aver}} \tag{3.14}$$

Where V_{ab}, V_{bc}, V_{ca} represent the line to line voltages. The V_{aver} represents the average line voltages. The $V_{abe}, V_{bce}, V_{cae}$ represent the difference between the line voltage and the average line voltages.

Figure 3.17 shows a 5 % unbalanced rate in the phase voltage, a scenario that is still permitted under the IEEE standard. The active power for both VSMs oscillated due to the effect of the unbalanced voltages, as is evident in Figure 3.18. If the enormous potential for the incorporation of interconnected renewable resources into an electrical system using power electronics converters is realized, system stability will be significantly affected because of the lack of inertia [26]. As well, commonly used three-phase distribution systems will cause unbalanced voltages when the loads are not equally distributed. During unbalanced voltage conditions, the active power usually oscillates around the reference command value, as indicated in Figure 3.18 when a step change in load happened at t = 2 sec (zero to 10kW).
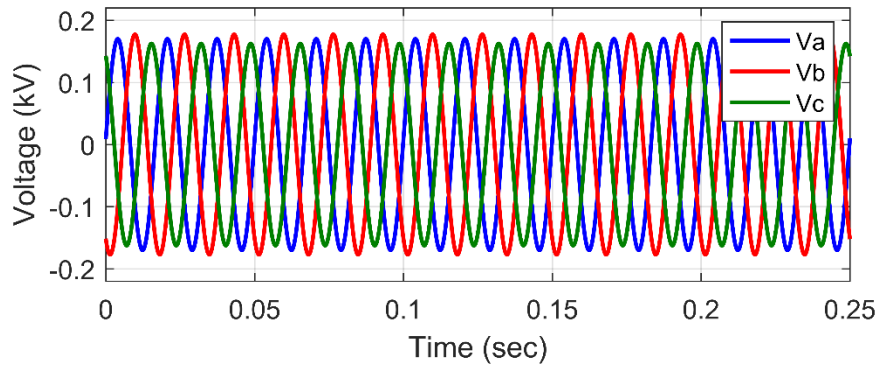
Figure 3-17: Unbalanced AC Voltage Performance shows Three-phase voltage unbalanced by a 5 % distortion.
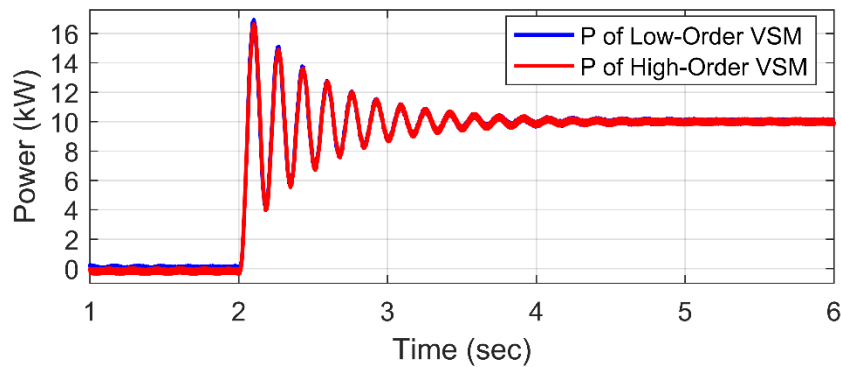
Figure 3-18: Unbalanced AC Voltage Performance Presents Effect of a 5 % voltage unbalance on active power for both VSMs.

In the case of a sudden increase in the unbalanced rate of the phase voltage to 25 % at t = 4 sec, the high-order VSM failed to emulate SM behaviour, and the average value of the active power was also decreased compared to that of the low-order VSM algorithm, as shown in Figure 3.19 at t = 4 sec. The extreme unbalanced voltage by 25% in distribution system could occur during a short circuit situation[84].
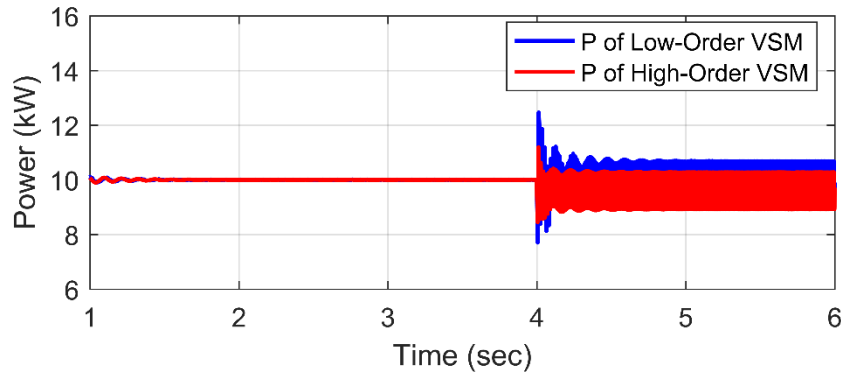
Figure 3-19: Unbalanced AC Voltage Performance Presents Effect of a 25 % voltage unbalance on active power for both VSMs.

It is obvious that the low-order VSM algorithm is more reliable than the high-order VSM control algorithm. In addition, according to [69], using a high-order model to emulate the inertia and control VSC might lead to numerical problems due to dependence primarily on measurements of the AC voltages, which is not ideal. The stability of both control algorithms was examined based on an unbalanced AC voltage, which is a usual occurrence in electrical systems. It is obvious that the low-order VSM based on a frequency droop mechanism control algorithm is the more promising algorithm and remains stable even during the abnormal conditions that are common in electrical distribution systems. The cascaded voltage and current control associated with the low-order VSM protect the converter from problems arising from overloading, and it also has a feature that can restrict the power flow direction.

3.4 Conclusion

The concept underlying VSM control algorithms has been reviewed with the goal of providing an efficient and stable VSC control algorithm that features the emulation of a classical SM. This paper has categorized a variety of VSM implementations in terms of additional control loops or equipment required and the simplicity of the control structures. It has been demonstrated that during normal and abnormal operating conditions. A low-order VSM algorithm is more stable than a high-order VSM algorithm. The possibility that the VSM will be unstable during abnormal operating conditions was therefore studied in order to investigate the numerical instability that might occur in a practical implementation. Because of its modified traditional droop control characteristics, the low-order VSM proved to be a valuable and useful option that enables a VSC to mimic SM behaviour. The impact of unbalanced AC voltage on VSM control algorithms was validated using a test system consisting of a detailed switching VSC terminal, simulated in a PSCAD/EMTDC environment.

44

A Novel Control Strategy for an IC in Hybrid AC/DC Microgrid [2]

The integration of renewable energy resources into electrical distribution systems through the use of power electronics converters is accompanied by challenges related to stability, especially under low inertia conditions. This chapter introduces a virtual synchronous machine (VSM) control strategy for a hybrid microgrid that addresses these issues by mimicking the properties of traditional synchronous machines (SMs) to improve the performance of a hybrid AC/DC microgrid. A novel method is presented for controlling an intertying converter (IC) that is based on a VSM while also ensuring the autonomous bidirectional power-sharing capability of the IC. The most significant factor investigated in this work is power exchange in both directions between an AC and a DC microgrid.

4.1 Introduction

Recently, the concept of microgrids, whether in AC or DC system, has become a widely acceptable option that can fully accommodate large-scale integration of RESs in distribution systems. Due to the advantages of both, the concept of combining both types of microgrid with each other as a hybrid microgrid was introduced [4]. A hybrid microgrid consists of both AC and DC sub-systems intertied by voltage source converter (VSC). The hybrid microgrid has two different operation modes: grid-connected mode and islanded mode. Maintaining the frequency of the AC sub-grid and the voltage of the DC sub-grid, to be within an acceptable standard range, is the most important issue, specifically in islanded hybrid microgrid. The high penetration of RESs affects the frequency and the voltage within the hybrid microgrid and, hence its stability [5]. The main pillar of ensuring the stable operation of the hybrid microgrid is the intertying converter (IC) control. The IC plays an important rule to ensure the stability of the hybrid microgrid via bidirectional power sharing among sub-grids.

Initially, power electronics interfacing is an essential component in order to integrate different types

_____

[2]Some parts of this chapter has been accepted to be published in:

- [85] H. Alrajhi Alsiraji, R.ElShatshat,and A A. Radwan, "A Novel Control Strategy for the Interlinking Converter in Hybrid Microgrid", Proc. IEEE PES General Meeting, Jul. 2017.
- [86]H. Alrajhi Alsiraji, A A. Radwan, and R. ElShatshat "Modelling and Analysis of a Synchronous Machine-Emulated Active Intertying Converter in Hybrid AC/DC Microgrids," in *IET Generation, Transmission & Distribution, Accepted.*

of distributed energy resources into all types of microgrid. Due to the numerous benefits of power electronics interfacing and the superior performance they offer, power converters have become a practical way to interface renewable sources. These are characterized by either variable frequencies or direct current, such as wind, photovoltaic, and fuel cells. However, unlike synchronous machines (SMs), the power converters that interface with RESs lack the inertia needed to support and participate in the frequency and voltage control of an AC system and, as a result, are unable to contribute to the improvement of system stability. Thus, high penetration level of VSCs may also lead to stability problems and affect system dynamics [4], [87], [88].

Standalone microgrids are generally considered a weak system as there is no frequency support to the AC sub-grid nor DC voltage support in the DC side. As a result, the power sharing between AC and DC sub-grids is extremely critical to the microgrid stability. Consequently, changing in the generation or loading condition causes large frequency deviations; which could cause instability problems [27]. In [28], the authors show that increasing the loading of the AC microgrid moves the dominant system poles to an unstable region. Therefore, the stability in hybrid microgrid is not only dependent on the AC microgrid, but also on the DC microgrid. Moreover, supplying or absorbing power via IC affects both the dynamics and performances of AC and DC sub-grids, this may lead to unstable operation for the whole hybrid system. With regards to power sharing, other attempts investigated and studied the autonomous operation of hybrid microgrids[23], [29] . Furthermore, studies were performed based on droop control for all distributed resources and the IC was proposed in [30].

This chapter, however, addresses the above issues through the application of the concept of virtual synchronous machine (VSM) controllers, which combines VSC and SM characteristics. The VSM control algorithm of a power electronics converter is a control feature that can be added to a converter controller to enable it to behave as an SM[56]. The algorithm allows for the incorporation of virtual inertia and damping behavior into the loop controllers of an interfacing converter[17], [57], [66], [72]. As a result, the VSC has no physical mass of inertia, as seen in the case of practical SMs.

The main contribution of this paper is the proposition of a new control algorithm for the IC to behave as a synchronous machine to support the AC sub-grid voltages and frequency, as well as the DC sub-grid voltage in islanded operation mode. This proposed research also considers the autonomous power sharing of the IC based on VSM as the second contribution. The proposed control consists of two controller loops, which include inner current controller and outer voltage controller. The main advantage of the current

46

controller loops, is the protection of the converter from over current situation. The proposed control algorithm is also applicable in the unbalanced hybrid system through the use of dual loop current controller. This chapter also compares the proposed control of IC with the existence control in the literature, in order to reveal its advantages. The system discussed in this paper is based on an average VSC model, which was simulated in a PSCAD/EMTDC environment.

The remainder of the chapter is organized as follows: Section II shows the configuration of the hybrid microgrid and its parameter. Section III presents the simulation results and analysis; and the finally section IV offers conclusions.

4.2 Hybrid AC/DC System Configuration and Control Structure

The hybrid microgrid structure is shown in Figure 4.1, and whose parameters are set out in Table I. The system is divided into three different divisions: AC microgrid sub-grid, DC microgrid sub-grid, and intertying converter. The control structure of AC subsystem and intertying converter is based on synchronous reference frame (SRF) for current and voltage controllers and is shown in previous chapter in Figure 3.5. Whereas the control structure for the DC sub-system inverters is based in cascaded voltage and current control [30], [89] that is illustrated in Figure 4.2, the IC controller consists of only the current loop and the current reference, which will be provided by droop controllers [6], [21].
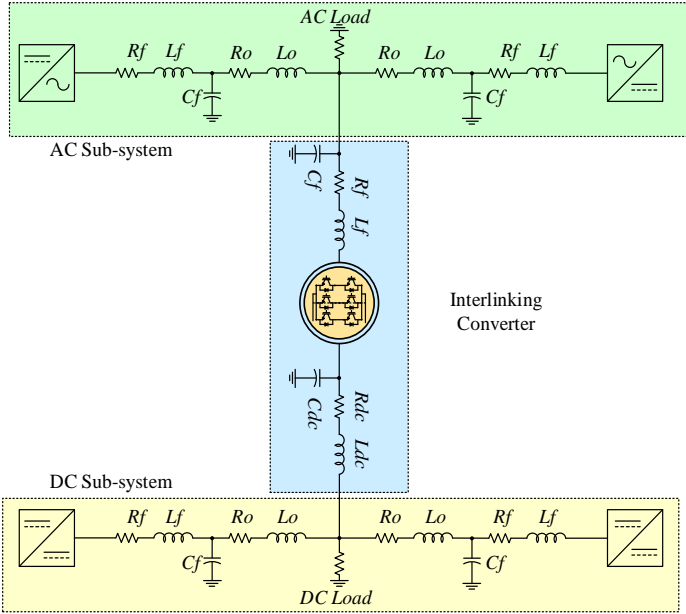
Figure 4-1: The Hybrid Microgrid Structure under Study.
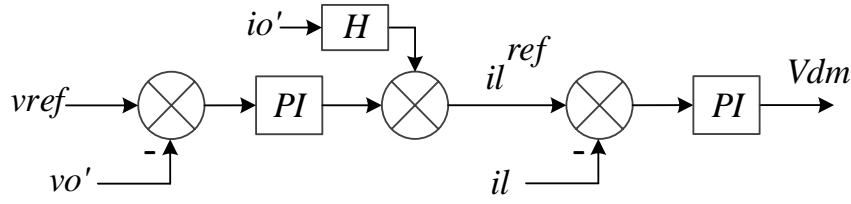
Figure 4-2: cascaded voltage and current control for DC DG Units.

Table 4-1: Hybrid Microgrid System Parameters.

Sub-grid	Quantity	Value	Unit
AC microgrid	Converter rated power	1	MVA
	AC Voltage (L-L) r.ms	690	V
	AC side resistance	0.01	Ω
	AC side inductance	1	mH
	AC side capacitance	50	μF
	System frequency	60	Hz
Intertying Converter	Virtual inertias	0.0025	Kg. m^2
	Virtual Damping Coefficient	16000	N.s/min
	AC side resistance	0.15	Ω
	AC side inductance	2	mH
	AC side capacitance	50	μF
DC microgrid	Converter rated power	1	MVA
	DC Voltage	2500	V
	DC side resistance	0.05	Ω
	DC side inductance	1	mH

4.2.1 AC Sub-grid

The DG units in the AC sub-grid consist of three-phase voltage source converters (VSCs) energized from DC sources. The DC voltage source is used to represent either dispatchable DG or non-dispatchable DG units, which are controlled by the conventional droop scheme [30]. Each DG unit feeds the load based on the predefined droop gains. As a result, in order to have equal power sharing for all DG units when the system parameters are symmetrical, the droop gains should also be identical. Furthermore, equal power sharing among DG units provides a stability margin for the system [28]. The supplying of active power into AC sub-grid must be satisfied by DG units. The summation of total power injected by each DG must be equal to the common AC load, as can be seen in equation (4.1).

$$P_{AC\ load} = \sum\nolimits_{i=1}^{n} P_{AC,DG}(i) \tag{4.1}$$

Where $P_{AC\ load}$ is denoted for the total AC load. The $P_{AC,DG}(i)$ represents the injected power from each DG unit in the AC microgrid, calculated from its droop coefficient (m_p^{ac}) at the operating system frequency. The variable (n) represents the number of DG units that is connected into AC microgrid.

4.2.2 DC Sub-grid

Each DG unit within the DC sub-grid consists of half-bridge DC-DC converter energized from DC sources. DC bus voltage in the DC sub-grid is controlled by the DG units based on droop control, which is correlated with the injected power. Droop control is similar to the AC sub-grid; therefore, each DG unit feeds the load based on the predefined droop gains. The summation of total power injected by each DG unit must be equal to the common DC load as can be seen in equation (4.2).

$$P_{DC\ load} = \sum_{i=1}^{n} P_{DC,DG}(i) \tag{4.2}$$

Where $P_{DC,DG}(i)$ represents the injected power from DG, calculated from the droop coefficient (m_p^{dc}) at the DC system voltage.

4.2.3 Intertying Converter

The intertying converter consists of a three-phase voltage source converter (VSC) energized from DC sub-grid, as well as AC sub-grid. The main functionality of this converter is to control the active power direction. The IC, however, is not responsible for reactive power support for the AC sub-grid [8],[30].

4.3 Autonomous Operation of Hybrid microgrid

The autonomous operation of hybrid microgrid will be discussed for AC sub-grid, DC sub-grid, and intertying converter.

The autonomous operation of the AC sub-grid is mainly based on droop control; thus, the supplied power is either active or reactive depending, on the system's frequency and the AC voltage at PCC. Increasing the AC load decreases the system's frequency, which is a sign for DGs to supply more active power and vice versa. On the other hand, decreasing the AC voltage at PCC is a sign for DGs to supply

49

the reactive power. Consequently, due to the use of vector control, the independent active control and the reactive power control can be achieved.

In DC sub-grid, the autonomous operation of DGs is similar to the AC microgrid. However, in this case, the DC voltage level determines the required injected power. The variation of the DC voltage is the main signal to DGs to maintain the DC voltage by injecting active power. Moreover, identical droop coefficients for all DGs in DC microgrid do not provide equal power sharing, due to the voltage drop associated with resistances lines [23], [29].
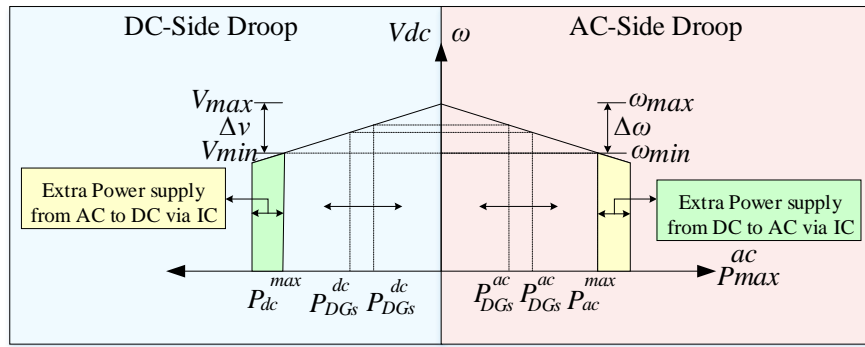
Figure 4-3: Combined AC and DC Droop Characteristics.

The autonomous operation of the intertying converter based on droop control is quite different in comparison to the AC and DC microgrids. In other words, the IC can be controlled autonomously based on droop control. This is determined by measuring the DC voltage level and AC sub-grid's frequency at its AC and DC terminals. Therefore, the input reference consists of a summation of AC droop associated with AC sub-grid frequency, and DC droop associated with DC sub-grid DC voltage as depicted in Figure 4.2.

The mathematical representation of combined AC and DC droop characteristics for the IC is shown in the following equation:

$$P_{IC}^{ref} = \begin{cases} 0 & if \quad \omega < \omega_{min} \,\& \, V_{dc} < V_{dc}^{min} \\ P_{IC}^{dc} - P_{IC}^{dc} & otherwise \end{cases} \tag{4.3}$$

$$P_{IC}^{dc} = \begin{cases} \dfrac{v_{min}^{dc} - v^{dc}}{m_p^{dc}} & if \quad V_{dc} < V_{dc}^{min} \\ 0 & otherwise \end{cases} \tag{4.5}$$

$$P_{IC}^{ac} = \begin{cases} \dfrac{\omega_{\min} - \omega}{m_p^{ac}} & if \quad \omega < \omega_{min} \\ 0 & otherwise \end{cases} \qquad (4.6)$$

Once the IC power reference is determine by equation (4.3), the current reference that should feed the current controller can be found by dividing the power reference by the voltage magnitude, in case of using only current controller loop. However, in the VSM control concept the power reference is directly fed to the swing equation model as shown in chapter 3 in Figure 3.4.

4.4 Simulation Results and Analysis

The system model used in this study consists of an average VSC model was built in PSCAD/EMTDC, whose system configuration is shown in Figure 4.1. The study presented here was concentrated on two important factors power exchange form DC to AC, and power exchange form AC to DC. Moreover, this chapter has studies and compared two hybrid microgrids based on the proposed VSM controller for IC and the only conventional current controller loop that is exists in the literature[10], [25].

4.4.1 Case 1: Dynamic Properties of Load Changes in AC and DC Sub-Grid during Under-Loading Conditions

In this case, both hybrid microgrids have identical operating conditions. Changing the loads for both sub-systems during the under loading condition is shown in Figure 4.4. Initially, the AC sub-system supplies 1MW for its AC load, while the DC sub-system supplies 0.8MW. At t = 5 sec, the AC load increases to 1.5MW as depicted in Figure 4.4.
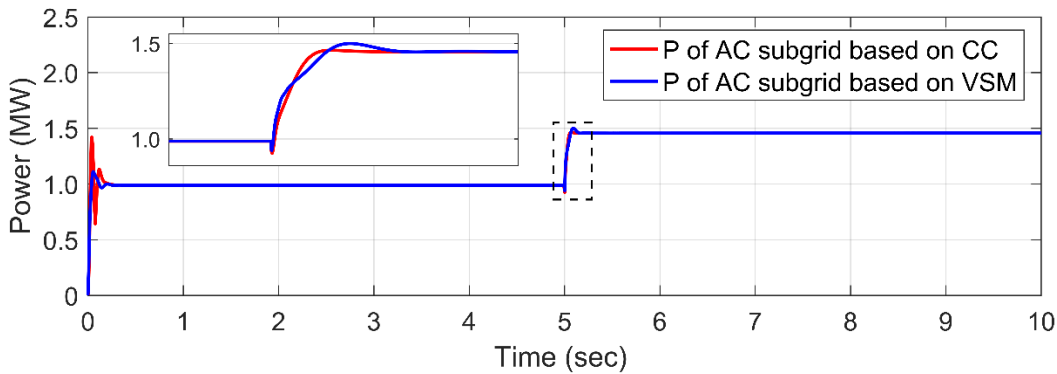
Figure 4-4: The AC Sub-grid's Load during under loading Condition.

51

It obvious that the IC does not operate in this situation according to Rule 2 in [8] as shown in Figure 4.5. However, supplying power during the transition might be preferable [29] in the case of slow response. In fact, this preferable situation is provided by the proposed control, where the control based on only current controller loop does not show this feature. Moreover, the proposed control based on VSM improves the starting transients for the DGs in the AC sub-system as evident in the beginning of Figure 4.4 and Figure 4.5, which decreases the overshoot.
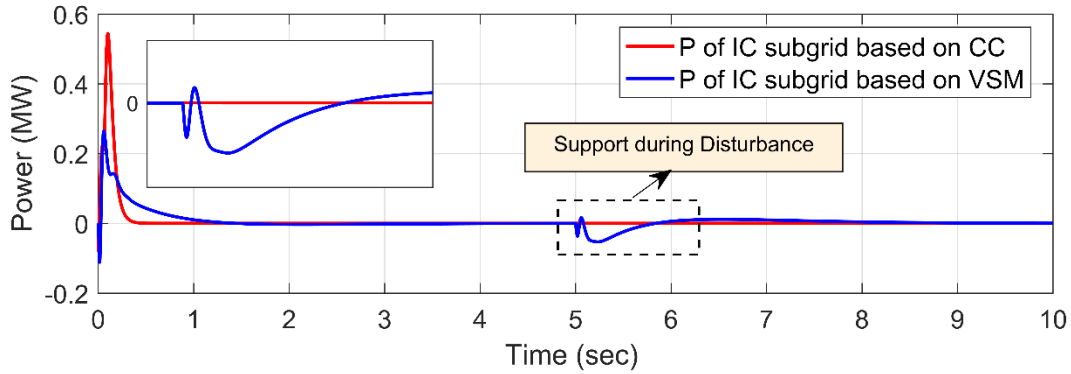
Figure 4-5: The IC Power Exchange during under loading Condition.

Due to the VSM in the IC controller, the effect of the inertia is just the response of the converter's power. At t = 3 sec, the DC load increases from 0.8MW to 1.6MW as shown in Figure 4.6; thus, there is no effect on the AC sub-grid. In this case, both sub-systems work under loading conditions due to the fact that both sub-systems DGs units can still supply more available an extra power, which is equal to 0.4MW for each DG unit.
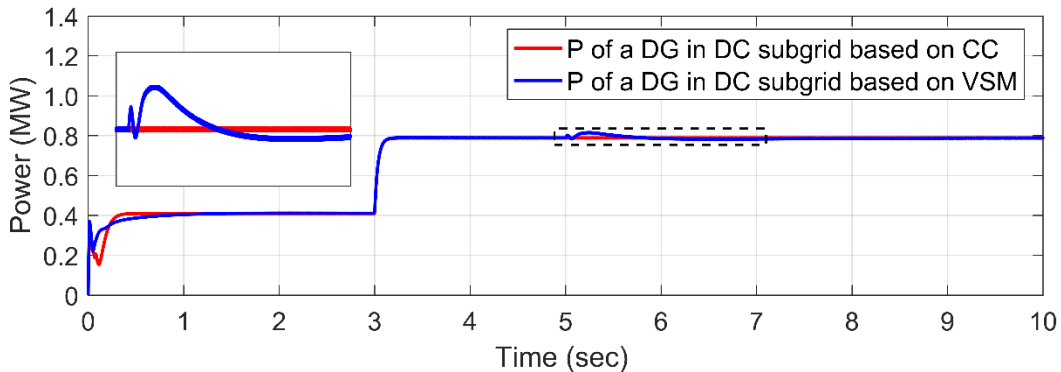
Figure 4-6: The DC Sub-grid's Load during under loading Condition.

The inertia means that some power is supplied by the intertying converter for a short period of time which represents the rotating mass during the frequency change. Therefore, as shown in Figure 4.5 and Figure 4.6 respectively, it is clear that at t = 5sec, the DC voltage follows the behaviour of the VSM due to the droop control characteristics in the DC sub-grid and the power exchange from the DC to AC sub-grid for a short time as illustrated in Figure 4.6. Furthermore, the DGs units in the DC sub-system supply power during transient disturbance, so the behaviour of the DC DGs units obey the VSM behaviour as well. The effect of the virtual inertia on the DC voltage sub-system is depicted in Figure 4.7.
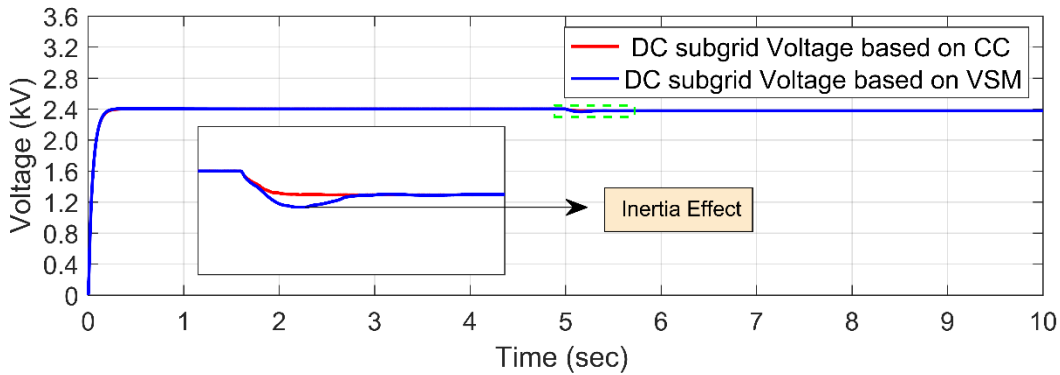
Figure 4-7: DC Sub-grid Bus Voltage during under Loading Condition.

4.4.2 Case 2: Power exchange from DC to AC sub-grid during AC sub-grid over loading conditions

Both hybrid microgrids were investigated in the case of a shortage power in the AC sub-system. The AC load of the AC sub-system increases from 1MW to 2.3 MW at t = 5 sec. which means that the AC sub-system is overloaded by 0.3MW as shown in Figure 4.8.
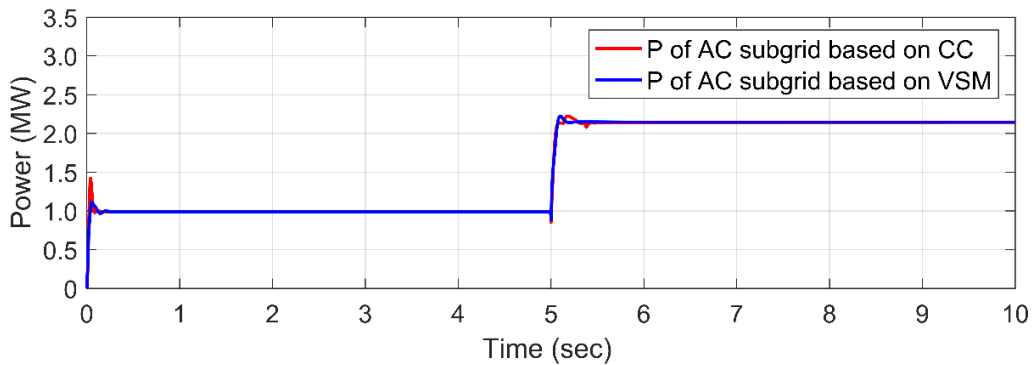
Figure 4-8: The AC sub-grid's load during over loading condition.

Furthermore, in this case the DC sub-grid is in an under-loaded condition that supplies its DC load with 1.6 MW as depicted in Figure 4.9. Therefore, the IC starts to provide the amount of power shortage to the AC sub-system from the DC sub-system, which is almost equal to 0.3 MW from DC sub-system as shown in Figure 4.10.
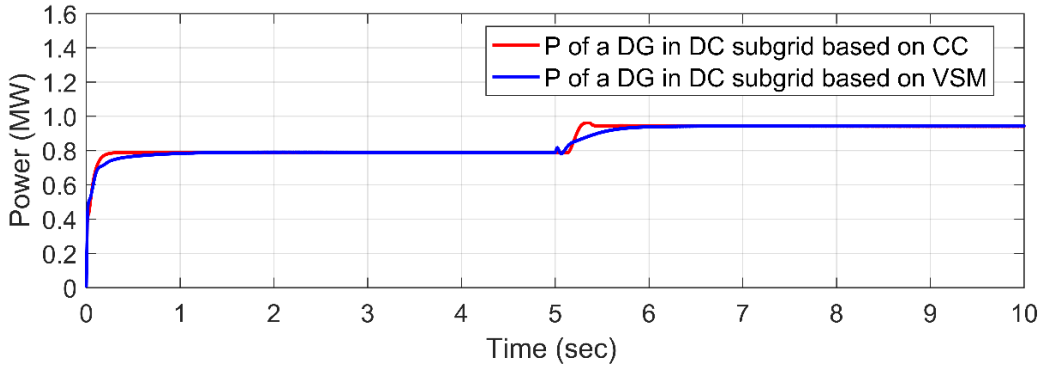
Figure 4-9: The DG Power generated in DC sub-grid.
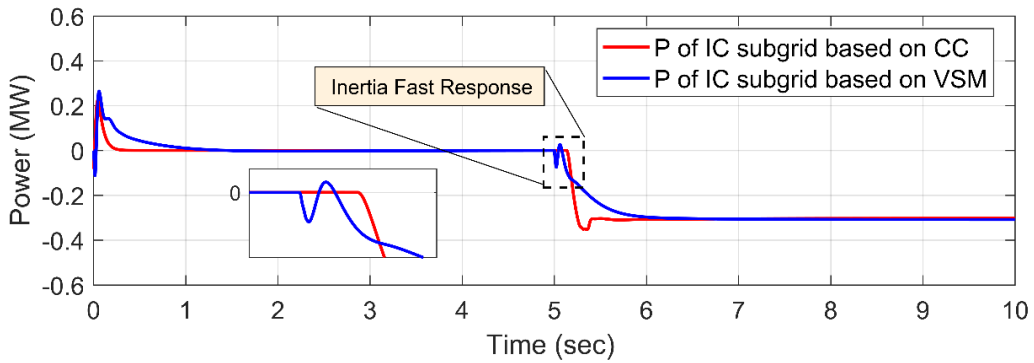
Figure 4-10: The IC Power exchange during over loading condition in AC sub-grid.

It is clear that the supplied power from DC sub-system into AC sub-system maintains both sub-grids within their rated power limits and prevents the possibility of overloading situations for all DGs units in AC and DC sub-systems as well.
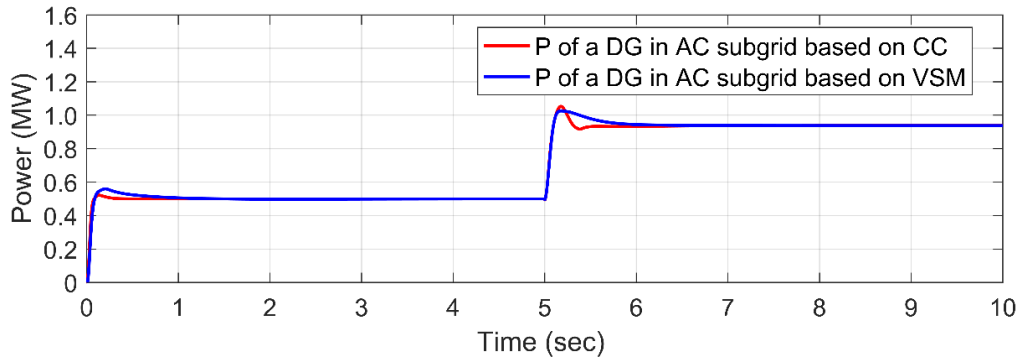
Figure 4-11: The DG Power generated in AC sub-grid.

The power generated via AC sub-system's DGs in this case is shown in Figure 4.11. Therefore, the supplied power from the AC DGs is less than its rated power, which is 1MVA due to the load voltage dependency. Considering the VSM control on the IC leads all DGs units to follow the SM behavior only in the case of a power exchange from DC to AC or AC to DC sub-systems or during transient disturbance. This advantage of the VSM is presented in this case.

4.4.3 Case 3: Power exchange from AC to DC sub-grid during DC sub-grid over loading conditions

The AC load voltage degraded is revealed in this case due to the fact that the power exchange from AC to DC affects the AC voltage of the point common coupling (PCC). Therefore, the proposed VSM control to IC supports the AC voltage, and it helps to improve the hybrid microgrid performance. In this case, both sub-systems work under low loading conditions. Thus, the AC sub-system load is equal to 1MW while the DC sub-grid load is equal to 1.5MW as shown in Figure 4.12 and Figure 4.13 respectively.
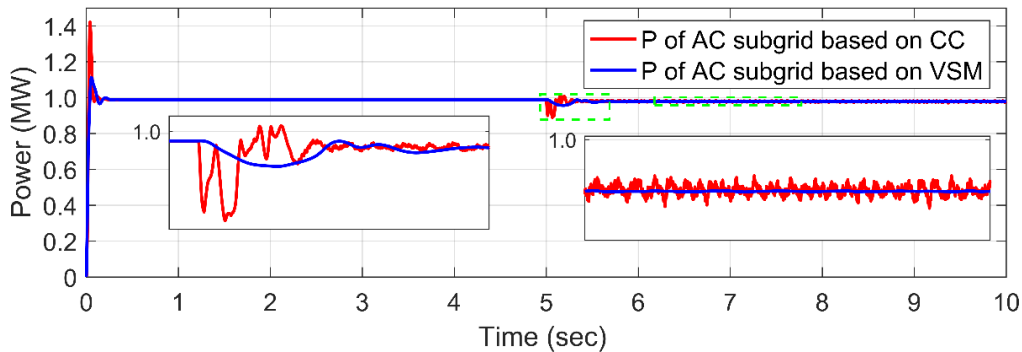
Figure 4-12: The AC sub-grid's load during power exchange for AC to DC sub-grid.

55
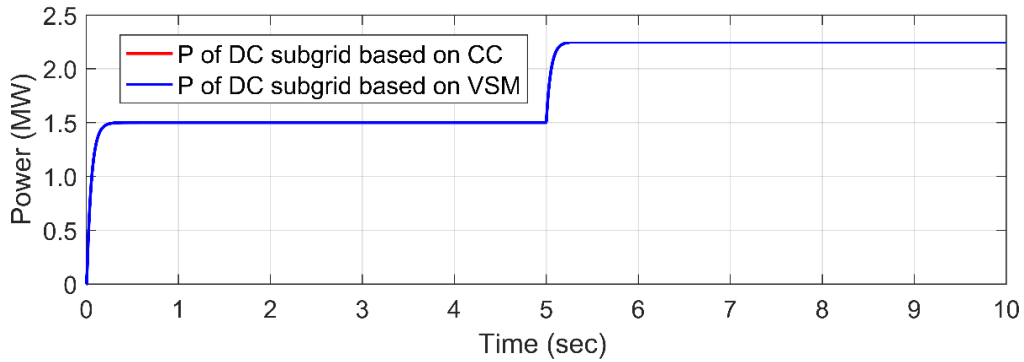
Figure 4-13: The DC sub-grid's load during power exchange for AC to DC sub-grid.

At t = 5 sec, the DC load increases from 1.5MW to 2.3MW, which represents an overloaded condition for the DC DGs units. As a result, the IC supplies the shortage of the power from the AC sub-system in order to maintain the DC sub-system in a healthier operation condition. Figure 4.14 shows the power exchange from AC to DC sub-system via IC.
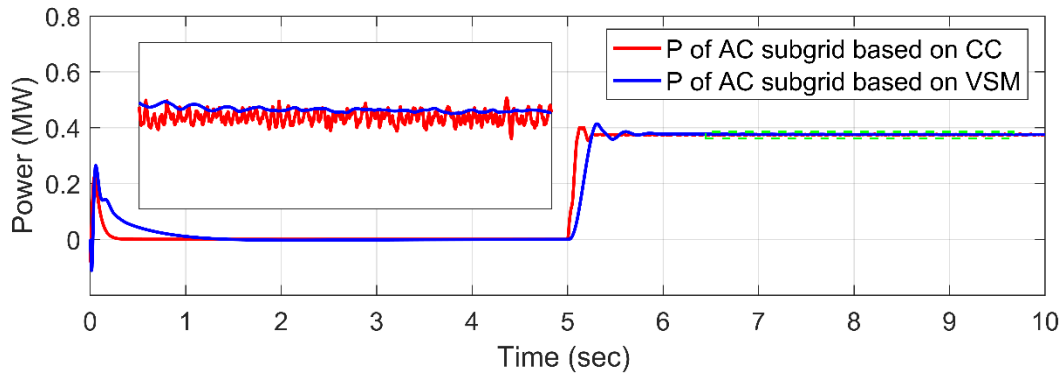
Figure 4-14: The IC Power exchange during over loading condition in DC sub-grid.

Referring to Figure 4.12, due to the load voltage dependence of the AC load, the power exchange from AC to DC sub-system affects the AC sub-system, and it causes fluctuation on the PCC voltage due to the lack of inertia. Therefore, the proposed VSM control to IC provides a remedy for this issue, and thus mitigates the PCC voltage dip during the power exchange from AC to DC sub-system. Moreover, integrating the proposed controller into the IC improves the power quality of the hybrid microgrid. In fact, in the case of using only current controller loop, the total power transfer experiences fluctuation due to the sensitivity of the droop controller. This fluctuation might reach the stability boundaries or violate the

required standards. As a result, the proposed controller of IC smooths out this fluctuation from the existence of inertia in the IC controller loop as can be seen in the Figure 4.15.
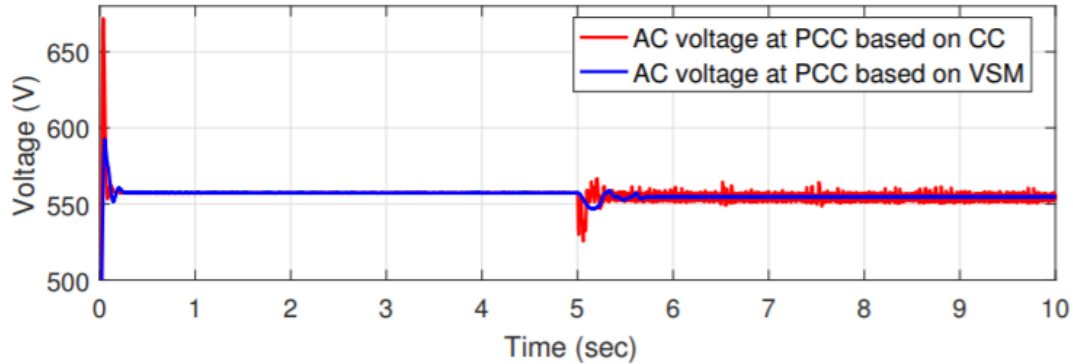
Figure 4-15 AC Voltage at the PCC.

4.4.4 Case 4: IC Switching between the Inversion and Rectification Modes

For further investigations, the IC is challenged to operate in the rectification mode; which the power flows from the AC sub-system into the DC sub-system at t = 5.0 sec and then suddenly switches to the inversion mode at t = 10.0 sec where the power flows from the DC sub-system into the AC sub-system as shown in Figure 4-16.
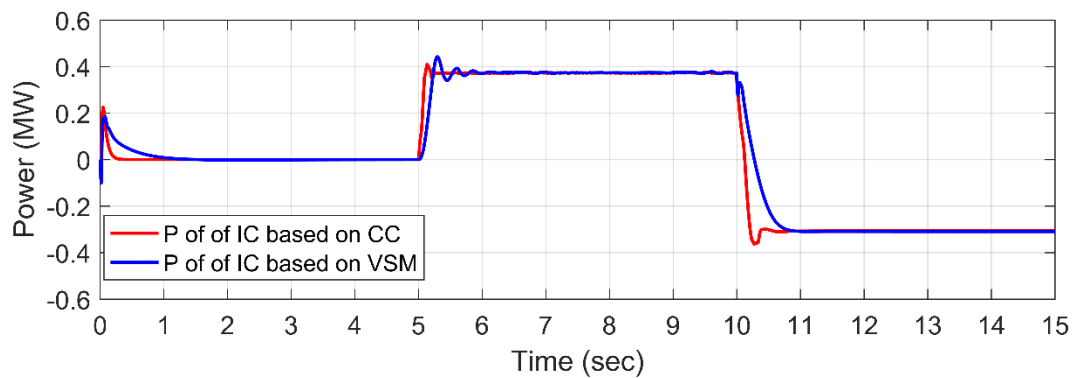
Figure 4-16 inverse the IC power exchange direction.

As shown in Figure 4.17, the VSM-based IC reflects a well-damped performance of AC voltage at the PCC as compared to the current-controlled IC.
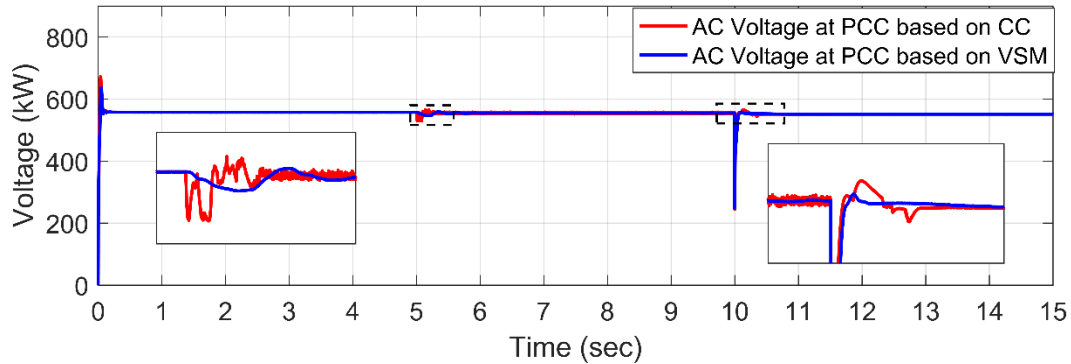
Figure 4-17 AC Voltage at the PCC during Switching between two different operation modes.

4.4.5 Case 5: Seamless Reconnection of the IC Following a Scheduled Maintenance

As compared to the SMs, the synchronization of the microgrids to another ac system might be challenging. In the autonomous mode, the DG units dictate the microgrid voltage and frequency based on the decentralized droop control, which might affect the system stability at the synchronization instants. In some situations, local adjustments throughout all DG units is required to facilitate the reconnection process [90]. In this case study, it is shown that the VSM-based IC provides superior synchronization characteristics as compared to the current-controlled IC. To challenge the VSM-based controller, the reconnection of the IC is investigated under the loaded and unloaded conditions.

4.4.5.1 Reconnection of IC under Loaded Conditions

As shown in Fig. 10(a), the IC is disconnected because of a scheduled maintenance at t = 6.0 s and hence a zero-power transfer is yielded. The overall system performance is still stable. However, load shedding actions shall be considered during the scheduled maintenance conditions in order to avoid overloading both sub-grids.
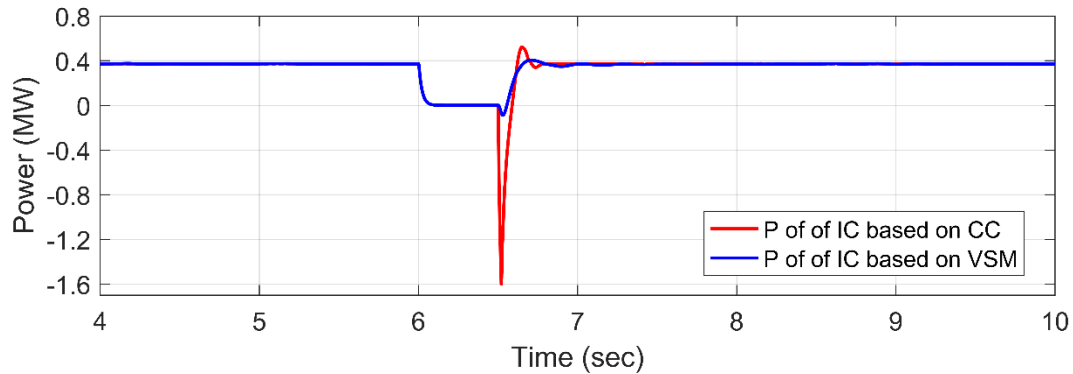
Figure 4-18 the Active power behavior of IC during reconnection IC under loaded conditions.

At t = 6.5 sec, the IC is reconnected to the system. In this case, the current-controlled IC produces a severe transient response as compared to the VSM-based control strategy. This severe performance might trigger the protection devices into nuisance trippings. On the other hand, the VSM-based controller has a unique self-synchronization feature. The virtual inertia and damping creates a smooth transient response which is clearly shown in Figure 4.19 for the AC voltage at PCC.
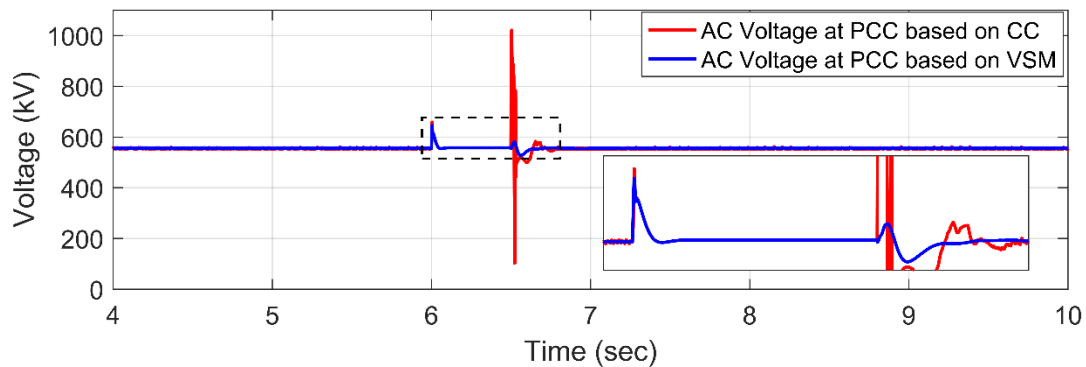
Figure 4-19 The PCC voltage at AC sub-system during reconnection IC under loaded conditions.

4.4.5.2 Reconnection of IC under Zero-Loaded Conditions

Similar to the preceding scenario, and as shown in Figure 4.20, the IC is disconnected at t = 4.0 s, and restored to operation at t = 4.5 s. Therefore, it is clear that the VSM-based controller

59

offers a superior behaviour as compare to the current-controlled IC. Note that the frequency stability is violated under the current-controlled IC as shown in Figure 4.21.
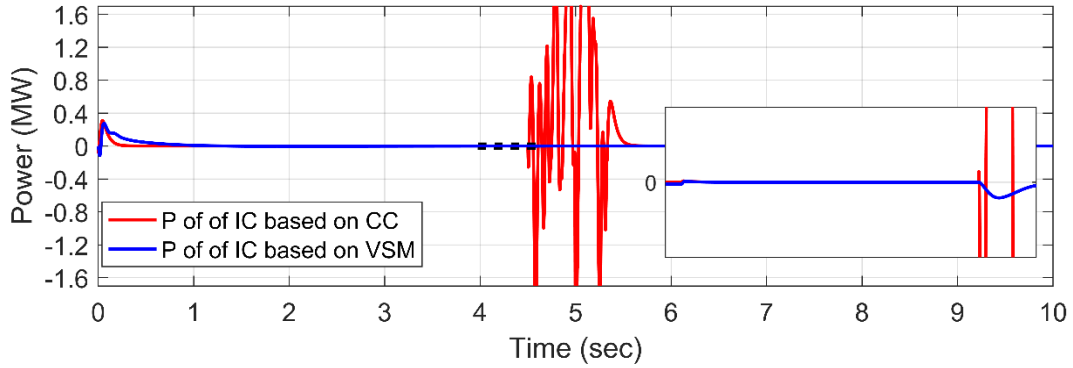
Figure 4-20 the Active power behavior of IC during reconnection IC under Zero-loaded conditions.
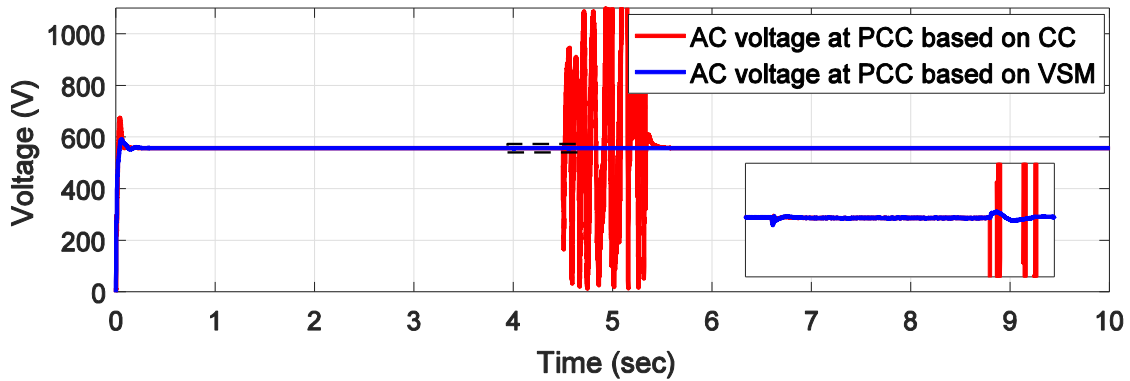
Figure 4-21 AC sub-system Frequency during reconnection IC under Zero-loaded conditions.

4.5 Conclusion

This chapter introduces the VSM-based control for the IC in the hybrid AC/DC microgrid. The VSM control strategy ensures the accurate bidirectional power flow between the AC and the DC sub-grids under different loading conditions. This chapter has studied and compared a two hybrid micro-grid with different control structures of the IC. It has been demonstrated that during variations of the loading conditions, the VSM algorithm is more efficient than using only the current control loop that is proposed in the literature due to the AC voltage degraded load. The results prove that the proposed control strategy improves the performance of the entire hybrid microgrid. The impact of the VSM control algorithms on the hybrid microgrid was validated using a test system simulated in a PSCAD/EMTDC environment.

Chapter 5
Modeling and Stability Analysis of Hybrid AC/DC Microgrid [3]

5.1 Introduction

Analyzing the dynamic performance and designing the controller of electrical system is commonly based on developing the small-signal dynamic model [91]. The main benefit of the small-signal modelling is to present further investigation of the hybrid microgrid once the eigenvalues and the stable region are determined. Particularly, the small-signal model of hybrid microgrid presents the system stability and also the effect of the system parameters changing such as PI controller coefficients. Therefore, it becomes necessary for studying the small-signal model to find the large-signal dynamic model of the hybrid microgrid first; which is represented using nonlinear differential equations.

The most important portion for the hybrid microgrid system is the stability study due to that fact that the behavior of the system when it is subjected to a temporary disturbance is the main concern. In hybrid microgrid, the disturbances take place continuously because of the load changing endlessly. Satisfying the hybrid microgrid operation during the disturbances conditions must be achieved in order to supply the demand. Furthermore, the power quality is another concern for the operation of a hybrid microgrid; which prefer for the hybrid microgrid to provide better response and less oscillatory behavior. The efficient and desire performance of the hybrid microgrid can be achieved by evaluating the linearized model of the nonlinear equations of the hybrid microgrid. Evaluating the eigenvalues and sensitivity modes of the hybrid microgrid are the most important aspect of studying the control system stability. The hybrid microgrid consists of AC sub-system (AC microgrid), DC sub-system (DC microgrid), and intertying converter (IC).

5.2 Small-Signal Dynamic Modeling of the Hybrid Microgrid

Deriving a dynamic model for the hybrid AC/DC microgrid is the most important component of the proposed control application design and stability assessment. Therefore, the hybrid microgrid should be

---

modelled as three subsystem stages, and then connected with each other based on the common model variable and reference frame as seen in Figure 5.1. The first sub-system model is the AC microgrid which is similar to the system that can be found in [20]. The configuration of the DC sub-system is similar to the AC sub-system while the converters are based on half-bridge DC-to-DC. The last sub-system model is the intertying converter. The following sections represents the deriving a dynamic model for each sub-system in details.
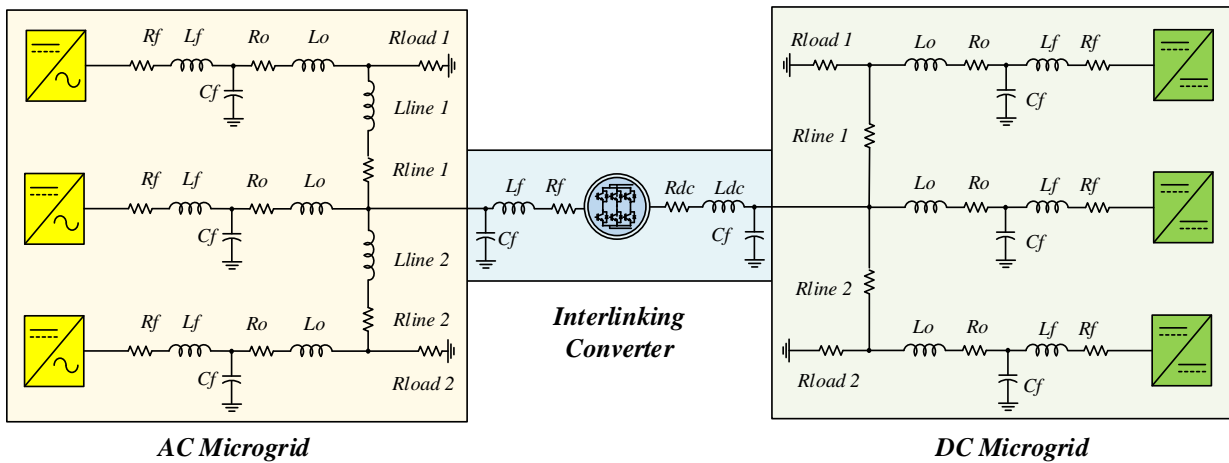
Figure 5-1 Systematic Configuration of the Hybrid AC/DC Microgrid.

5.3 AC Microgrid small-signal Model

The AC microgrid configuration is depicted in Figure 5.2. The small-signal state space model of AC microgrid divided into several sub-modules that are output LCL filer, network lines, load, power controller, voltage control and current controller.
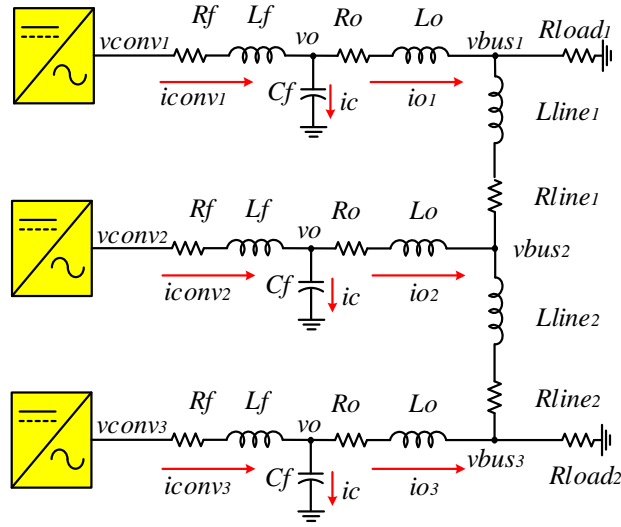
Figure 5-2 AC Microgrid Sub-system.

5.3.1 Small-signal Model of VSC in AC Sub-system

With referring to chapter 2, a small-signal model of VSC interfacing a DG unit into AC microgrid is discussed. The large signal model was derived in the control structure of the VSC section; thus, linearizing equations (2.3)-(2.8), (2.11), (2.12), (2.15), (2.16), (2.19), and (2.20) leads to determine the small-signal dynamic model. It is evident that the large signal model consists of 13 equations [20], [28], [30]. In other words, the small-signal model consists of 13 state variables for LCL filter, current controller, voltage controller, power controller, and AC load.

5.3.1.1 Linearized Power Circuit State Space Model

The linearized equations and state space representation form of the power circuit that consist of LCL filter and coupling inductance is shown in the following equations [20]:

$$\Delta \dot{\iota con v}_d = \frac{1}{Lf} \Delta V conv_d - \frac{1}{Lf} \Delta Vo_d - \frac{Rf}{Lf}.\Delta iconv_d + \omega.\Delta iconv_q \qquad (5.1)$$

$$\Delta \dot{\iota con v}_q = \frac{1}{Lf} \Delta V conv_q - \frac{1}{Lf} \Delta Vo_q - \frac{Rf}{Lf}.\Delta iconv_q - \omega.\Delta iconv_d \qquad (5.2)$$

$$\Delta \dot{vo}_d = \omega.\Delta vo_q + \frac{1}{Cf} \Delta iconv_d - \frac{1}{Cf} \Delta io_d \qquad (5.3)$$

$$\Delta \dot{vo}_q = -\omega.\Delta vo_d + \frac{1}{Cf} \Delta iconv_q - \frac{1}{Cf} \Delta io_q \qquad (5.4)$$

63

$$\Delta \dot{io}_d = \frac{1}{Lo}\Delta Vo_d - \frac{1}{Lo}\Delta Vg_d - \frac{Ro}{Lo}.\Delta io_d + \omega.\Delta io_q \qquad (5.5)$$

$$\Delta \dot{io}_q = \frac{1}{Lo}\Delta Vo_q - \frac{1}{Lo}\Delta Vg_q - \frac{Ro}{Lo}.\Delta io_q - \omega.\Delta io_d \qquad (5.6)$$

The power circuit linearized equations of the LCL filter are written in standard form of state space representation as following:

$$\begin{bmatrix} \Delta \dot{iconv}_d \\ \Delta \dot{iconv}_q \\ \Delta \dot{io}_d \\ \Delta \dot{io}_q \\ \Delta \dot{vo}_d \\ \Delta \dot{vo}_q \end{bmatrix} = \mathbb{A}_{LCL} \begin{bmatrix} \Delta iconv_d \\ \Delta iconv_q \\ \Delta io_d \\ \Delta io_q \\ \Delta vo_d \\ \Delta vo_q \end{bmatrix} + \mathbb{B}_{LCL1} \begin{bmatrix} \Delta \dot{vconv}_d \\ \Delta \dot{vconv}_q \end{bmatrix} + \mathbb{B}_{LCL2} \begin{bmatrix} \Delta \dot{vg}_d \\ \Delta \dot{vg}_q \end{bmatrix} + \mathbb{B}_{LCL3}[\Delta \dot{\omega}] \qquad (5.7)$$

Where:

$$\mathbb{A}_{LCL} = \begin{bmatrix} -Rf/Lf & \omega & 0 & 0 & -1/Lf & 0 \\ -\omega & -Rf/Lf & 0 & 0 & 0 & -1/Lf \\ 0 & 0 & -Ro/Lo & \omega & -1/Lo & 0 \\ 0 & 0 & -\omega & -Ro/Lo & 0 & -1/Lo \\ 1/Cf & 0 & -1/Cf & 0 & 0 & \omega \\ 0 & 1/Cf & 0 & -1/Cf & -\omega & 0 \end{bmatrix} ; \mathbb{B}_{LCL1} = \begin{bmatrix} 1/Lf & 0 \\ 0 & 1/Lf \\ 0 & 0 \\ 0 & 0 \\ 0 & 0 \\ 0 & 0 \end{bmatrix}$$

$$\mathbb{B}_{LCL2} = \begin{bmatrix} 0 & 0 \\ 0 & 0 \\ -1/Lo & 0 \\ 0 & -1/Lo \\ 0 & 0 \\ 0 & 0 \end{bmatrix} ; \quad \mathbb{B}_{LCL3} = \begin{bmatrix} iconv_q \\ -iconv_d \\ io_q \\ -io_d \\ vo_q \\ -vo_d \end{bmatrix}$$

5.3.1.2 Linearized Current Controller State Space Model

Based on equations (2.11) and (2.12), the state space model of the current controller loops have two extra state variables. The variables which come from the PI controller are called axillary state, and they are notated as $\Delta \gamma_d$ and $\Delta \gamma_q$. Therefore, the current state space model can be written as follows:

$$
\begin{bmatrix} \Delta\dot{\gamma}_d \\ \Delta\dot{\gamma}_q \end{bmatrix} = [0]\begin{bmatrix} \Delta\gamma_d \\ \Delta\gamma_q \end{bmatrix} + \mathbb{B}_{c1}\begin{bmatrix} \Delta vconv_d \\ \Delta vconv_q \end{bmatrix} + \mathbb{B}_{c2}\begin{bmatrix} \Delta iconv_d \\ \Delta iconv_q \\ \Delta io_d \\ \Delta io_q \\ \Delta vo_d \\ \Delta vo_q \end{bmatrix} \tag{5.8}
$$

Where:

$$
\mathbb{B}_{c1} = \begin{bmatrix} K_{ic} & 0 \\ 0 & K_{ic} \end{bmatrix}; \quad \mathbb{B}_{c2} = \begin{bmatrix} -K_{ic} & 0 & 0 & 0 & 1 & 0 \\ 0 & -K_{ic} & 0 & 0 & 0 & 1 \end{bmatrix};
$$

Where equation (5.8) represents the axillary states of the PI controller states, and equation (5.9) represents the current controller states. The inputs are split into feedback and references for the purpose of simplicity.

$$
\begin{bmatrix} \Delta vc\dot{o}nv_d \\ \Delta vc\dot{o}nv_q \end{bmatrix} = \mathbb{C}_c\begin{bmatrix} \Delta\gamma_d \\ \Delta\gamma_q \end{bmatrix} + \mathbb{D}_{c1}\begin{bmatrix} \Delta vconv_d \\ \Delta vconv_q \end{bmatrix} + \mathbb{D}_{c2}\begin{bmatrix} \Delta iconv_d \\ \Delta iconv_q \\ \Delta io_d \\ \Delta io_q \\ \Delta vo_d \\ \Delta vo_q \end{bmatrix} \tag{5.9}
$$

Where:

$$
\mathbb{C}_c = \begin{bmatrix} 1 & 0 \\ 0 & 1 \end{bmatrix}; \quad \mathbb{D}_{c1}\begin{bmatrix} K_{pc} & 0 \\ 0 & K_{pc} \end{bmatrix}; \quad \mathbb{D}_{c2} = \begin{bmatrix} -K_{pc} & -\omega Lf & 0 & 0 & 1 & 0 \\ \omega Lf & -K_{pc} & 0 & 0 & 0 & 1 \end{bmatrix}
$$

5.3.1.3 Linearized Voltage Controller State Space Model

The state space model of the voltage controller follows the same procedure that is applied in the current controller state space model. Based on equations (2.15) and (2.16), the state space model of the voltage controller loops have two extra state variables as well. These state variables are notated as $\Delta\varphi_d$ and $\Delta\varphi_q$. Therefore, the voltage state space model can be written as follows:

$$\begin{bmatrix} \Delta\dot{\varphi}_d \\ \Delta\dot{\varphi}_q \end{bmatrix} = [0]\begin{bmatrix} \Delta\varphi_d \\ \Delta\varphi_q \end{bmatrix} + \mathbb{B}_{v1}\begin{bmatrix} \Delta vo_d \\ \Delta vo_q \end{bmatrix} + \mathbb{B}_{v2}\begin{bmatrix} \Delta iconv_d \\ \Delta iconv_q \\ \Delta io_d \\ \Delta io_q \\ \Delta vo_d \\ \Delta vo_q \end{bmatrix} \quad (5.10)$$

Where:

$$\mathbb{B}_{v1} = \begin{bmatrix} K_{iv} & 0 \\ 0 & K_{iv} \end{bmatrix}; \quad \mathbb{B}_{v2} = \begin{bmatrix} -1 & 0 \\ 0 & -1 \end{bmatrix};$$

Equation (5.11) represents the voltage controller states. Also, the inputs are divided for the purpose of simplicity into feedback and references.

$$\begin{bmatrix} \Delta \dot{io}_d \\ \Delta \dot{io}_d \end{bmatrix} = \mathbb{C}_v \begin{bmatrix} \Delta\gamma_d \\ \Delta\gamma_q \end{bmatrix} + \mathbb{D}_{v1}\begin{bmatrix} \Delta vconv_d \\ \Delta vconv_q \end{bmatrix} + \mathbb{D}_{v2}\begin{bmatrix} \Delta iconv_d \\ \Delta iconv_q \\ \Delta io_d \\ \Delta io_q \\ \Delta vo_d \\ \Delta vo_q \end{bmatrix} \quad (5.11)$$

$$\mathbb{C}_v = \begin{bmatrix} 1 & 0 \\ 0 & 1 \end{bmatrix}; \quad \mathbb{D}_{v1}\begin{bmatrix} K_{pv} & 0 \\ 0 & K_{pv} \end{bmatrix}; \quad \mathbb{D}_{v2} = \begin{bmatrix} 0 & 0 & H & 0 & -K_{pv} & -\omega Cf \\ 0 & 0 & 0 & H & \omega Cf & -K_{pv} \end{bmatrix}$$

5.3.1.4 Linearized Power Controller State Space Model

Referring to Figure 2-6, the power control consists of three integrators; thus, the power controller state space model has three state variables. By rearranging equations (2.19) and (2.20), the linearized differential equations of the power controllers become the following:

$$\Delta\dot{P} = \left(\frac{3}{2}\right)\left(\omega_f\left((\Delta vo_d * io_d) + (\Delta vo_q * io_q) + (vo_d * \Delta io_d) + (vo_q * \Delta io_q) - \Delta P\right)\right) \quad (5.12)$$

$$\Delta\dot{Q} = \left(\frac{3}{2}\right)\left(\omega_f\left((\Delta vo_d * io_q) + (vo_d * \Delta io_q) - (vo_q * \Delta io_d) - (vo_q * \Delta io_d) - \Delta Q\right)\right) \quad (5.13)$$

According to Figure 2-6, the phase angle θ represents the angle difference between the converter reference and the common reference in the AC sub-system (AC microgrid). It is obvious that the phase angle θ equation for the power controller is written as follows (5.14):

$$\theta = \int \omega^{inv} - \omega_{com} \tag{5.14}$$

Therefore the linearization of the previous equation and the substitution into the power droop equation leads to achieving the phase angle state equation as written below in (5.15):

$$\dot{\Delta\theta} = -m_p\Delta P - \Delta\omega_{com} \tag{5.15}$$

The power controller state space representation model can be written as equation (5.16) while the output equations of the power controller are correlated with the system's voltages as shown in (5.17):

$$\begin{bmatrix} \dot{\Delta\theta} \\ \dot{\Delta P} \\ \dot{\Delta\theta} \end{bmatrix} = \mathbb{A}_p \begin{bmatrix} \Delta\delta \\ \Delta P \\ \Delta Q \end{bmatrix} + \mathbb{B}_{p1} \begin{bmatrix} \Delta iconv_d \\ \Delta iconv_q \\ \Delta io_d \\ \Delta io_q \\ \Delta vo_d \\ \Delta vo_q \end{bmatrix} \tag{5.16}$$

$$\begin{bmatrix} \Delta w \\ \Delta vo_d \\ \Delta vo_q \end{bmatrix} = \begin{bmatrix} \mathbb{C}_{dw} \\ \mathbb{C}_{dv} \end{bmatrix} \begin{bmatrix} \Delta Q \\ \Delta P \end{bmatrix} \tag{5.17}$$

Where:

$$\mathbb{A}_d = \begin{bmatrix} -\omega f & 0 & 0 \\ 0 & -\omega f & 0 \\ -m_p & 0 & 0 \end{bmatrix}; \quad \mathbb{B}_d = \frac{3}{2}\begin{bmatrix} 0 & 0 & 0 & 0 & 0 & 0 \\ 0 & 0 & \omega.vo_d & \omega.vo_q & \omega.io_d & \omega.io_q \\ 0 & 0 & -\omega.vo_q & \omega.vo_d & \omega.io_q & -\omega.io_d \end{bmatrix}$$

$$\mathbb{C}_{dw} = [0 \quad -m_p \quad 0] \; ; \qquad \mathbb{C}_{dv} = \begin{bmatrix} 0 & -n_p & 0 \\ 0 & 0 & 0 \end{bmatrix}$$

5.3.1.5 Complete Linearized State Space Small-signal Model of VSC

The total state space model of a VSC that is interfacing a DG unit into AC microgrid is achieved by combining the linearized state space models with each other. Equation (5.18) represents the complete state space model of a converter Interfacing DG Unit into AC Microgrid. [The readers are referred to Appendix B for further details].

$$[\Delta\dot{x}_{inv}] = \mathbb{A}_{inv}[\Delta x_{inv}] + \mathbb{B}_{inv1}[\Delta V_{busdq}] + \mathbb{B}_{inv2}[\Delta\delta] \tag{5.18}$$

Where Δx_{inv} represents the all state variables of the VSC including its controllers.

$$[\Delta x_{inv}] = \begin{bmatrix} \Delta\delta & \Delta P & \Delta Q & \Delta\varphi_{dq} & \Delta\gamma_{dq} & \Delta iconv_{dq} & \Delta vo_{dq} & \Delta io_{dq} \end{bmatrix}$$

$$\mathbb{A}_{inv} = \begin{bmatrix} (\mathbb{A}_p)_{3\times3} & ((0)_{2\times2}) & (0)_{2\times2} & (\mathbb{B}_p)_{3\times6} \\ (\mathbb{B}v_1 * \mathbb{C}p_v)_{2\times3} & ((0)_{2\times2}) & (0)_{2\times2} & (\mathbb{B}v_2)_{3\times6} \\ \begin{pmatrix} \mathbb{B}c_1 * \\ \mathbb{D}v_1 * \\ \mathbb{C}p_v \end{pmatrix}_{2\times3} & \begin{pmatrix} \mathbb{B}c_1 * \\ \mathbb{C}v_1 \end{pmatrix}_{2\times2} & (0)_{2\times2} & \begin{pmatrix} \mathbb{B}c_1 * \\ \mathbb{D}v_2 * \\ \mathbb{B}c_2 \end{pmatrix}_{2\times6} \\ \begin{pmatrix} \begin{pmatrix} \mathbb{B}LCL_1 * \\ \mathbb{D}c_1 * \\ \mathbb{D}v_1 * \\ \mathbb{C}pv \end{pmatrix} \\ +\begin{pmatrix} \mathbb{B}LCL_2 * \\ \begin{bmatrix} T_v^{-1} & (0)_{3\times2} \\ (0)_{4\times1} & (0)_{3\times2} \end{bmatrix} \end{pmatrix} \\ +(\mathbb{B}LCL_3 * \mathbb{C}pw) \end{pmatrix}_{6\times3} & \begin{pmatrix} \mathbb{B}LCL_1 * \\ \mathbb{D}C_1 * \\ \mathbb{C}v \end{pmatrix}_{6\times2} & \begin{pmatrix} \mathbb{B}LCL_1 * \\ \mathbb{C}c \end{pmatrix}_{6\times2} & \begin{pmatrix} \begin{pmatrix} \mathbb{A}LCL + \\ \mathbb{B}LCL_1 * \\ \mathbb{D}c_1 * \mathbb{D}v_2 \\ \mathbb{B}LCL_1 * \mathbb{D}c_2 \end{pmatrix} \end{pmatrix}_{6\times6} \end{bmatrix}$$

$$\mathbb{B}_{1inv} = \begin{bmatrix} ((0)_{3\times2}) \\ ((0)_{2\times2}) \\ ((0)_{2\times2}) \\ \begin{pmatrix} \mathbb{B}LCL_2 * \begin{bmatrix} (0)_{4\times2} \\ T_s^{-1} \end{bmatrix} \end{pmatrix}_{6\times2} \end{bmatrix} \begin{bmatrix} \Delta v_{busd} \\ \Delta v_{busq} \end{bmatrix}; \quad \mathbb{B}_{1inv} = \begin{bmatrix} [\mathbb{B}_{pcom}] \\ (0)_{2\times1} \\ (0)_{2\times1} \\ (0)_{6\times1} \end{bmatrix}[\Delta\delta]$$

$$\mathbb{C}_{inv_w1} = \begin{cases} [(\mathbb{C}p_w)_{1\times3} \quad (0)_{1\times10}][\Delta\delta] & if\ Inverter\ index = 1 \\ [(0)_{1\times13}] \quad [\Delta\delta] & if\ Inverter\ index \neq 1 \end{cases}$$

$$\mathbb{C}_{inv_c} = [(T_C)_{2\times1} \quad (0)_{2\times10} \quad (T_S)_{2\times2}][\Delta x_{inv}]$$

Referring to Figure 5.2, the AC sub-system contains of three VSCs interfacing DG units; therefore, by taking one of the converter interfacing the DG unit as a common reference for the rest of the other converter helps to combine all state space converter models with each other as explained in equation (5.19) and (5.20). The readers are referred to [20] for further details about combining state space model of several converters.

$$
\begin{bmatrix} \Delta \dot{x}_{inv1} \\ \Delta \dot{x}_{inv2} \\ \Delta \dot{x}_{inv3} \\ \vdots \\ \Delta \dot{x}_{invn} \end{bmatrix} = \begin{bmatrix} \mathbb{A}_{inv}^{total} \end{bmatrix} \begin{bmatrix} \Delta x_{inv1} \\ \Delta x_{inv2} \\ \Delta x_{inv3} \\ \vdots \\ \Delta x_{invn} \end{bmatrix} + \begin{bmatrix} \mathbb{B}_{1inv1} \\ \mathbb{B}_{1inv2} \\ \mathbb{B}_{1inv3} \\ \vdots \\ \mathbb{B}_{1invn} \end{bmatrix} \begin{bmatrix} \Delta v_{bus_{dq}}1 \\ \Delta v_{bus_{dq}}2 \\ \Delta v_{bus_{dq}}3 \\ \vdots \\ \Delta v_{bus_{dq}}n \end{bmatrix} + \begin{bmatrix} \mathbb{B}_{2inv1} \\ \mathbb{B}_{2inv2} \\ \mathbb{B}_{2inv3} \\ \vdots \\ \mathbb{B}_{2invn} \end{bmatrix} \begin{bmatrix} \Delta \delta_1 \\ \Delta \delta_2 \\ \Delta \delta_3 \\ \vdots \\ \Delta \delta_n \end{bmatrix} \tag{2.19}
$$

$$
\begin{bmatrix} \Delta vo_{dq}1 \\ \Delta vo_{dq}2 \\ \Delta vo_{dq}3 \\ \vdots \\ \Delta vo_{dq}n \end{bmatrix} = \begin{bmatrix} \mathbb{C}_{inv_c1} & 0 & 0 & 0 & 0 \\ 0 & \mathbb{C}_{inv_c2} & 0 & 0 & 0 \\ 0 & 0 & \mathbb{C}_{inv_c3} & 0 & 0 \\ \vdots & \vdots & \vdots & \ddots & \vdots \\ 0 & 0 & 0 & 0 & \mathbb{C}_{inv_cn} \end{bmatrix} \begin{bmatrix} \Delta x_{inv1} \\ \Delta x_{inv2} \\ \Delta x_{inv3} \\ \vdots \\ \Delta x_{invn} \end{bmatrix} \tag{5.20}
$$

$$
\begin{bmatrix} \mathbb{A}_{inv}^{total} \end{bmatrix} = \begin{bmatrix} \begin{pmatrix} \mathbb{A}_{inv1} + \\ \mathbb{B}_{2inv1} * \mathbb{C}_{inv_w1} \end{pmatrix} & 0 & 0 & 0 & 0 \\ 0 & \begin{pmatrix} \mathbb{A}_{inv2} + \\ \mathbb{B}_{2inv2} * \mathbb{C}_{inv_w2} \end{pmatrix} & 0 & 0 & 0 \\ 0 & 0 & \begin{pmatrix} \mathbb{A}_{inv3} + \\ \mathbb{B}_{2inv3} * \mathbb{C}_{inv_w3} \end{pmatrix} & 0 & 0 \\ \vdots & \vdots & \vdots & \ddots & \vdots \\ 0 & 0 & 0 & 0 & \begin{pmatrix} \mathbb{A}_{invn} + \\ \mathbb{B}_{2invn} * \mathbb{C}_{inv_wn} \end{pmatrix} \end{bmatrix}
$$

5.3.1.6 Linearized State Space Model of AC sub-system network

The AC sub-system network contains of two electrical storage elements; which are the lines' inductances as shown in Figure 5.3. Therefore, the small-signal state space model of the network consists of four state variables; two of these state are in the d- and q- directions, respectively.
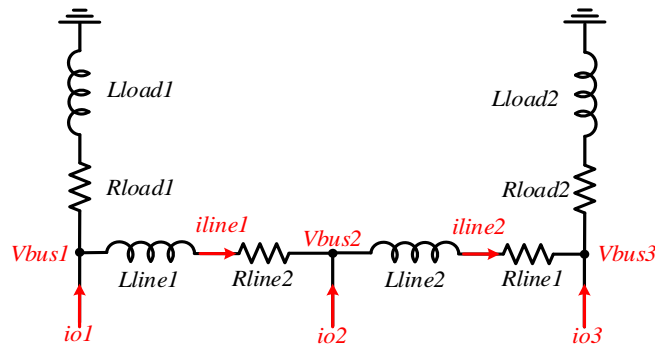
Figure 5-3 AC sub-system network configuration

The state space equations of the AC sub-grid network follow the same procedure that is applied in the circuit state space model of the power LCL filter. Based on Figure 5.3, the linearized state space equations can be written as:

$$\Delta \dot{\iota}_{Lined1} = \frac{1}{L_{Line1}}\Delta V_{busd1} - \frac{1}{L_{Line1}}\Delta V_{busd2} - \frac{R_{Line1}}{L_{Line1}}.\Delta i_{Lined1} + w.\Delta i_{Lineq1} + i_{Lineq1}.\Delta \omega \quad (5.21)$$

$$\Delta \dot{\iota}_{lineq1} = \frac{1}{L_{Line1}}\Delta V_{busq1} - \frac{1}{L_{Line1}}\Delta V_{busq2} - \frac{R_{Line1}}{L_{Line1}}.\Delta i_{Lineq1} - w.\Delta i_{Lined1} - i_{Lined1}.\Delta \omega \quad (5.22)$$

$$\Delta \dot{\iota}_{Lined2} = \frac{1}{L_{Line2}}\Delta V_{busd2} - \frac{1}{L_{Line2}}\Delta V_{busd3} - \frac{R_{Line2}}{L_{Line2}}.\Delta i_{Lined2} + w.\Delta i_{Lineq2} + i_{Lineq2}.\Delta \omega \quad (5.23)$$

$$\Delta \dot{\iota}_{lineq2} = \frac{1}{L_{Line2}}\Delta V_{busq2} - \frac{1}{L_{Line2}}\Delta V_{busq3} - \frac{R_{Line2}}{L_{Line2}}.\Delta i_{Lineq2} - w.\Delta i_{Lined2} - i_{Lined2}.\Delta \omega \quad (5.24)$$

The standard state space representation form of AC sub-system network can be obtained as following equation:

$$\begin{bmatrix} \Delta \dot{\iota}_{Lined1} \\ \Delta \dot{\iota}_{lineq1} \\ \Delta \dot{\iota}_{Lined2} \\ \Delta \dot{\iota}_{lineq2} \end{bmatrix} = \mathbb{A}_{net}\begin{bmatrix} \Delta i_{Lined1} \\ \Delta i_{lineq1} \\ \Delta i_{Lined2} \\ \Delta i_{lineq2} \end{bmatrix} + \mathbb{B}_{net1}\begin{bmatrix} \Delta V_{busd1} \\ \Delta V_{busq1} \\ \Delta V_{busd2} \\ \Delta V_{busq2} \\ \Delta V_{busd3} \\ \Delta V_{busq3} \end{bmatrix} + \mathbb{B}_{net2}[\Delta\omega] \quad (5.25)$$

Where:

$$\mathbb{A}_{net} = \begin{bmatrix} -\dfrac{R_{Line1}}{L_{Line1}} & \omega & 0 & 0 \\ -\omega & -\dfrac{R_{Line1}}{L_{Line1}} & 0 & 0 \\ 0 & 0 & -\dfrac{R_{Line1}}{L_{Line1}} & \omega \\ 0 & 0 & -\omega & -\dfrac{R_{Line1}}{L_{Line1}} \end{bmatrix}$$

$$\mathbb{B}_{net1} = \begin{bmatrix} \dfrac{1}{L_{Line1}} & 0 & -\dfrac{1}{L_{Line1}} & 0 & 0 & 0 \\[2ex] 0 & \dfrac{1}{L_{Line1}} & 0 & -\dfrac{1}{L_{Line1}} & 0 & 0 \\[2ex] 0 & 0 & \dfrac{1}{L_{Line2}} & 0 & -\dfrac{1}{L_{Line2}} & 0 \\[2ex] 0 & 0 & 0 & \dfrac{1}{L_{Line2}} & 0 & -\dfrac{1}{L_{Line2}} \end{bmatrix}; \quad \mathbb{B}_{net2} = \begin{bmatrix} +i_{Lineq1} \\ -i_{Lined1} \\ +i_{Lineq2} \\ -i_{Lined2} \end{bmatrix}$$

5.3.1.7 Linearized State Space Model of AC sub-system Loads

The state space equations of the AC sub-system loads are similar to the AC sub-grid network. Based on Figure 5.3, the linearized state space loads equations can be written as:

$$\Delta \dot{i}_{Loadd1} = \frac{1}{L_{Load1}} \Delta V_{busd1} - \frac{R_{Load1}}{L_{Load1}} . \Delta i_{Loadd1} + \omega . \Delta i_{Loadq1} + i_{Loadq1} . \Delta \omega \tag{5.26}$$

$$\Delta \dot{i}_{loadq1} = \frac{1}{L_{Load1}} \Delta V_{busq1} - \frac{R_{Load1}}{L_{Load1}} . \Delta i_{Loadq1} - \omega . \Delta i_{Loadd1} - i_{Loadd1} . \Delta \omega \tag{5.27}$$

$$\Delta \dot{i}_{Loadd2} = \frac{1}{L_{Load2}} \Delta V_{busd3} - \frac{R_{Load2}}{L_{Load2}} . \Delta i_{Loadd2} + \omega . \Delta i_{Loadq2} + i_{Loadq2} . \Delta \omega \tag{5.28}$$

$$\Delta \dot{i}_{loadq2} = \frac{1}{L_{Load2}} \Delta V_{busq3} - \frac{R_{Load2}}{L_{Load2}} . \Delta i_{Loadq2} - \omega . \Delta i_{Loadd2} - i_{Loadd2} . \Delta \omega \tag{5.29}$$

The standard state space representation form of AC sub- system loads can be obtained as following equation:

$$\begin{bmatrix} \Delta \dot{i}_{Loadd1} \\ \Delta \dot{i}_{loadq1} \\ \Delta \dot{i}_{Loadd2} \\ \Delta \dot{i}_{loadq2} \end{bmatrix} = \mathbb{A}_{load} \begin{bmatrix} \Delta i_{Loadd1} \\ \Delta i_{loadq1} \\ \Delta i_{Loadd2} \\ \Delta i_{loadq2} \end{bmatrix} + \mathbb{B}_{load1} \begin{bmatrix} \Delta V_{busd1} \\ \Delta V_{busq1} \\ \Delta V_{busd2} \\ \Delta V_{busq2} \\ \Delta V_{busd3} \\ \Delta V_{busq3} \end{bmatrix} + \mathbb{B}_{load2} [\Delta \omega] \tag{5.30}$$

$$\mathbb{A}_{net} = \begin{bmatrix} -\dfrac{R_{Load1}}{L_{Load1}} & \omega & 0 & 0 \\[2ex] -\omega & -\dfrac{R_{Load1}}{L_{Load1}} & 0 & 0 \\[2ex] 0 & 0 & -\dfrac{R_{Load1}}{L_{Load1}} & \omega \\[2ex] 0 & 0 & -\omega & -\dfrac{R_{Load1}}{L_{Load1}} \end{bmatrix}$$

$$\mathbb{B}_{Load1} = \begin{bmatrix} \dfrac{1}{L_{Load1}} & 0 & 0 & 0 & 0 & 0 \\[2ex] 0 & \dfrac{1}{L_{Load1}} & 0 & 0 & 0 & 0 \\[2ex] 0 & 0 & 0 & 0 & \dfrac{1}{L_{Load2}} & 0 \\[2ex] 0 & 0 & 0 & 0 & 0 & \dfrac{1}{L_{Load2}} \end{bmatrix} ; \quad \mathbb{B}_{Load2} = \begin{bmatrix} +i_{Loadq1} \\ -i_{Loadd1} \\ +i_{Loadq2} \\ -i_{Loadd2} \end{bmatrix}$$

According to equation (2.19), (5.20), (5.25), and (5.30), all these equations contain of a common voltage node as can be illustrated in Figure 5.4. Embedding a virtual resistance (Rv) leads to combine the entire AC sub-system state space models with each other as presented in equation(5.31); which is proposed in [20]. Subsequently, the AC sub-system stability analysis can be evaluated. Nevertheless, it becomes necessary to include these state space models based on the system configuration using mapping matrices (see appendix B).
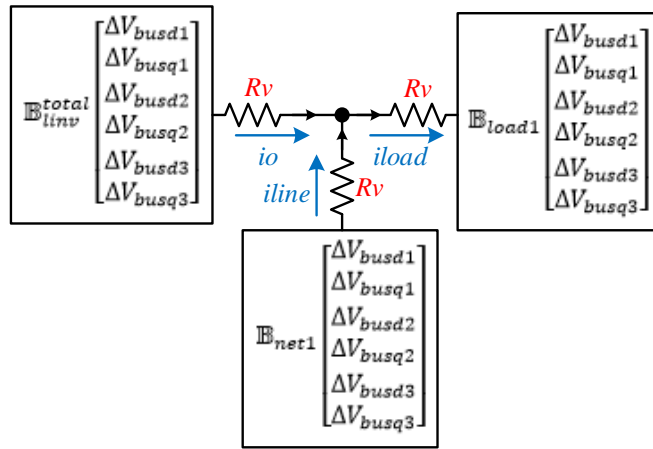
Figure 5-4 Embedding Virtual Resistance among Sub-module

$$[\Delta V_{busdq}] = Rv([\mathcal{M}ap_{inv}][\Delta vo_{dq}] + [\mathcal{M}ap_{line}][\Delta i_{Linedq}] + [\mathcal{M}ap_{load}][\Delta i_{Loaddq}]) \qquad (5.31)$$

Where:

$\mathcal{M}ap_{inv}$ is a mapping matrix that represents all VSC based on the AC sub-grid configuration.

$\mathcal{M}ap_{line}$ is a mapping matrix that represents all lines based on the AC sub-grid configuration.

$\mathcal{M}ap_{load}$ is a mapping matrix that represents all loads based on the AC sub-grid configuration.

5.3.1.8 Complete State Space of Entire AC Sub-grid

The complete state space model of the AC sub- system is presented in equation (5.32), and the eigenvalues of the AC sub-grid are shown in Figure 5.5 using the initial operating points that are extracted from the time-domain simulations in PSCAD/EMTDC. For further investigations, the trajectory of the dominant eigenvalue as a function of the active power droop coefficient (m_p) is shown in Figure 5.6, while Figure 5.7 shows the trajectory of the dominant eigenvalue as a function of the reactive power droop coefficient (n_q).

$$\mathbb{A}_{subgrid}^{AC} = \begin{bmatrix} \begin{pmatrix} \mathbb{A}inv + (\mathbb{B}inv * \\ Rv * \mathcal{M}ap_{inv} * \mathbb{C}inv) \end{pmatrix} & \begin{pmatrix} \mathbb{B}inv * Rv \\ * \mathcal{M}ap_{line} \end{pmatrix} & \begin{pmatrix} \mathbb{B}inv * \\ Rv * \mathcal{M}ap_{load} \end{pmatrix} \\ \begin{pmatrix} (\mathbb{B}1net * RN * \\ \mathcal{M}ap_{inv} * \mathbb{C}inv) \\ +(\mathbb{B}2net * \mathbb{C}invw) \end{pmatrix} & \begin{pmatrix} \mathbb{A}net + (\mathbb{B}1net * \\ Rv * \mathcal{M}ap_{line}) \end{pmatrix} & \begin{pmatrix} \mathbb{B}1net * \\ Rv * \mathcal{M}ap_{load} \end{pmatrix} \\ \begin{pmatrix} (\mathbb{B}1load * Rv * \\ \mathcal{M}ap_{inv} * \mathbb{C}inv) \\ +(\mathbb{B}2load * \mathbb{C}invw) \end{pmatrix} & \begin{pmatrix} \mathbb{B}1load * \\ Rv * \mathcal{M}ap_{line} \end{pmatrix} & \begin{pmatrix} \mathbb{A}load + (\mathbb{B}1load \\ * Rv * \mathcal{M}ap_{load}) \end{pmatrix} \end{bmatrix}_{47 \times 47} \qquad (5.32)$$
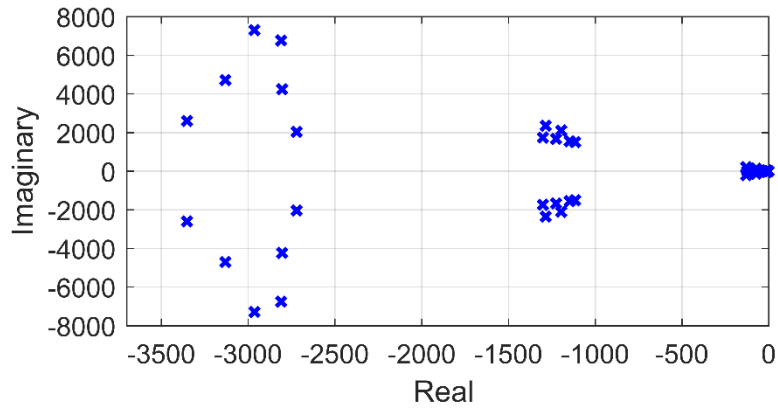
Figure 5-5 Eigenvalues spectrum of the AC Sub-system.
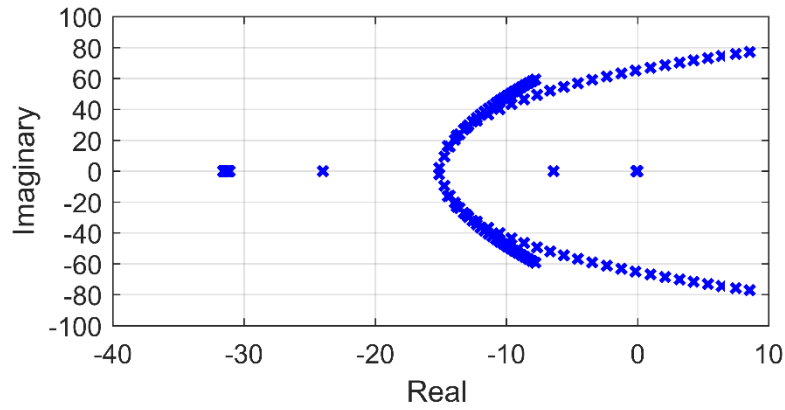
Figure 5-6 Impact of increasing the Active Power Droop coefficient (m_p) with respect to the low frequency modes of the AC Sub-system: 1.57e-5 $<m_p<$3.14e-4
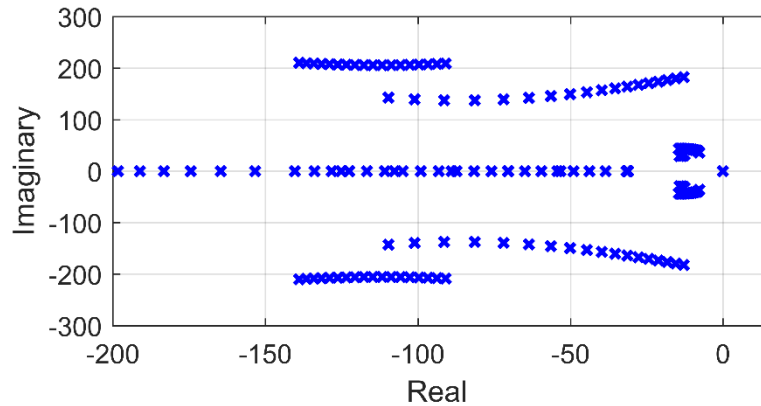
Figure 5-7 Impact of increasing the Reactive Power Droop coefficient (n_q) with respect to the low frequency modes of the AC Sub-system: 3.17e-4 $< n_p <$4.8e-3

5.4 DC Microgrid small-signal Model

The DC microgrid is the second subsystem which is similar to the AC sub-system system configuration that is discussed previously as depicted in Figure 5.8. The small-signal state space model of DC microgrid consists of several state variables that are output LCL filer, network lines, load, power controller, voltage control and current controller.
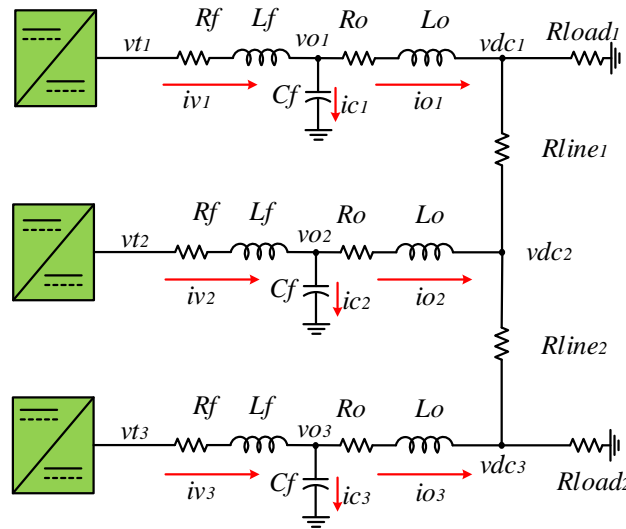
Figure 5-8 AC Microgrid Sub-system

5.4.1 Small-signal Model of VSC in DC sub-grid

A small-signal model of DC/DC half-bridge interfacing a DG unit into DC microgrid is discussed. The large signal model was derived in the control structure of the DC/DC half-bridge section of the proposal; thus, linearizing equations (2.23)-(2.25), (2.26), (2.27), and (2.28) leads to the small-signal dynamic model. It is evident that the large signal model consists of 5 equations.

5.4.1.1 Linearized Power Circuit State Space Model

The linearized equations and state space representation form of the power circuit that consist of LCL filter and coupling inductance is shown in the following equations [20]:

$$\Delta \dot{\imath v} = \frac{1}{Lf} \cdot \Delta vt - \frac{1}{Lf} \cdot \Delta vo - \frac{Rf}{Lf} \cdot \Delta iv \tag{5.33}$$

$$\Delta \dot{\imath o} = \frac{1}{Lo} \cdot \Delta vo - \frac{1}{Lo} \Delta vdc - \frac{Ro}{Lo} \cdot \Delta io \tag{5.34}$$

$$\Delta \dot{vo} = \frac{1}{Cf} \cdot \Delta iv - \frac{1}{Cf} \cdot \Delta io \tag{5.35}$$

The power circuit linearized equations are written in standard form of state space representation as following:

$$\begin{bmatrix} \Delta \dot{\imath v} \\ \Delta \dot{\imath o} \\ \Delta \dot{vo} \end{bmatrix} = \begin{bmatrix} A_p \end{bmatrix} \begin{bmatrix} \Delta \dot{\imath v} \\ \Delta \dot{\imath o} \\ \Delta \dot{vo} \end{bmatrix} + \begin{bmatrix} B1_p \end{bmatrix} [\Delta vt] + \begin{bmatrix} B2_p \end{bmatrix} [\Delta vdc] \tag{5.36}$$

Where:

$$\mathbb{A}_p = \begin{bmatrix} -\dfrac{R_f}{L_f} & 0 & -\dfrac{1}{L_f} \\ 0 & -\dfrac{R_o}{L_o} & -\dfrac{1}{L_o} \\ \dfrac{1}{C_f} & -\dfrac{1}{C_f} & 0 \end{bmatrix} \;;\; \mathbb{B}1_p = \begin{bmatrix} \dfrac{1}{L_f} \\ 0 \\ 0 \end{bmatrix} \;;\; \mathbb{B}2_p = \begin{bmatrix} 0 \\ -\dfrac{1}{L_o} \\ 0 \end{bmatrix}$$

5.4.1.2 Linearized Current Controller State Space Model

Based on equation (2.27) in chapter 2, the state space model of the current controller loop have only one extra state variable. The variable which comes from the PI controller are called axillary state, and it is notated as $\Delta\gamma_i$. Equation (2.37) represents the current controller states. Therefore, the current state space model can be written as presented in (2.38):

$$[\dot{\gamma_i}] = [0][\Delta\gamma_i] + [Kp_i][\Delta io^*] + [-Kp_i][\Delta io] \tag{5.37}$$

$$[vt] = [1][\Delta\gamma_i] + [Kp_i][\Delta io^*] + [-Kp_i][\Delta io] \tag{5.38}$$

5.4.1.3 Linearized Voltage Controller State Space Model

The state space model of the voltage controller is similar to the current controller state space model. Referring to equation (2.15), the state space model of the voltage controller has an extra state variable that is notated as $\Delta\vartheta_v$. Therefore, the voltage state space model can be written as follows:

$$[\Delta io^*] = [1][\Delta\vartheta_v] + [Kp_v][\Delta vo^*] + [-Kp_v][\Delta v_{dc}] + [H][\Delta io] \tag{5.39}$$

$$[\dot{\vartheta}_v] = [0][\Delta\vartheta_v] + [Ki_v][\Delta\dot{vo}] + [-Ki_v][\Delta\dot{vdc}] \tag{5.40}$$

5.4.1.4 Linearized Power Controller State Space Model

Referring to Figure 2-11, the power control consists of one integrator that exists in the low pass filter (LPF); thus, the power controller state space model has one state variable. By rearranging the power equation, the linearized differential equations of the power controllers become the following:

$$[\dot{P_{dc}}] = [\omega_f.v_{dc}][\Delta io] + [\omega_f.io][\Delta v_{dc}] + [-\omega_f][\Delta P_{dc}] \tag{5.41}$$

Therefore the linearization of the DC droop equation leads to achieving the DC voltage reference equation as written below in (2.42):

$$[\Delta v_{dc}] = [-m_{dc}][\Delta P_{dc}] \tag{5.42}$$

77

5.4.1.5 Complete Linearized State Space Small-signal Model of DC-to-DC converter

The total state space model of a VSC that is interfacing a DG unit into DC sub-system is achieved by combining the linearized state space models with each other. Equation (2.43) represents the complete state space model of a converter Interfacing DG Unit into AC Microgrid. [The readers are referred to Appendix B for further details].

$$[\Delta \dot{x}_{inv}^{dc}] = \mathbb{A}_{inv}^{dc}[\Delta x_{inv}] + \mathbb{B}_{inv1}^{dc}[\Delta V_{dc}] \tag{5.43}$$

Where:

$$[\Delta x_{inv}^{dc}] = [\Delta ii \quad \Delta io \quad \Delta vo \quad \Delta P_{dc} \quad \Delta \vartheta_v \quad \Delta \Delta \gamma_i]^T$$

$$\mathbb{A}_{inv}^{dc} = \begin{bmatrix} \left(Ap + \begin{bmatrix} \left[([B1_p][-Kp_c]) \begin{bmatrix} 0 & 0 \\ 0 & 0 \\ 0 & 0 \end{bmatrix} \right] + \\ \begin{bmatrix} 0 \\ 0 \\ 0 \end{bmatrix} ([Kp_c][B1_p][H]) \begin{bmatrix} 0 \\ 0 \\ 0 \end{bmatrix} \end{bmatrix} \right)_{3\times3} & \begin{pmatrix} [Kp_c][B1_p] \times \\ [Kp_v][-m_{dc}] \end{pmatrix}_{3\times1} & \begin{pmatrix} [Kp_c] \times \\ [B1_p] \end{pmatrix}_{3\times1} & (B1_p)_{3\times1} \\ (0 \quad [\omega_f.vo] \quad [\omega_f.io])_{1\times3} & (-\omega_f)_{1\times1} & (0)_{1\times1} & (0)_{1\times1} \\ \begin{pmatrix} [0 \quad 0 \quad 0] + \\ [[-Ki_c] \; ([Ki_c][H]) \; 0] \end{pmatrix}_{2\times3} & \left(\begin{bmatrix} \begin{pmatrix} [Ki_v] \times \\ [-m_{dc}] \end{pmatrix} \\ \begin{pmatrix} [Ki_c] \times \\ [Kp_v] \times \\ [-m_{dc}] \end{pmatrix} \end{bmatrix} \right)_{2\times1} & \left(\begin{bmatrix} 0 \\ [Ki_c] \end{bmatrix} \right)_{2\times1} & (0)_{2\times1} \end{bmatrix}_{6\times6}$$

$$Bp_{dc} = \begin{bmatrix} \begin{pmatrix} [Kp_c] * [B1_p] * [-Kp_v] \\ +[B2_p] \end{pmatrix}_{3\times1} \\ (0)_{1\times1} \\ ([-Ki_v])_{1\times1} \\ ([Ki_c][-Kp_v])_{1\times1} \end{bmatrix}_{6\times1} [\Delta v_{dc}]$$

5.4.1.6 Complete State Space of Entire DC Sub-grid

In order to implement the state space model for the entire DC microgrid, the DC loads and lines resistances must be included in the system matrix. Therefore, the A matrix of inverter # 1 and #3 will be changed due to the loads connection at these electrical nodes according to Figure 5.9.

78
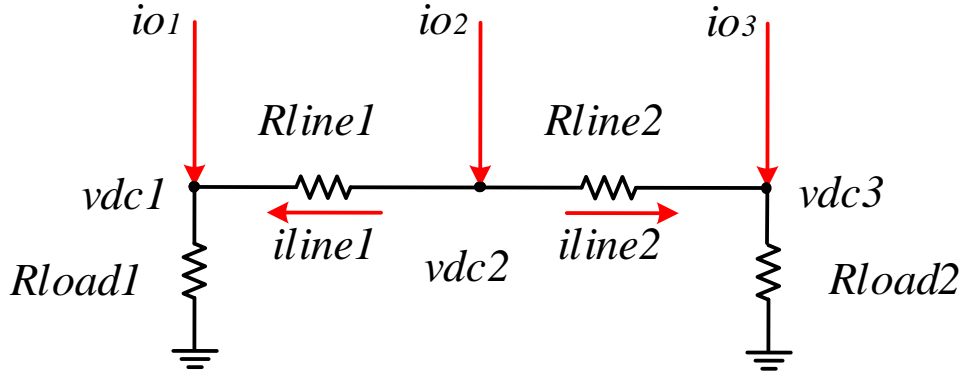
Figure 5-9 DC Sub-system Network Configuration.

The DC sub-system contains of three DC-to-DC half-bridge converters interfacing DG units. It is clear that includeing the DC loads shows some elements are related to the state matrix. For any converter has common connection node with the DC load, the system matrix must contains the DC load elements. Therefore; the ($\mathbb{A}_{inv}^{dc}$) and ($\mathbb{B}_{inv}^{dc}$) becomes as written below including the load and lines resistances as presented in equation (2.44) and (2.45) respectively. [The readers are referred to Appendix B for further details].

$$\mathbb{B}_{inv}^{dc} = \begin{bmatrix} \begin{bmatrix} [Kp_c] * [B1_p] * [-Kp_v] * [R_{load}] \\ + [B2_p] * [R_{load}] \end{bmatrix}_{3\times1} \\ [0]_{1\times1} \\ [[-Ki_v] * [R_{load}]]_{1\times1} \\ [[Ki_c][-Kp_v][R_{load}]]_{1\times1} \end{bmatrix} [\Delta i_{line}] \tag{5.44}$$

$$\mathbb{A}_{inv}^{dc} = \begin{bmatrix} \begin{bmatrix} \begin{bmatrix} Ap + \\ \left[[B1_p][-Kp_c] \quad [0]_{3\times2} \right] + \\ \begin{bmatrix} \begin{bmatrix} 0 \\ 0 \\ 0 \end{bmatrix} & \begin{bmatrix} \left[\begin{pmatrix} [Kp_c] \times \\ [B1_p] \times \\ [-Kp_v] \times \\ [R_{load}] \times \end{pmatrix} \\ + \begin{pmatrix} [B2_p] \\ [R_{load}] \end{pmatrix} \end{bmatrix}_{3\times1} \\ [0]_{1\times1} \\ \begin{bmatrix} [-Ki_v] \times \\ [R_{load}] \end{bmatrix}_{1\times1} \\ \begin{bmatrix} [Ki_c] \times \\ [-Kp_v] \times \\ [R_{load}] \times \end{bmatrix}_{1\times1} \end{bmatrix} & \begin{bmatrix} 0 \\ 0 \\ 0 \end{bmatrix} \end{bmatrix}_{3\times3} \end{bmatrix} & \begin{bmatrix} [Kp_c] \times \\ [B1_p] \times \\ [Kp_v] \times \\ [-m_{dc}] \times \end{bmatrix}_{3\times1} & \begin{bmatrix} [Kp_c] \times \\ [B1_p] \end{bmatrix}_{3\times1} & [B1_p]_{3\times1} \\[5em] \begin{bmatrix} 0 & [w.vo] & [w.io] \end{bmatrix}_{1\times3} & [-w]_{1\times1} & [0]_{1\times1} & [0]_{1\times1} \\[2em] \begin{bmatrix} [0 \quad 0 \quad 0] + \\ \left[[-Ki_c] \quad ([Ki_c][H]) \quad 0 \right] \end{bmatrix}_{2\times3} & \begin{bmatrix} \begin{bmatrix} [Ki_v] \times \\ [-m_{dc}] \end{bmatrix} \\ \begin{bmatrix} [Ki_c] \times \\ [Kp_v] \times \\ [-m_{dc}] \end{bmatrix} \end{bmatrix}_{2\times1} & \begin{bmatrix} 0 \\ [Ki_c] \end{bmatrix}_{2\times1} & [0]_{2\times1} \end{bmatrix} \tag{5.45}$$

5.4.1.7 Complete State Space of Entire DC Sub-grid

The complete state space model of the DC sub-system is presented in equation (2.46), and the eigenvalues of the DC sub-system are shown in Figure 5.10. Using the initial operating points that are extracted from the time-domain simulations in PSCAD/EMTDC. For further investigations, the trajectory of the dominant eigenvalue as a function of the active DC power droop coefficient (m_p) is shown in Figure 5.11.

$$[\dot{X}_P] = \begin{bmatrix} Ap_{dc1} & (0)_{6\times6} & (0)_{6\times6} \\ (0)_{6\times6} & Ap_{dc2} & (0)_{6\times6} \\ (0)_{6\times6} & (0)_{6\times6} & Ap_{dc3} \end{bmatrix} [\Delta X_P] + \begin{bmatrix} Bp_{dc1} \\ Bp_{dc2} \\ Bp_{dc3} \end{bmatrix} \begin{bmatrix} (\Delta i_{o1} + \Delta i_{line1}) * R_{load1} \\ \Delta v_{dc2} \\ (\Delta i_{o3} + \Delta i_{line2}) * R_{load3} \end{bmatrix} \tag{5.46}$$
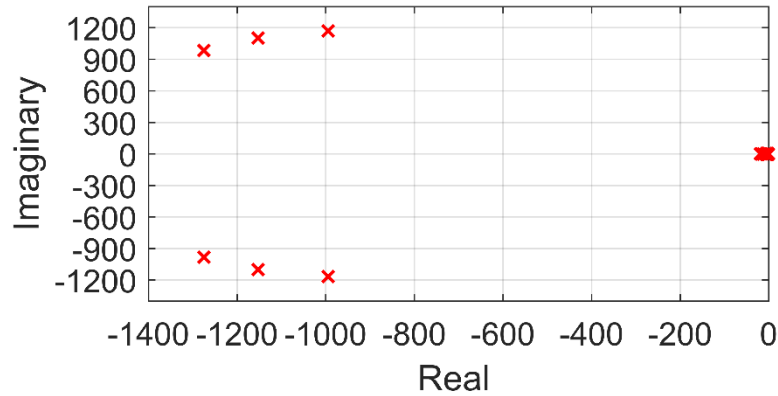
Figure 5-10 Eigenvalues spectrum of the DC Sub-system.
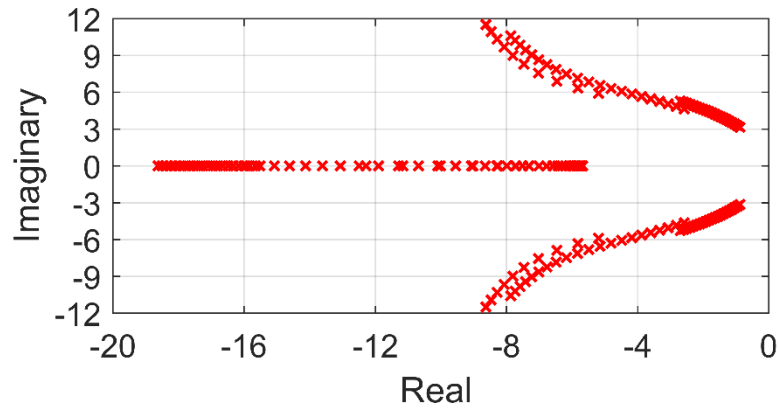
Figure 5-11 Impact of Changing the Active DC Power Droop coefficient with respect to the low frequency modes of the DC Sub-system: 1.25e-4 $<m_p<$3.25e-4

5.4.2 Small-signal model of Intertying converter.

5.4.2.1 The State-Space Model of the IC Power controller

The model of the IC converter is similar to that of the VSC in the AC sub-system, except the power controller state space model. The power control for the IC is based on the swing equation, shown in (5.47) and (5.48).

$$\frac{d\omega}{dt} = \frac{P_{ref}}{2J} - \frac{P_{ele}}{2J} - \frac{K_d * \omega_{VSM}}{2J} + \frac{K_d * \omega_g^*}{2J} \qquad (5.47)$$

81

$$\frac{d\delta}{dt} = \omega_{VSM} \tag{5.48}$$

The state space representation of the IC's power controller after replacing the electrical power by calculated power in d-q frame is presented in equation (5.49).

$$
\begin{bmatrix} \Delta\dot{\omega}_{VSM} \\ \Delta\dot{\theta}_{vsm} \end{bmatrix} = \underbrace{\begin{bmatrix} -\dfrac{K_d}{2J} & 0 \\ 1 & 0 \end{bmatrix}}_{A_s} \begin{bmatrix} \Delta\omega_{VSM} \\ \Delta\theta_{vsm} \end{bmatrix} + \underbrace{\begin{bmatrix} -\dfrac{1.5v_d}{2J} & -\dfrac{1.5v_q}{2J} \\ 0 & 0 \end{bmatrix}}_{B_s1} \begin{bmatrix} \Delta io_d^c \\ \Delta io_q^c \end{bmatrix}
$$
$$
+ \underbrace{\begin{bmatrix} -\dfrac{1.5io_d}{2J} & -\dfrac{1.5io_q}{2J} \\ 0 & 0 \end{bmatrix}}_{B_s2} \begin{bmatrix} \Delta v_d^c \\ \Delta v_q^c \end{bmatrix} + \underbrace{\begin{bmatrix} \dfrac{K_d}{2J} \\ 0 \end{bmatrix}}_{B_s3} \begin{bmatrix} \Delta\omega_g \end{bmatrix} \tag{5.49}
$$

5.4.2.2 The State-Space Model of the IC Power Circuit

The dynamic equations of the voltages and currents of the IC are known collectively as the large signal model, and can be written based on the Figure 5.13 as follows:
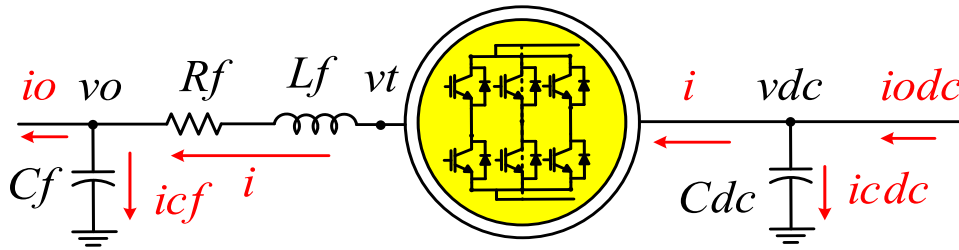
Figure 5-12 Systematic IC to Intertying AC Sub-system with DC Sub-system

$$\frac{di_d}{dt} = \frac{1}{L_f} vt_d - \frac{1}{L_f} vo_d - \frac{R_f}{L_f} i_d + \omega i_q \tag{5.50}$$

$$\frac{di_q}{dt} = \frac{1}{L_f} vt_q - \frac{1}{L_f} vo_q - \frac{R_f}{L_f} i_q - \omega i_d \tag{5.51}$$

$$\frac{dvo_d}{dt} = \frac{1}{C_f} io_d - \frac{1}{C_f} i_d + \omega v_q \tag{5.52}$$

$$\frac{dvo_q}{dt} = \frac{1}{C_f} io_q - \frac{1}{C_f} i_q - \omega v_d \tag{5.53}$$

$$\frac{dv_{dc}}{dt} = \frac{1}{C_{dc}} io_{dc} - \frac{1}{C_f} i \qquad (5.54)$$

The converter voltages and currents in d-q frame can be written as a function in modulation index of the IC as shown in equation (5.55) and (5.56).

$$vt_d + vt_q = m_d v_{dc} + m_q v_{dc} \qquad (5.55)$$

$$i_d + i_q = 1.5 \, m_d v_{dc} + 1.5 m_q v_{dc} \qquad (5.56)$$

The linearized small-signal state space representation of the IC power circuit is as follows.

$$[\Delta \dot{x}_{pIC}] = \mathbb{A}_{PIC}[\Delta x_{pIC}] + \mathbb{B}_{PIC1}\begin{bmatrix} \Delta m_d \\ \Delta m_q \end{bmatrix} + \mathbb{B}_{PIC2}\begin{bmatrix} \Delta io_d \\ \Delta io_q \end{bmatrix} + \mathbb{B}_{PIC3}[\Delta w] + \mathbb{B}_{PIC4}[\Delta io_{dc}] \qquad (5.57)$$

Where:

$$[\Delta \dot{x}_{pIC}] = [\Delta i_d \quad \Delta i_q \quad \Delta v_d \quad \Delta v_q \quad \Delta v_{dc}]$$

$$\mathbb{A}_{PIC} = \begin{bmatrix} -\dfrac{R_f}{L_f} & \omega & -\dfrac{1}{L_f} & 0 & \dfrac{m_d}{L_f} \\ -\omega & -\dfrac{R_f}{L_f} & 0 & -\dfrac{1}{L_f} & \dfrac{m_q}{L_f} \\ \dfrac{1}{C_f} & 0 & 0 & \omega & 0 \\ 0 & \dfrac{1}{C_f} & -\omega & 0 & 0 \\ -\dfrac{1.5 m_d^o}{C_{dc}} & -\dfrac{1.5 m_q^o}{C_{dc}} & 0 & 0 & 0 \end{bmatrix} ; \quad \mathbb{B}_{PIC1} = \begin{bmatrix} -\dfrac{v_{dc}}{L_f} & 0 \\ 0 & -\dfrac{v_{dc}}{L_f} \\ 0 & 0 \\ 0 & 0 \\ -\dfrac{1.5 I_d^o}{C_{dc}} & -\dfrac{1.5 I_q^o}{C_{dc}} \end{bmatrix}$$

$$\mathbb{B}_{PIC2} = \begin{bmatrix} 0 & 0 & -\dfrac{1}{C_f} & 0 & 0 \\ 0 & 0 & 0 & -\dfrac{1}{C_f} & 0 \end{bmatrix}$$

83

$$\mathbb{B}_{PIC3} = [i_q \quad -i_d \quad v_q \quad -v_d \quad 0]; \; \mathbb{B}_{PIC4} = \begin{bmatrix} 0 & 0 & 0 & 0 & -\dfrac{1}{C_{dc}} \end{bmatrix}$$

5.4.3 The State-Space Model of the IC Controllers

In order to avoid the repetition, the procedures of the state space modelling of the IC controller is not shown here because they are similar to the VSC interfacing a DG unit into AC microgrid. The overall states and inputs matrices of the IC, given in the Appendix, consist of ten state variables based on the following equation:

$$\left[\Delta \dot{x}_{inv_{IC}} \right] = \mathbb{A}_{inv_{IC}} \left[\Delta x_{inv_{IC}} \right] + \mathbb{B}_{inv_{IC1}} \begin{bmatrix} \Delta io_d \\ \Delta io_q \\ \Delta io_{dc} \end{bmatrix} \tag{5.58}$$

Where:

$$[\Delta \dot{x}_{invIC}] = [\Delta i_d \quad \Delta i_q \quad \Delta v_d \quad \Delta v_q \quad \Delta v_{dc} \quad \Delta \gamma_d \quad \Delta \gamma_q \quad \Delta \varphi_d \quad \Delta \varphi_q \quad \Delta w]^T$$

$$\mathbb{A}_{inv_{IC}} = \begin{bmatrix} \begin{pmatrix} Ap + \\ [Bp1Di2 \quad Bp1Di1Dv2 \quad 0] \end{pmatrix} & Bp1Ci & Bp1Di1Cv & \begin{pmatrix} Bp1Di1Dv1Dvr2 \\ +Bp2 \end{pmatrix} \\ (Bi2 \quad Bi1Dv2 \quad 0) & 0 & Bi1Cv & Bi1Dv1Dvr2 \\ (0 \quad Bv2 \quad 0) & 0 & 0 & Bv1Dvr2 \\ (0 \quad Bs2 \quad 0) & 0 & 0 & As \end{bmatrix}$$

$$\mathbb{B}_{inv_{IC1}} = \begin{bmatrix} \begin{pmatrix} (Bp1Di1Dv1Cvr) \\ +(Bp1Di1Dv3) \\ +Bp2 \end{pmatrix} \\ \begin{pmatrix} (Bi1Dv1Cvr) \\ +(Bi1Dv3) \end{pmatrix} \\ Bv1 * Cvr \\ Bs2 \end{bmatrix}; \quad \mathbb{B}_{inv_{IC2}} = \begin{bmatrix} Bp4 \\ 0 \\ 0 \\ 0 \end{bmatrix} [\Delta io_{dc}]$$

5.5 Small-Signal Stability Analysis of the Hybrid AC/DC Microgrid

The complete state space model of the overall hybrid AC/DC microgrid is shown in equation (5.59), and is given in details (see appendix C). The evaluation of the system stability can be investigated by analysing the eigenvalues of the state matrix in (5.59).

$\mathbb{A}_{\text{Hybrid}}$

$$= \begin{bmatrix} \mathbb{A}_{inv_{AC}} & \mathbb{B}_{inv_{ac}} & 0 \\ \begin{pmatrix} \left(\mathbb{B}_{p1IC} * \mathbb{D}_{i1IC} * \mathbb{D}_{v1IC} * \mathbb{C}_{vrIC} \right) + \\ \left(\mathbb{B}_{p1IC} * \mathbb{D}_{i1IC} * \mathbb{D}_{v3IC} \right) + \mathbb{B}_{p2IC} \\ \mathbb{B}_{p4IC} \end{pmatrix} & \mathbb{A}_{inv_{IC}} & \begin{pmatrix} \left(\mathbb{B}_{i1IC} * \mathbb{D}_{v1IC} * \mathbb{C}_{vrIC} \right) \\ \left(\mathbb{B}_{i1IC} * \mathbb{D}_{v3IC} \right) \end{pmatrix} \quad \mathbb{B}_{sw1IC} \\ 0 & \mathbb{B}_{inv_{dc}} & \mathbb{A}_{inv_{dc}} \end{bmatrix} \qquad (5.59)$$

The complete eigenvalues for the hybrid AC/DC microgrid shown in Figure 5.14 are based on the initial operating values that were determined from the time domain simulation conducted in PSCAD/EMTDC.
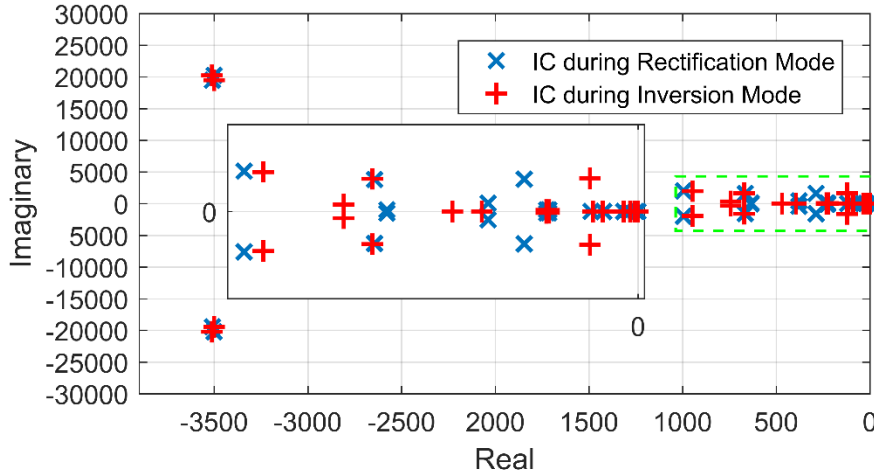
Figure 5-13: Eigenvalue spectrum for the hybrid AC/DC microgrid.

Analysis of the eigenvalues for the overall hybrid AC/DC microgrid using the participation factors reveals the dominant sensitive low-frequency eigenvalue. The state variable for virtual damping is the most dominant in the hybrid AC/DC microgrid. The trajectory of the sensitive low-frequency dominant eigenvalue is therefore a function of the virtual damping coefficient (K_d), as shown in Figure 5.15. The inversion mode of the IC is in fact the most important mode because of the sensitivity of the AC sub-grid to power loading. It is therefore apparent that the dynamic of the virtual damping during the IC inversion mode affects system stability. The assessment of the stability of the hybrid AC/DC microgrid should thus be evaluated in an IC inversion operation mode, which will ensure the stability of the system during the

rectification mode. In other words, the stability margin of the rectification mode is larger than that of the inversion mode.
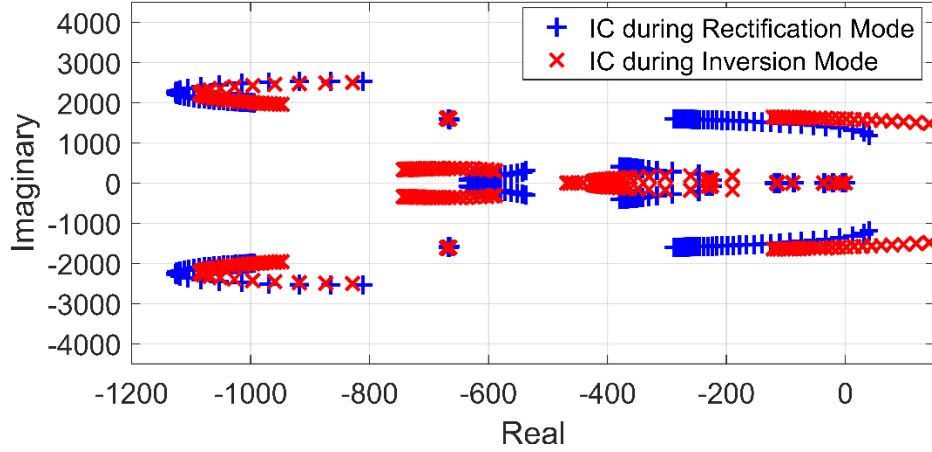
Figure 5-14 Impact of decreasing the virtual damping with respect to the low-frequency modes of the hybrid microgrid: $0.3e4 < K_d < 1e3$.

The stability for the hybrid AC/DC microgrid is evaluated to reveal the effect of the virtual inertia and damping on the entire hybrid microgrid. The impact of varying the virtual inertia on the system eigenvalues is less than the impact of varying the virtual damping gain as illustrated in Figure 5.16. The reason behind this impact is that the virtual damping gain is an inverse form the droop coefficient that can be seen in (5.60)[72]. Where m_{ac} represents the droop coefficient, and K_d represents the virtual damping gain.

$$K_d = \frac{1}{m_{ac}} \tag{5.60}$$
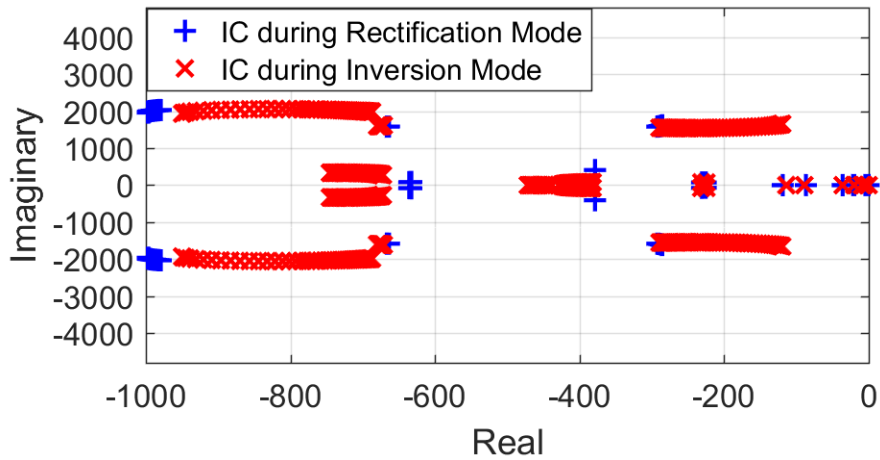
Figure 5-15 Trajectory of hybrid microgrid based on VSM controller as a function of virtual inertia**.**

5.6 Conclusion

This chapter has presented the development of the small-signal model of the hybrid AC/DC microgrid that contains VSM-based control for the IC. The small-signal model of the hybrid AC/DC microgrid has been divided into three main parts. These parts are AC microgrid, DC microgrid, and IC. The stability analysis has been evaluated based on determining the most dominant eigenvalues using participation factors percentage calculation. This chapter has studied and compared a two hybrid micro-grid with different control structures of the IC based on small-signal models.

This chapter has studied and compared the stability analysis of two hybrid microgrid with different control structures of the IC. It has been demonstrated that during variations of the AC droop coefficients, DC droop coefficients, and virtual inertia and damping coefficients.

Chapter 6

Issues and Solution-based Virtual Synchronous Machine for Parallel Intertying Converters (ICs) Interfacing Hybrid AC/DC Microgrids [4]

This chapter reveals three serious issues of operating a hybrid AC/DC microgrid. Two of these issues are temporary, depending on the system's operating conditions. In a hybrid AC/DC microgrid, an Intertying converter (IC) becomes a harmonics voltage source due to the antiparallel diodes and the shunt capacitor on its DC side, so this is the first issue. The nonlinear behavior of ICs introduces the second operational issue of circulating current in the case of parallel ICs. Reconnecting an IC after abnormal operating conditions or scheduled maintenance requires especially challenging synchronization control due to the variation of the AC subgrid voltages and frequency. This is the third issue. This chapter proposes a solution for these three issues by developing a new control strategy that combines the virtual synchronous machine (VSM) control concept with a dual-based droop control. The results indicate that the proposed solution provides a positive outcome in addressing the above issues, hence improving hybrid microgrid operations and the quality of the delivered power. The theoretical expectations are verified by digital simulation using the PSCAD/EMTDC simulation package.

6.1 INTRODUCTION

Recognizing the sensitivity of the system dynamics in a hybrid microgrid during power exchange between the sub-systems led the authors of [9] and [93] to propose a control strategy that makes use of energy storage systems already existing in the AC and/or DC side. However, most of the literature uses a VSM control strategy for unidirectional power flow except only one; which focuses on integrating that DC microgrid into AC grid [94]. In this case the AC voltage and frequency are fix; therefore, the study does not investigate the hybrid AC/DC microgrid in islanded operation mode; which means AC voltage and frequency are changing according to the load variation. To the authors' best knowledge, no studies have included considerations of the IC as a nonlinear load once the power exchanges from AC to DC

---

subsystem; an issue that extremely violates the standards requirements of the power quality. Also, there is no studies have included the variation of the AC voltage, frequency, and DC voltage variation on the VSM control concept Indeed, the majority of the literature works were conducted under an assumption that the DC side of the converter based on VSM controller concept is connected to an ideal DC source. However, this is not the case of interconnecting the DC sub-system into AC sub-system to form the hybrid AC/DC microgrid.

The concept of multiple parallel converters that provide an interface between the AC and the DC sides has been employed in numerous applications, including motor drives, microgrids, and distributed generation (DG) systems. Multiple parallel converter architectures have been observed to increase system reliability [95], to permit the use of low-rating converters in high-power applications, and to improve the simplicity and cost-effectiveness of maintenance because of the ease of replacing individual malfunctioning converters [96]. The performance and reliability of both sub-systems are dependent primarily on the reliability of the ICs, which can directly affect the stability and efficiency of the entire hybrid microgrid. Load curtailment might be an effective solution for stabilizing both the AC and DC sub-systems; however, this technique provides a low degree of reliability with respect to the overall hybrid microgrid. Further, hybrid AC/DC microgrid generally requires both voltage and frequency support for the AC sub-system, plus DC voltage support on the DC sub-system side, which means that power sharing between the sub-systems is critical for ensuring the stability and reliability of such systems. Any change in generation or loading conditions causes substantial frequency deviations, which can result in instability [77]. A further consideration is that hybrid AC/DC microgrid dynamics are also affected during power exchanges between the two sub-systems, which could potentially lead to stability issues due to the lack of inertia and load-dependent voltages [23], [97], [98].

The main challenge of a hybrid AC/DC microgrid is the power sharing among AC and DC sub-systems through the IC. Designing the coordinating control of the IC is another challenge, but it was introduced and investigated based on normalized droop control using just current controller loop[31]. Since each sub-system has a power generation limitation based on dispatchable DGs units rating, the power sharing between sub-systems requires a coordinate controller for the IC; seen from either side, to behave as a load for the sub-system exporting power to another sub-system. Also, the IC simultaneously behaves as a supply for the sub-system importing power from another. When the IC provides power to the DC sub-system, the effect of the IC on the AC sub-system is identical to a non-linear load involves several issues. These issues are similar to ones that are associated with nonlinear load and were investigated in

the literature based on the DG inverters controllers[99]–[103]. However, in the hybrid AC/DC microgrid these issues are raised by the IC operation behaviour.

Electric power systems are often subject to abnormal operation conditions, such as short circuits, and thus, must also undergo regularly scheduled maintenance. After a fault or scheduled maintenance has been cleared or completed, the system must be restored to its normal operational state and this involves reconnection of the isolated portion. The resynchronization of the isolated part with the rest of the system is an important and crucial step, and any associated issues must be resolved in order to achieve a smooth reconnection and stable operation. As a result, for seamless reconnection, the inclusion of a resynchronization algorithm as a part of the overall controller is necessary for each IC in a hybrid AC/DC system as well as for DG units in an AC microgrid. None of the reports in the literature discusses this issue, despite the enormous effect this issue has on overall system stability. Thus, an urgent need exists for the development of a dependable controller that is capable of offering reliable IC operation along with a self-synchronization control feature. Moreover, according to [104], the circulating current of the parallel inverters connected into common AC and DC bus using droop control can also occur. When power flows from the AC sub-system into to DC sub-system, the IC behaviour is seen from the AC sub-system as a nonlinear load. Therefore, the nonlinear load issues exist on the AC sub-system, and the THD of voltage increases while the power quality is degraded.

The primary contribution of this chapter is to solve the previous issues, including: 1) non-linear load behaviour of the IC, 2) re-synchronization issue of the IC after disturbance, and 3) circulating current issue between parallel ICs. The solution for these issues is based on the VSM control concept by including the dual droop control to achieve a bi-directional power flow capability. Applying the concept of the VSM with power reference modification, based on considering the AC and DC electrical quantities variation for the ICs, solves these issues. The applied controller enables multiple parallel ICs to behave as a synchronous machine (SM) for supporting both sub-systems, with consideration of the variations of the DC voltage and the AC frequency during the islanded operation of a hybrid AC/DC microgrid. The paper also addresses the stability analysis, resynchronization issue and its effect on system stability; as well as including a comparison with existing solution in the literature. Further, the application of the VSM control concept prevents the issue of circulating current that occurs in the parallel ICs during the rectification operation mode.

6.2 Issues Associated with IC

The parallel IC option offers a high level of system reliability. However, due to variations in the AC and DC voltages and the AC system frequency, the effect of the dynamics within each individual sub-system is increased, especially during isolated operation mode. This results in various issues that are associated with the existence of the IC in a hybrid AC/DC microgrid.

In a hybrid AC/DC microgrid application, the IC controller does not consider the voltage loop controller, as can be seen in [10], [29], [30], [89]. Therefore, it is more beneficial to include a voltage controller loop with the virtual synchronous machine concept applied on the IC converter. As a result, the model of the VSM control concept proposed in [46], [72], [105] is more reasonable for use based on a comprehensive assessment presented in [61].

6.2.1 Non-linear load issue

A nonlinear load is defined as an electrical load that infrequently draws current or whose impedance changes during the cycle of the AC waveform voltage. The hybrid microgrid IC consists of an antiparallel diodes rectifier and a shunt capacitor at the DC side to feed the variable frequency VSC in the AC subgrid. Subsequently, the power supplies via the antiparallel diodes rectifier to stiff voltage loads draw a discontinuous and non-sinusoidal AC current, which results in a higher current THD and distortions of the AC voltage at the point of common coupling (PCC) [106]. The readers are referred to Chapter 9 in [106] for further details. As a result, in this situation the IC becomes a harmonic voltage source instead of a harmonic current source [107], which is the case in this paper.

The DC sub-system interfaced with an IC will be seen from the AC side as a nonlinear load, as experimentally proven in [108]. In addition, the currents in different phases will differ, as explained in the quotation below from an ABB white paper:

"The diodes in a typical rectifier switch when the switching threshold voltage is exceeded in the positive direction. During each half cycle, two phases will exceed the switching threshold voltage, as one is decaying another is rising and vice versa-thus producing two peaks in the line current draw. When operating correctly and the voltage is balanced, the AC supply current waveform has a double pulse per half cycle shape"[109].

91

One associated issue with a non-linear load is regarding voltage and current distortion. Once the power flows from the AC sub-system into the DC sub-system, the impact of the IC on the AC sub-system is similar to that of a non-linear load. In this case, the voltage THD will increase beyond the allowable range and result in an unbalanced AC voltage at the PCC [110]. This issue has been discussed in the literature as a nonlinear load connected to an AC microgrid, and several solutions have been proposed [99]–[101], [103], [110]. However, in a hybrid AC/DC microgrid, this issue has different aspects due to the required functionalities of the IC in order to allow coordination between the sub-systems based on bidirectional power flow, and to support the AC sub-system's voltage and frequency.

6.2.2 Re-synchronization issue

Microgrid synchronization is a bit different in comparison to synchronizing a traditional synchronous machine with a classical electrical system. This is due to the fact that many DG units form the microgrid voltage and frequency based on decentralized droop control. The main challenge is to determine the successful synchronizing criteria for the AC microgrid, which is required to adjust all DG units [90]. Intensive works based on AC microgrid synchronization have been done, as reviewed in [111], which involved the use of a PLL as a synchronization controller unit, but this has significant adverse effects on overall system stability [112]. This issue results in the requirement for the development of a controller that does not require a synchronization unit in the inverter controller, as reviewed in [61]. Therefore, this paper presents a unique self-synchronization feature of a VSM controller through the inclusion of the AC and DC electrical quantity variations, such that reconnecting the IC based on the VSM controller results in stable operation when the IC is subjected to reconnection to the entire system after abnormal conditions, as presented in the simulation results and analysis section.

6.2.3 Circulating currents issue

Zero-sequence and cross currents between ICs form circulating current issues. Circulating currents appears in parallel converter application due to many reasons, such as switching frequency, dead-time, and hardware drifting components[104]. Transferring power from the AC into DC sub-system leads to circulating current issues; due to the IC behaving as non-linear load. Determining the circulating currents values for cross and zero-sequence can be calculated using (6.1), and (6.2) respectively based on Figure 6-1.

$$I_{cir}^{cross} = \frac{1}{2} * \left(\frac{v_{o1}}{R_{f1} + jL_{f1}} - \frac{v_{o2}}{R_{f2} + jL_{f2}} \right) \tag{6.1}$$

$$I_{cir}^{zero} = \frac{1}{3} * \left((I_{a1} + I_{b1} + I_{c1}) - (I_{a2} + I_{b2} + I_{c2}) \right) \tag{6.2}$$

Where v_{o1} and v_{o2} are the output voltages of each converter. The R_{f1}, R_{f2}, L_{f1} and L_{f2} are AC filter components of the converters. The phase currents are represented as $I_a, I_b, and I_c$ for each converters.
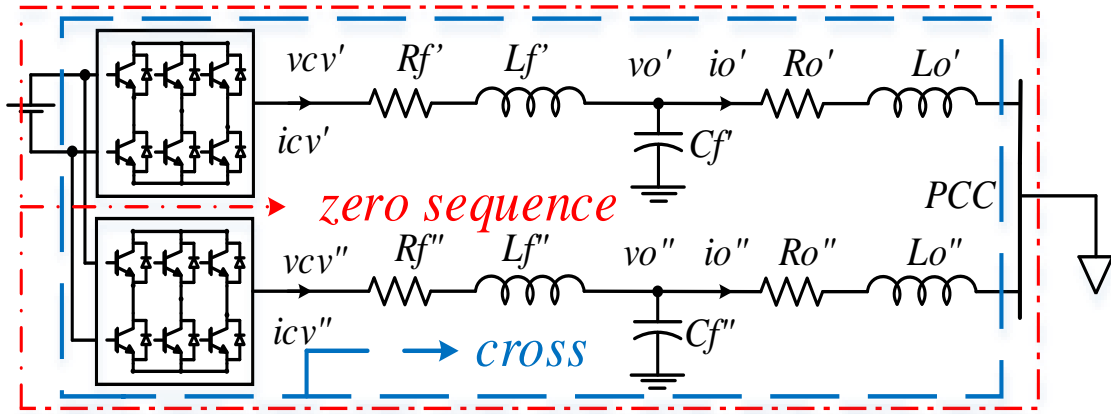
Figure 6-1 Circulating Currents paths of Parallel ICs.

6.2.4 Traditional IC based on current controller

The traditional IC controller based on just a current loop is studied based on centralized control in [30], while the dual droop control based on a current controller is investigated in [8], [25]. However, the previous works do not consider the voltage controller loop, despite the fact that this element will improve the disturbance rejection performance of the converter.

The advantages of including a voltage controller loop include the provision of a degree of freedom for the IC to support and control the AC voltage, which does not currently exist. The primary function of the IC is to control the direction of the active power; however, it is not responsible for providing reactive power support for the AC sub-system [8], [30].

The main drawback of using only a current controller energized via droop control (as shown in Figure 6-2) is that it causes fluctuations in the AC PCC voltage. Therefore, due to the load voltage dependence

of the AC load, the power exchange from the AC sub-system to the DC sub-system affects the AC sub-system voltage and power load, and produces more harmonics and circulating current in the case of parallel ICs.
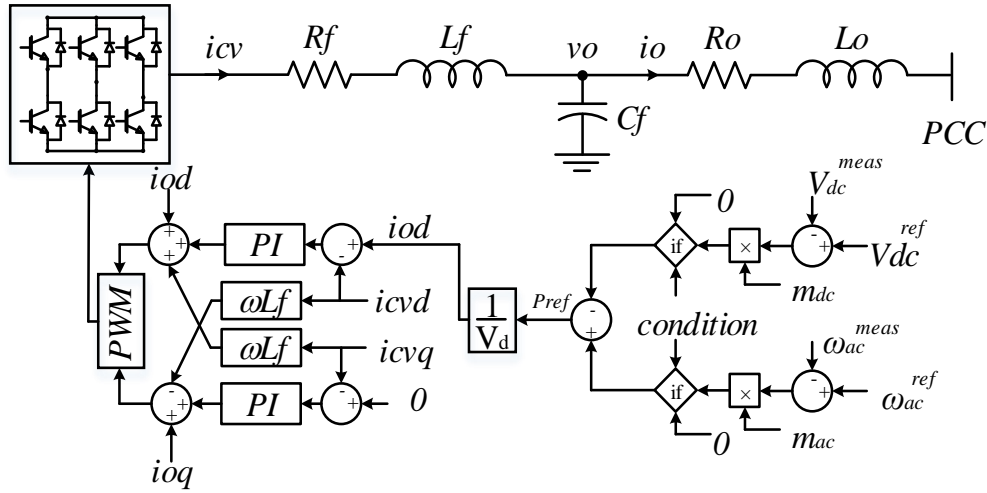
Figure 6-2 Control structure of IC based on only a current controller.

6.2.5 ICs based on VSM controller

VSM control concept can be implemented through a slight modification to the general control structure of VSC interfacing a DG unit. A number of VSM control algorithms have been developed to enable a VSC to mimic the behavior of an SM. The appropriate VSM control algorithm based on second-order model was chosen due to the fact that it is more stable during abnormal conditions such as short circuits [61]. Thus, in order to implement the second-order VSM control strategy, it is required to replace the power controller loop with the swing equation. Since the power controller loop provides the converter controller with phase angle and angular speed that are necessary to convert the voltages and the currents in d-q vector control frame as shown in Figure 6.3 (a); the swing equation can also produce these required quantities as depicted in Figure 6.3 (b). The overall IC's controller structure is shown in Figure 6-4.
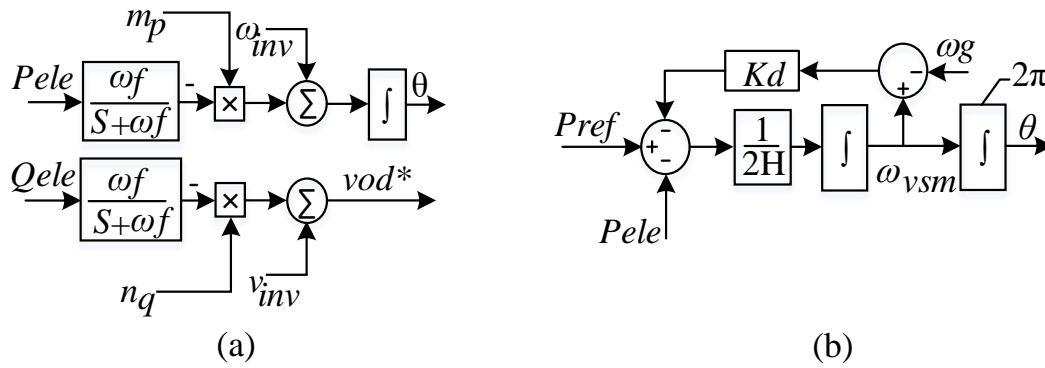
Figure 6-3 Power Controller (a) based on Droop, (b) based on VSM.
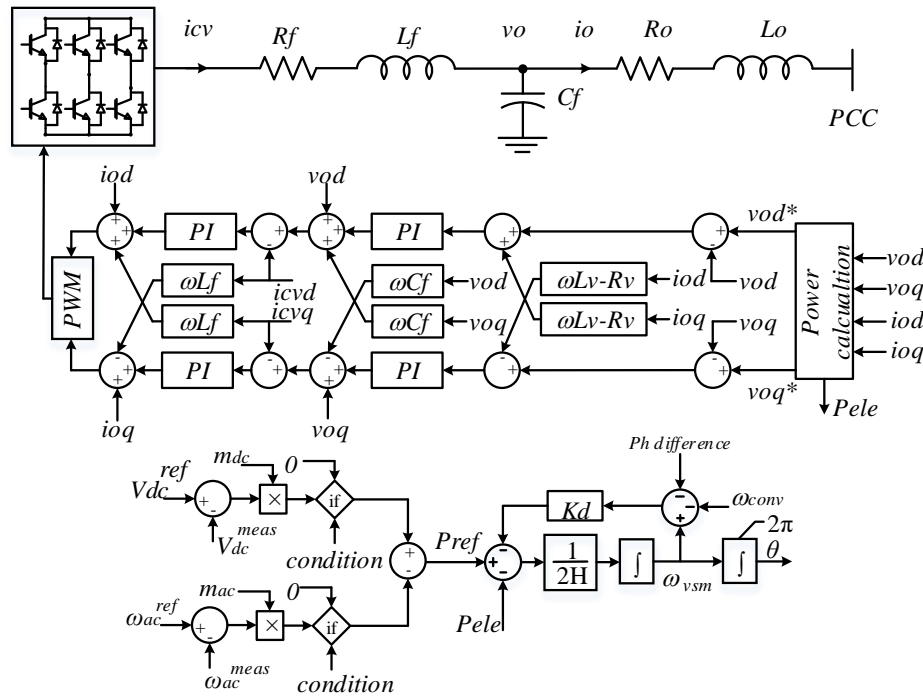
Figure 6-4 Control structure of IC based on VSM control concept.

6.3 Architecture of a Hybrid AC/DC System

The MV hybrid AC/DC system configuration employed in this study was obtained from [30] based on IEEE Standard 399, but modified to include parallel ICs. According to the secondary distribution system configuration, a spot network configuration provides the highest reliability compare to the other configurations such as a radial system or secondary-bank system. The spot network configuration consists of more than one transformer connected in parallel, which increases the distribution system reliability

[113]. A similar concept will be proposed for the Intertying converter in order to increase the hybrid AC/DC system reliability. Therefore, the MV hybrid AC/DC system with multiple Intertying converters is illustrated in Figure 6-5 based on the VSM control concept.

The hybrid AC/DC system consists of two dispatchable distributed generators (DGs) in the AC and DC subgrids. The interfacing power electronics converter with its parameters for the AC subgrid based on IEEE Standard 399 consists of a three-phase converter [33], while the interfacing converter in the DC subgrid is based on a half-bridge converter.

The system is divided into three different components: the AC subgrid, the ICs, and the DC subgrid. The control structure of the AC subgrid converters and the ICs are based on d-q cascaded synchronous reference frame (SRF) controllers, while the control structure for the DC subgrid converters is based on cascaded voltage and current control [30]. However, the use of a Park transformation is unnecessary because the control quantities are already constant as DC values.
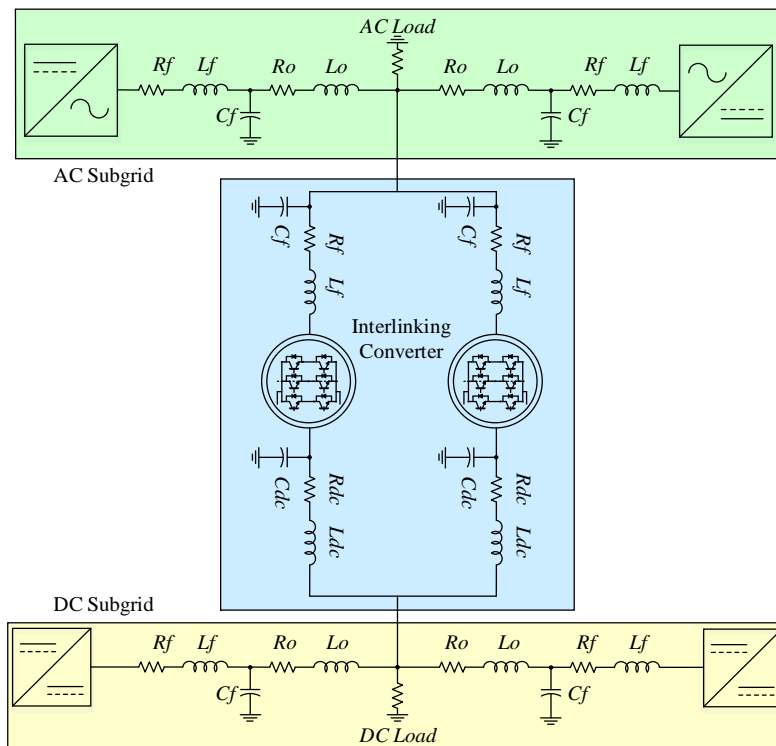
Figure 6-5: Medium Voltage MV hybrid AC/DC system architecture employed for this study.

Table 6-1: Hybrid Microgrid System Parameters.

Subsystem	Quantity	Value	Unit
AC sub-system	Converter rated power	1	MVA
	AC voltage (L-L) r.ms	690	V
	AC side resistance	0.01	Ω
	AC side inductance	1	mH
	AC side capacitance	50	µF
	System frequency	60	Hz
Intertying Converter	Virtual inertias	0.0025	Kg. m^2
	Virtual damping coefficient	16,000	N.s/min
	AC side resistance	0.15	Ω
	AC side inductance	2	mH
	AC side capacitance	50	µF
DC sub-system	Converter rated power	1	MVA
	DC voltage	2500	V
	DC side resistance	0.05	Ω
	DC side inductance	1	mH

6.4 Simulation Results and Analysis

The work presented in this paper involved the examination and comparison of two hybrid AC/DC systems: one based on the proposed modified VSM controller for the IC, and the other based on dual droop with only current control, as reported in the literature [10], [25], [30]. The cases that were simulated to evaluate the effectiveness of the modified VSM control strategy are explained below. The investigation presented here concentrated on four important cases, including small-signal analysis and assessment, IC behavior as a non-linear load, the re-connection of an IC after that has been disconnected from the system, and the occurrence of circulating current between the ICs.

Due to the sensitivity of isolated microgrid stability to the droop coefficient [20], the hybrid AC/DC microgrid stability is the most important issue to be evaluated based on eigenvalue assessment. Therefore, the first case (Case 1) studied hybrid microgrid stability with different IC controllers. The second case (Case 2) dealt with the effect of the IC behaving as a non-linear load. The third case (Case 3) aimed at establishing system performance given equal power-sharing among parallel ICs. Hence, the VSM controller illustrates the benefit of the proposed modified VSM controller based on dual droop control by using the existence of virtual inertia to prevent the occurrence of unstable operations in the case of reconnecting an IC that has been disconnected from the system. The goal of the fourth case (Case 4) was to investigate the overall performance of the hybrid AC/DC system to eliminate the occurrence of circulating current.

6.4.1 Small Signal Analysis based on eigenvalue assessment

The overall eigenvalues of the entire hybrid AC/DC microgrid were evaluated, as shown in Figure 6-6, and Figure 6-7 based on the initial operation values that were determined from the time domain simulation in PSCAD/EMTDC. Figure 6-6 presents the evolution of the hybrid microgrid eigenvalues using a VSM controller for the IC, while Figure 6-7 presents the eigenvalues of the hybrid microgrid using just a current controller for the IC, as reported in the literature. It is therefore to be noted that the existence of the voltage controller loop in the IC moves all the eigenvalues close to the origin, as shown in Figure 6-8, by varying the AC droop coefficient. As shown in Figure 6-8, the hybrid AC/DC microgrid's stability is most sensitive to the AC droop coefficient when the IC is in inversion operation mode. Clearly, it can be seen that varying the AC droop coefficients for 2 systems with identical ranges causes the hybrid microgrid based on VSM control for the IC to be unstable compared to the system that its IC's controller based on current controller loop, as shown in Figure 6-9. Nevertheless, including the voltage controller loop provides a valuable disturbance rejection function and prevents AC voltage degradation.
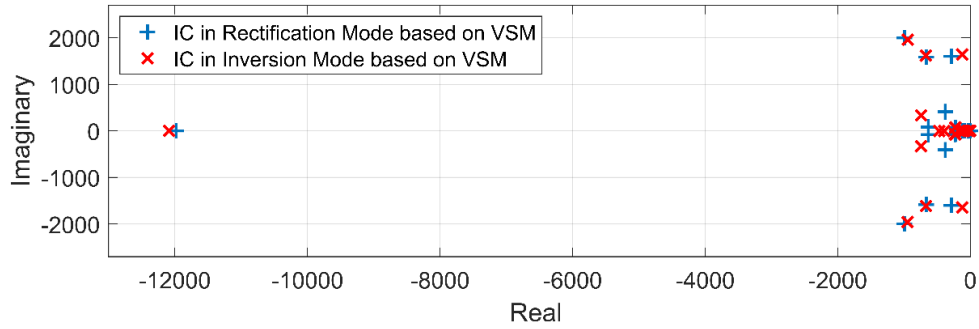
Figure 6-6: The eigenvalues of the hybrid microgrid based on VSM.
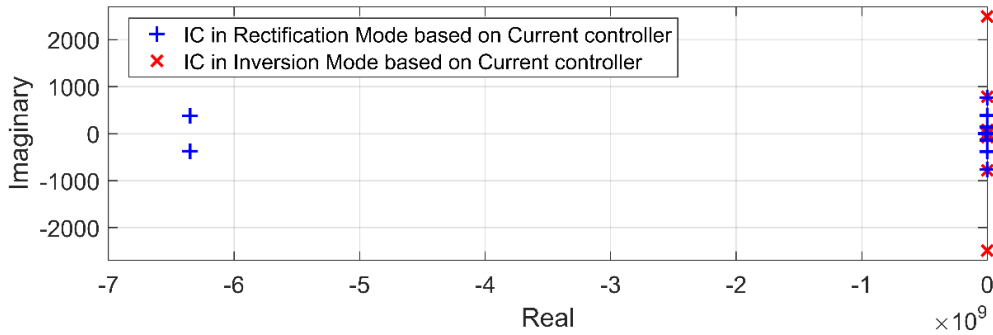
Figure 6-7: The eigenvalues of the hybrid microgrid based on Current controller.
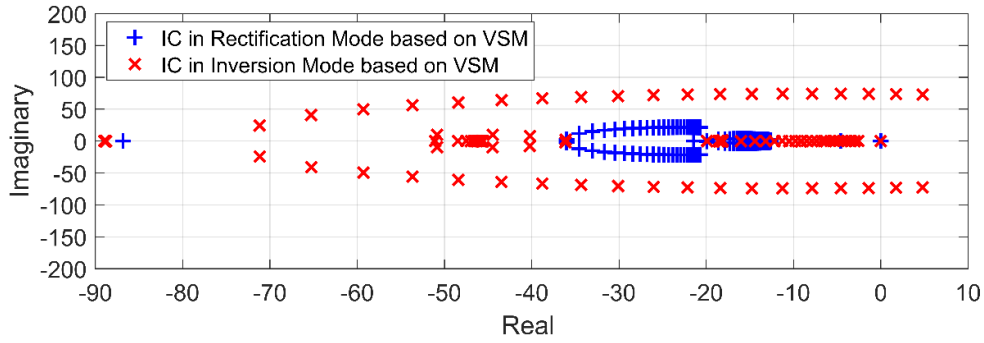
Figure 6-8: Trajectory of the eigenvalues as a function of AC active power droop coefficient based on VSM.
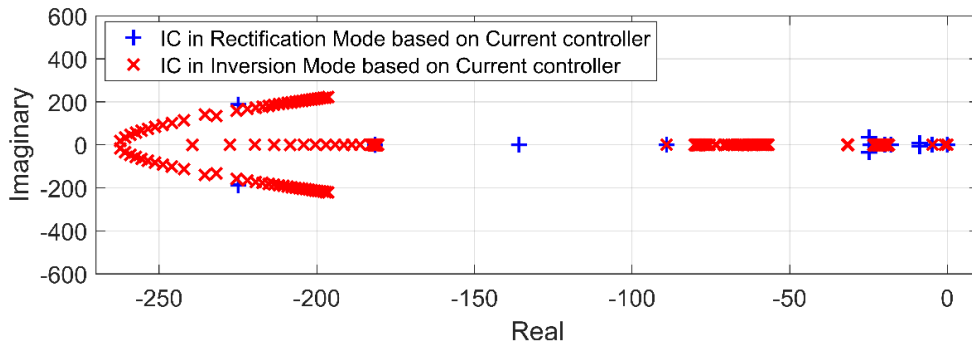
Figure 6-9: Trajectory of the eigenvalues as a function of AC active power droop coefficient based on Current controller.

Figure 6-10 and Figure 6-11 show the effect of the DC droop coefficients on the system stability. The stability margin of the hybrid AC/DC microgrid is less sensitive to the DC droop coefficient compared to the AC droop coefficient. When the IC is in inversion operation mode based on the VSM control concept, as shown in Figure 6-10, varying the DC droop coefficient moves the dominant eigenvalue to an unstable region. On the other hand, the system based on just the current controller loop is stable with the same condition, as shown in Figure 6-11.
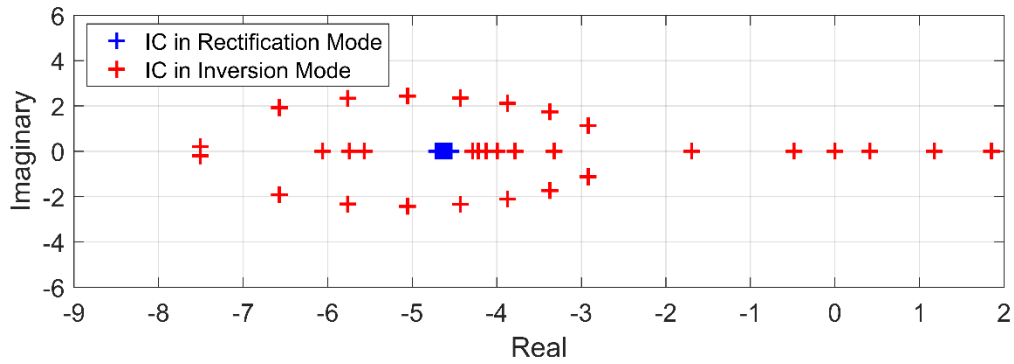
Figure 6-10: Trajectory of the eigenvalues as a function of DC active power droop coefficient based on VSM.

Figure 6-11: Trajectory of the eigenvalues as a function of DC active power droop coefficient based on Current controller.

The stability of the system is evaluated to reveal the effect of the virtual inertia and damping on the entire hybrid microgrid, as depicted in Figure 6-12 and Figure 6-13. The impact of varying the virtual inertia on the system eigenvalues is less than the impact of varying the virtual damping gain, as illustrated in Figure 6-12, and Figure 6-13. The reason behind this is that the virtual damping gain is an inverse form of the droop coefficient, which can be seen in Equation (6-3) [72].

$$K_d = \frac{1}{m_{AC}}$$

(6-3)

where m_{ac} represents the droop coefficient, and K_d represents the virtual damping gain.
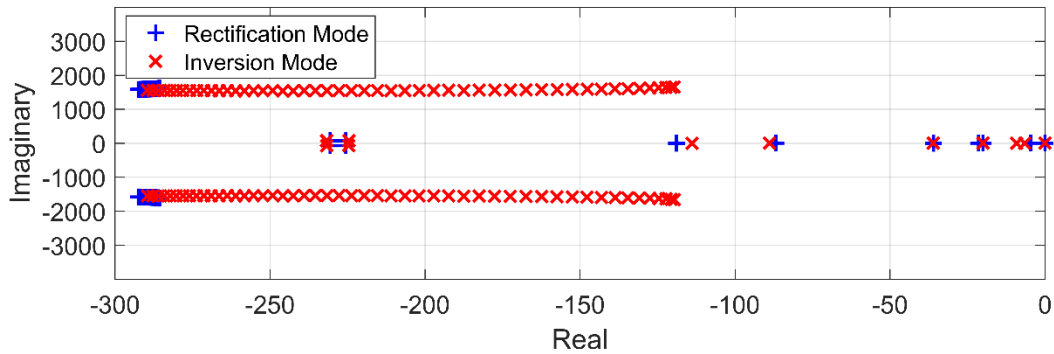
Figure 6-12: Trajectory of hybrid microgrid based on VSM controller as a function of virtual inertia.
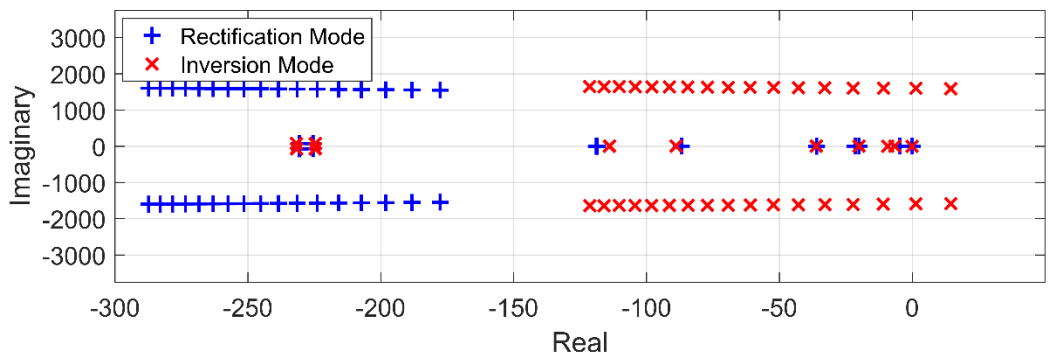
Figure 6-13: Trajectory of hybrid microgrid based on VSM controller as a function of virtual damping.

6.4.2 Case 1: The IC behavior as Non-linear load

In this case, the focus is on the issue of the IC behaviour as non-linear load. Both sub-systems operate under low-load conditions: the AC sub-system load is equal to 1 MW while the load in the DC sub-system is equal to 1.5 MW. At t = 2 sec, the DC load increases from 1.5 MW to 2.3 MW, which represents an overloaded condition for the DC DG units. In response, the IC compensates for the shortage of power from the dispatchable DG unit in the AC sub-system to maintain the DC sub-system in a healthier operating condition, as shown in Figure 6.14, which indicates the power exchange from the AC to the DC sub-system via the IC.
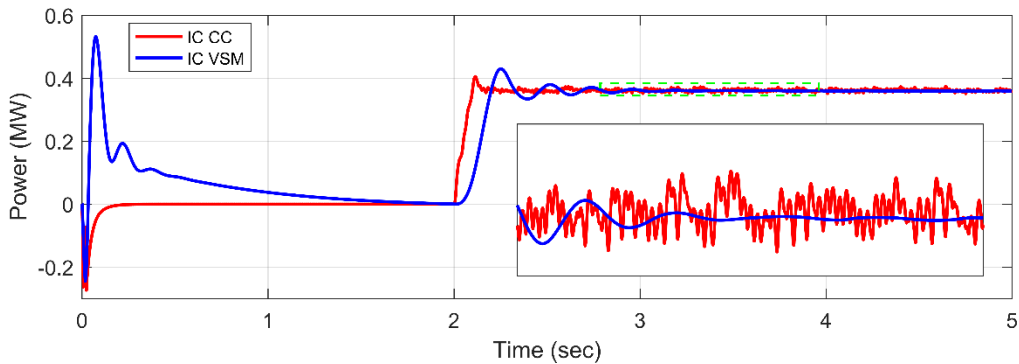
Figure 6-14: IC Power Exchange during DC Sub-system Overloading Conditions.

In the case of using just current control technique, the AC voltage in the AC sub-system is degraded due to the power exchange from AC to DC sub-system, as illustrated in Figure 6.15.
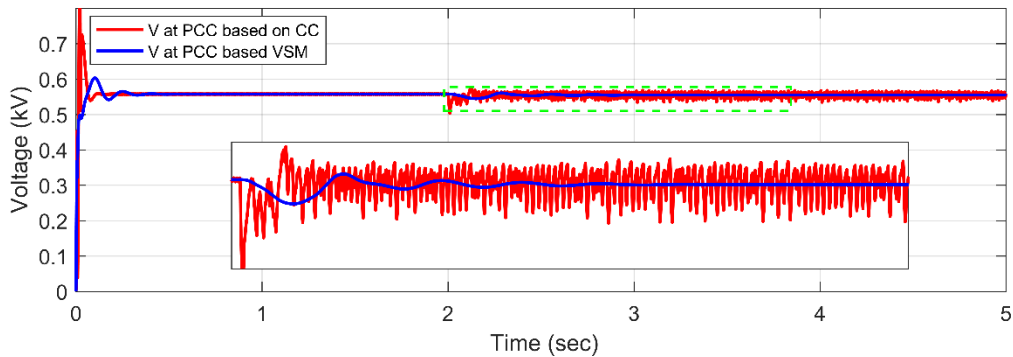
Figure 6-15 AC Voltage during the Exchange of Power from the AC to the DC Sub-system.

The AC voltage fluctuations issue leads to violations of the standard requirements. The AC sub-system voltage becomes unbalanced during this situation, as shown in Figure 6.16.The applied VSM control strategy on IC utilizes this effect to support the AC voltage and helps to enhance the performance of the hybrid microgrid. Also, the applied IC controller based on VSM smooths out these fluctuations by introducing inertia into the IC controller loop. In the systems reported in the literature, the DC sub-system affects the AC sub-system voltage and power load, and causes fluctuations in the PCC voltage due to the lack of inertia.
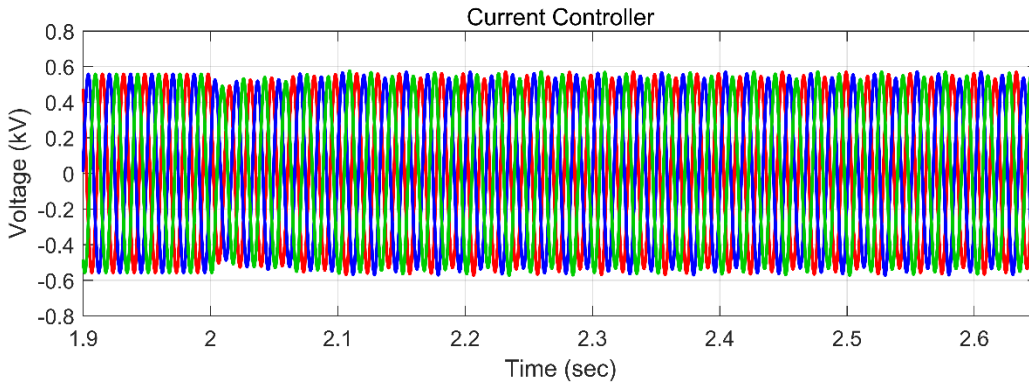
Figure 6-16: AC Voltage at the PCC with Current Control.

The introduced modified VSM control for IC offers a remedy for this problem, which occurs during the exchange of power from the AC to the DC sub-system, as shown in Figure 6.17. In addition, integrating the VSM controller into the IC also improves power quality in the entire hybrid AC/DC system.

The results in this case show the effect of the exchange of power from the to the DC sub-system through parallel ICs. At t = 2 sec, the DC sub-system imports about 0.35 MW, including power losses attributable to converters and line resistance; which is shown in Figure 6-14. Using multiple ICs based on a conventional current controller clearly produces more voltage fluctuations, along with their associated power quality issues. In contrast, the virtual inertia, and damping that accompanies the use of the proposed modified VSM IC controller, eliminates these difficulties.
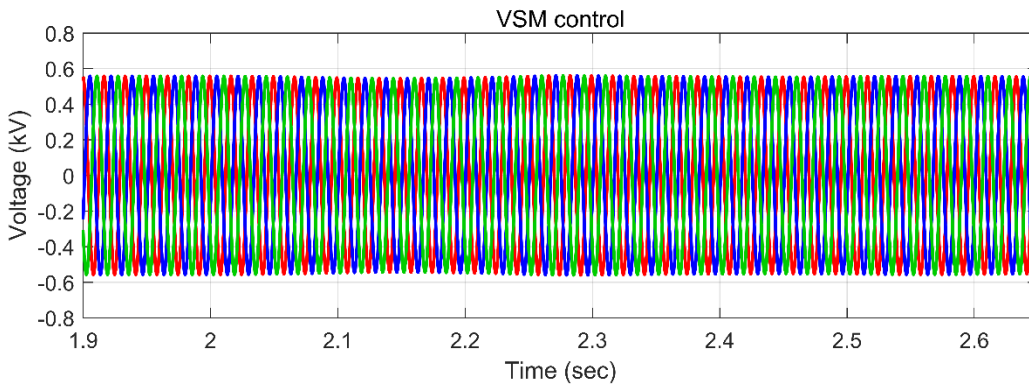
Figure 6-17: AC Voltage at the PCC with the VSM Control Concept.

6.4.3 Case 2: Hybrid AC/DC System Performance during an Outage of One IC

This case highlights the benefits of the proposed VSM IC controller over current control methods that employ just inner loop. Multiple ICs offer advantages similar to those provided by parallel transformers in a distribution system, including**:** increased availability of the electrical system during maintenance activities, increased power system reliability in the case of fault-initiated tripping, and easier load transportation.

At t = 6 sec as shown in Figure 6-18, Figure 6-19, and Figure 6-20, one of the ICs disconnected because of a schedule maintenance situation in both hybrid AC/DC systems. Overall system performance is still reliable, with respect to supplying the required load, and using a conventional current controller for just one IC decreased the AC voltage fluctuations. Nevertheless, for one or for multiple ICs, the proposed modified VSM controller is unaffected by this issue. At t = 9 sec, the IC is reconnected to the system when it is assumed that the schedule maintenance has been done. In this case, the IC based on a conventional current controller loses its synchronization and causes unstable operation for the entire hybrid AC/DC system, as illustrated in Figure 6.19. However, the proposed VSM controller has a unique self-synchronization feature, such that reconnecting the IC based on the VSM controller results in stable operation even in abnormal conditions. The Figure 6.20 indicates that the virtual inertia and damping creates a smooth transient response to the reconnection of the parallel ICs. It is apparent that the concept of parallel ICs increases overall system reliability and availability.
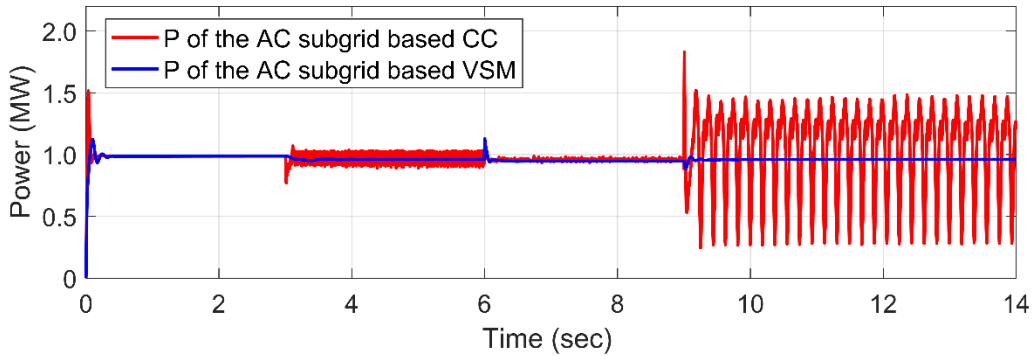
Figure 6-18: The Effect of Power Exchange on the AC Sub-system Load in the Case of Multiple ICs.
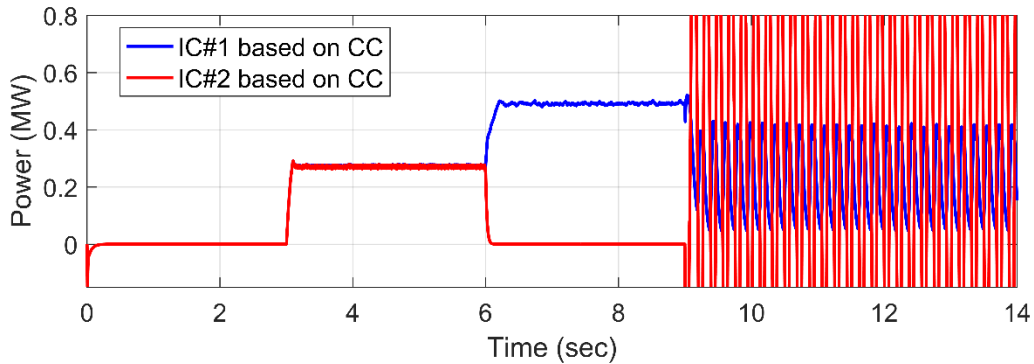
Figure 6-19: Power Supplied to the DC Sub-system via Parallel ICs based on CC.
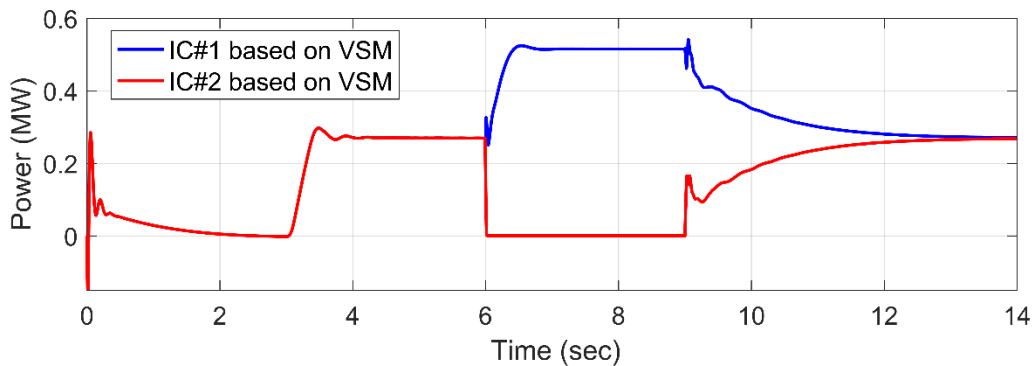
Figure 6-20: Power Supplied to the DC Sub-system via Parallel ICs based on VSM.

6.4.4 Case 3: Circulating Currents issue in Hybrid AC/DC System with Parallel ICs

The main issue examined in this case is the circulating current between the parallel ICs, which has been the subject of numerous published studies, whose goal was to minimize and mitigate this current [114]–[117]. This case involved the evaluation of two identical hybrid AC/DC systems consisting of parallel ICs. The IC controller of one of the hybrid systems was based on dual droop control using just the inner current loop, as proposed in [10], [25], and [30]. The ICs of the second hybrid system relied on the VSM control concept introduced in this paper.

In this case study, the operating conditions that were explained in case 1 were applied at t = 2 sec. the results show the existence of the circulating current during power exchange from the AC to the DC sub-system. As mentioned earlier, the components of the circulating current are namely cross and zero sequence circulating currents. The cross circulating current is defined as the current circulated between the AC side and the DC capacitor. On the other hand, the zero sequence circulating current is the current

105

flow from the AC PCC voltage to DC side PCC. Based on the outcome results, the cross circulating current is higher in comparison to the zero sequence circulating current. Figure 6.21 shows that the total cross circulating current based on the use of a current controller is about 2.5mA, but it is equal to zero when VSM controller is applied. The zero sequence circulating current is depicted in Figure 6.22 for both systems with different IC controller. Using just current controller for the IC produces almost 0.025 pA, compared to the VSM that equals to zero. It can be seen that with the current controller loop, the total power transfer fluctuates due to the sensitivity of the droop controller and the absence of the voltage controller, while the VSM IC control concept suppresses this effect.
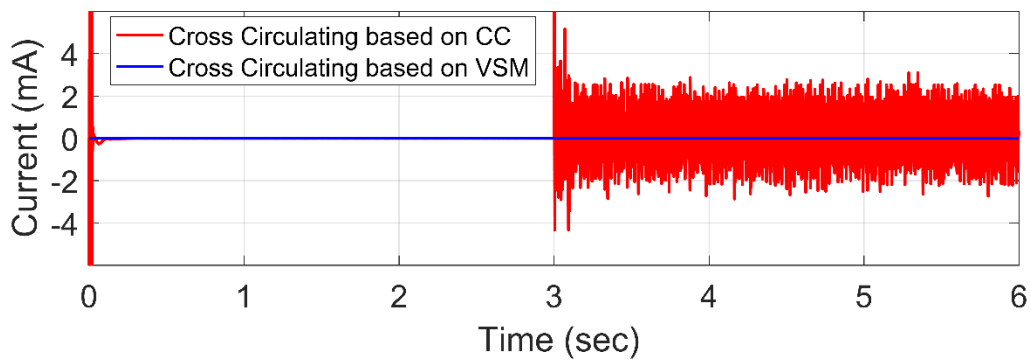
Figure 6-21: Circulating current between the ICs Shows Cross Circulating Current.
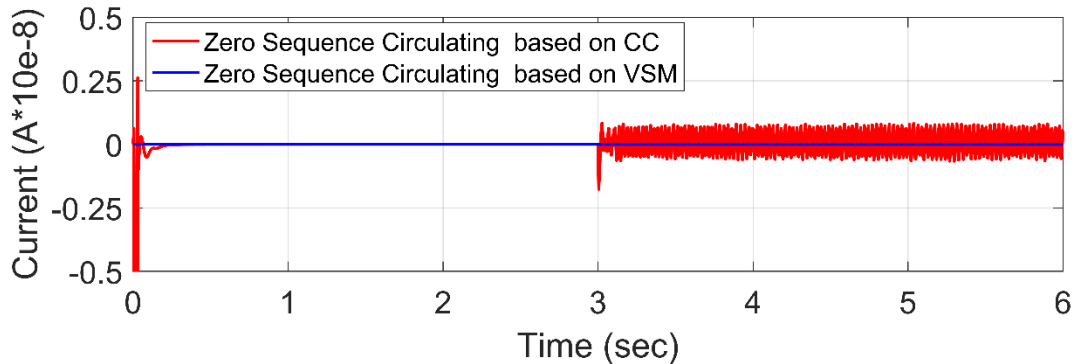
Figure 6-22: Circulating current between the ICs Shows Zero Sequence Circulating Current.

It is thus clear that using traditional current control of parallel ICs introduces more operational difficulties, such as voltage and current harmonics, as well as unbalanced AC voltage at the PCC due to the lack of inertia. The introduced IC controller based on a VSM control concept smooths out fluctuations and improves overall system performance. The benefits associated with the ability of a VSM control

106

algorithm to emulate the properties of traditional SMs in a hybrid AC/DC system mean that it offers greater efficiency, rather than just using current controller loop. As is evident from results, compared to the traditional current control methods reported in the literature, the introduced concept for controlling ICs uses virtual inertia and damping to prevent the development of a circulating current between the parallel ICs during power exchange from the AC into DC sub-system.

6.5 Conclusion

This chapter reveals operation issues associated with parallel ICs, and a novel control strategy application for multiple ICs in a hybrid AC/DC system. The usage of VSM control also provides self-synchronization when an IC is reconnected, following a short circuit or required scheduled maintenance. The work reported in this chapter involved the examination and comparison of two hybrid AC/DC systems with different IC control structures. The impact of the VSM control algorithms on a hybrid AC/DC system was validated using a test system which was simulated in a PSCAD/EMTDC environment. The system stability evaluation based on VSM control concept for IC is proposed as well as for IC based on the current controller. The results demonstrate that during variations in loading conditions, the VSM algorithm is more efficient than the current control method described in the literature, which is affected by the voltage-dependent load issue. Further, when the IC is reconnected following abnormal operating conditions, the performance offered by the VSM control concept is superior to that provided by previously reported controllers.

Chapter 7
Summary, Contributions, and Future

7.1 Summary

This thesis focused on the hybrid AC/DC microgrid modelling, design the controller for the IC, power sharing control for the IC based on VSM, and hybrid AC/DC microgrid stability. The motivations and the goal objectives of this thesis were presented in Chapter 1

In Chapter 2 relative background of the voltage source converter (VSC) control strategy and a literature survey reviews of the earlier work on hybrid ac/dc microgrid were discussed including several control concepts of VSM.

In Chapter 3 comprehensive assessment of virtual synchronous machine based voltage source converter controllers was introduced. Therefore, the most of VSM models in the literature were classified and evaluated based on the extra components required, in addition to VSC components to emulate the SM behaviour, simplicity algorithm to be implemented, and viability and stability during different operation conditions.

In Chapter 4 the benefit of a virtual synchronous machine (VSM) control strategy that mimics the properties of traditional synchronous machines in the hybrid AC/DC microgrid intertying converter was proposed. The proposed control application of VSM controller on the IC has shown better performance of the hybrid AC/DC microgrid via modified dual droop control characteristics. The most significant factor investigated in this chapter was the power exchange from the AC into the DC microgrid, and vice versa.

Chapter 5 has presented the development of the small-signal state-space model for the entire hybrid AC/DC microgrid to investigate the overall system stability under different operating points. The main benefit of the small-signal modelling is to present further investigation of the hybrid microgrid stability. Due to the fact that the behaviour of the hybrid AC/DC microgrid when it is subjected to a temporary disturbance is the main concern. In hybrid microgrid, the disturbances take place continuously because of the load changing endlessly. Satisfying the hybrid microgrid operation during the disturbances conditions was achieved in order to supply the demand. Furthermore, the power quality was another concern for the operation of a hybrid microgrid; which prefer for the hybrid microgrid to provide better response and less oscillatory behaviour. The efficient and desire performance of the hybrid microgrid were evaluated using

the linearized model of the hybrid microgrid. As a result, evaluating the eigenvalues and sensitivity modes of the hybrid microgrid were discussed due to its necessity of studying the control system stability.

Chapter 6 was revealed three serious issues of operating hybrid AC/DC microgrid; some of these issues are temporary take a place based on the system operating conditions. In hybrid AC/DC microgrid, an intertying converter (IC) becomes harmonics voltage source due to the antiparallel diodes and the shunt capacitor at its DC side. The nonlinearity behaviour of ICs was introduced another operation issue that was circulating current in case of parallel ICs. Reconnecting an IC after abnormal operation condition or schedule maintenance was required an extra challenging synchronization control due the variation of the AC subgrid voltages and frequency; which was the third issue. This chapter has proposed a solution for all these issues by developing a new control strategy that combines the VSM control concept with a dual based droop control.

7.2 Contributions

The main contributions of the research presented in this thesis are as follows:

- A comprehensive assessment of VSM control algorithms has been carried out. This study has presented the similarity of the equivalence of the low-order VSM control algorithm with high-order VSM control algorithm under different operation conditions. A key contribution in the study is the determination of the suitable choice of VSM control algorithm to be implemented and used for the hybrid AC/DC microgrid application.

- A novel control strategy for the Intertying converter in hybrid AC/DC microgrid was proposed to ensure the benefit of a virtual synchronous machine (VSM) control algorithm in the hybrid AC/DC microgrid. The VSM controller application was proposed to enable an IC converter to support the AC-side voltage and frequency as well as the DC-side voltage.

- Developing an autonomous operation control of the VSM intertying converter based on dual droop characteristics which is quite different compared to using only current controller. The autonomous operation of the intertying converter based on dual droop control is modified and proposed to be capable to feed the VSM controller (swing equation) to ensure accurate power exchange management between the AC and DC sub-systems.

- A generic small-signal state space model of the hybrid AC/DC microgrid system has been proposed, and built to carry out the stability analysis. The development of the small-signal state-space model for the entire hybrid AC/DC microgrid was developed to investigate the overall system stability under different operating points.

- The hybrid AC/DC microgrid performance with multiple ICs was investigated to achieve reliable operation. Due to the existence of the parallel ICs some serious operation issues and challenges have been revealed such as circulating currents. The developed VSM controller on the IC was solved these issues.

7.3 Direction of Future Work

Based on this thesis research, some research points require further future research work, as follows:

- The AC sub-system of the hybrid AC/DC microgrid in this thesis is considered as a balanced AC source, but it is important to study the system performance during unbalanced AC sub-system. Also the effect of the unbalance AC sub-system on the DC sub-system performance.

- Fault analysis is the most important aspect that must be considered and studied in both AC and DC sub-systems due to the existence of the DC circuit breakers in the market.

- Recently, there is a trend to consider the model productive control (MPC) strategy in the practical application due to its advantages that does not need any controller tuning. Therefore, MPC might be a good direction for future investigation of microgrid applications.

- Considering different load types such as pumping load, which might affect the AC sub-system performance and the overall system stability.

Bibliography

[1]   H. A. Alsiraji, "Cooperative Power Sharing control in Multi- terminal VSC-HVDC," University of Waterloo, 2014.

[2]   H. K. A. Alsiraji and E. F. El-saadany, "Cooperative autonomous control for active power sharing in multi-terminal VSC-HVDC," *Int. J. Process Syst. Eng.*, vol. 2, no. 4, pp. 303–319, 2014.

[3]   R.H. Lasseter, "MicroGrids," in *Power Engineering Society Winter Meeting*, 2002, pp. 305–308.

[4]   M. Davari and Y. A. R. I. Mohamed, "Robust multi-objective control of VSC-based DC-voltage power port in hybrid AC/DC multi-terminal micro-grids," *IEEE Trans. Smart Grid*, vol. 4, no. 3, pp. 1597–1612, 2013.

[5]   C. Wang, S. Member, K. Yuan, S. Member, and P. Li, "A Projective Integration Method for Transient Stability Assessment of Power Systems with a High Penetration of Distributed Generation," vol. 3053, no. c, 2016.

[6]   M. E. Baran and N. R. Mahajan, "DC distribution for industrial systems: opportunities and challenges," *IEEE Trans. Ind. Appl.*, vol. 39, no. 6, pp. 1596–1601, 2003.

[7]   X. L. X. Liu, P. W. P. Wang, and P. C. L. P. C. Loh, "A hybrid AC/DC micro-grid," in *IPEC, Conference Proceedings*, 2010, pp. 746–751.

[8]   F. Blaabjerg, P. C. Loh, D. Li, and Y. K. Chai, "Autonomous operation of ac–dc microgrids with minimised interlinking energy flow," *IET Power Electron.*, vol. 6, no. 8, pp. 1650–1657, 2013.

[9]   X. Liu, P. Wang, and P. C. Loh, "A hybrid AC/DC microgrid and its coordination control," *IEEE Trans. Smart Grid*, vol. 2, no. 2, pp. 278–286, 2011.

[10]   P. C. Loh, D. Li, Y. K. Chai, and F. Blaabjerg, "Hybrid AC-DC microgrids with energy storages and progressive energy flow tuning," *IEEE Trans. Power Electron.*, vol. 28, no. 4, pp. 1533–1543, 2013.

[11]   S. A. Arefifar, Y. A. R. I. Mohamed, and T. H. M. El-Fouly, "Optimum microgrid design for enhancing reliability and supply-security," *IEEE Trans. Smart Grid*, vol. 4, no. 3, pp. 1567–1575, 2013.

[12]   C. Gao, R. Yang, J. Jiao, and Z. Dou, "Power Control Strategy Design in an Islanded Microgrid Based on Virtual Frequency," in *Renewable Power Generation Conference*, 2013, pp. 3–6.

[13]   J. Driesen and F. Katiraei, "Design for distributed energy resources," *IEEE Power Energy Mag.*, vol. 6, no. 3, pp. 30–40, 2008.

[14]   O. Hafez and K. Bhattacharya, "Optimal planning and design of a renewable energy based supply

system for microgrids," *Renew. Energy*, vol. 45, pp. 7–15, 2012.

[15] J. G. Slootweg and W. L. Kling, "Impacts of distributed generation on power system transient stability," in *IEEE Power Engineering Society Summer Meeting*, 2002, vol. 2, pp. 862–867.

[16] Y. Chen, R. Hesse, D. Turschner, and H.-P. Beck, "Improving the grid power quality using virtual synchronous machines," in *International Conference on Power Engineering, Energy and Electrical Drives*, 2011, no. May, pp. 1–6.

[17] J. Liu, Y. Miura, and T. Ise, "Comparison of Dynamic Characteristics Between Virtual Synchronous Generator and Droop Control in Inverter-Based Distributed Generators," *IEEE Trans. Power Electron.*, vol. 31, no. 5, pp. 3600–3611, 2016.

[18] Y. Chen, R. Hesse, D. Turschner, and H. Beck, "Comparison of methods for implementing virtual synchronous machine on inverters," in *International Conference on Renewable Energies and Power Quality*, 2012, pp. 1–6.

[19] K. Lee, G. Venkataramanan, and T. M. Jahns, "Source current harmonic analysis of adjustable speed drives under input voltage unbalance and sag conditions," *IEEE Trans. Power Deliv.*, vol. 21, no. 2, pp. 567–576, 2006.

[20] N. Pogaku, M. Prodanović, and T. C. Green, "Modeling, Analysis and Testing of Autonomous Operation of an Inverter-Based Microgrid," *IEEE Trans. Power Electron.*, vol. 22, no. 2, pp. 613–625, 2007.

[21] E. Unamuno and J. A. Barrena, "Hybrid ac/dc microgrids - Part I: Review and classification of topologies," *Renew. Sustain. Energy Rev.*, vol. 52, pp. 1251–1259, 2015.

[22] D. J. Hammerstrom, "AC versus DC distribution systems-did we get it right?," in *2007 IEEE Power Engineering Society General Meeting, PES*, 2007, pp. 1–5.

[23] P. Wang, C. Jin, D. Zhu, Y. Tang, P. C. Loh, and F. H. Choo, "Distributed control for autonomous operation of a three-port ac/dc/ds hybrid microgrid," *IEEE Trans. Ind. Electron.*, vol. 62, no. 2, pp. 1279–1290, 2015.

[24] X. Liu, P. C. Loh, P. Wang, and F. Blaabjerg, "A Direct Power Conversion Topology for Grid Integration of Hybrid AC / DC Energy Resources," *IEEE Trans. Ind. Electron.*, vol. 60, no. 12, pp. 5696–5707, 2013.

[25] P. C. Loh, D. Li, Y. K. Chai, and F. Blaabjerg, "Autonomous control of interlinking converter with energy storage in hybrid AC-DC microgrid," *IEEE Trans. Ind. Appl.*, vol. 49, no. 3, pp. 1374–1382, 2013.

[26] J. M. Guerrero, P. C. Loh, T. L. Lee, and M. Chandorkar, "Advanced control architectures for

intelligent microgridsPart II: Power quality, energy storage, and AC/DC microgrids," *IEEE Trans. Ind. Electron.*, vol. 60, no. 4, pp. 1263–1270, 2013.

[27] M. Guan, W. Pan, J. Zhang, and Q. Hao, "Synchronous Generator Emulation Control Strategy for Voltage Source Converter (VSC) Stations," *IEEE Trans. POWER Syst.*, vol. 30, no. 1, pp. 1–9, 2015.

[28] Y. A. R. I. Mohamed and E. F. El-Saadany, "Adaptive decentralized droop controller to preserve power sharing stability of paralleled inverters in distributed generation microgrids," *IEEE Trans. Power Electron.*, vol. 23, no. 6, pp. 2806–2816, 2008.

[29] P. C. Loh, D. Li, Y. K. Chai, and F. Blaabjerg, "Autonomous operation of hybrid microgrid with ac and dc subgrids," *IEEE Trans. Power Electron.*, vol. 28, no. 5, pp. 2214–2223, 2013.

[30] A. A. A. Radwan and Y. A. R. I. Mohamed, "Networked Control and Power Management of AC/DC Hybrid Microgrids," *IEEE Syst. J.*, pp. 1–12, 2014.

[31] P. C. Loh and F. Blaabjerg, "Autonomous Operation of Hybrid Microgrid with AC and DC Sub-Grids Keywords," in *Proceedings of the 2011 14th European Conference on Power Electronics and Applications*, 2011, pp. 1–10.

[32] M. Albu, M. Calin, D. Federenciuc, and J. Diaz, "The measurement layer of the Virtual Synchronous Generator operation in the field test," in *2011 IEEE International Workshop on Applied Measurements for Power Systems, AMPS 2011 - Proceedings*, 2011, pp. 85–89.

[33] A. Kahrobaeian and Y. Ibrahim, "Mitigation of Low-Frequency Oscillations in Autonomous Converter-Based Micro-Grids with Induction Motor Load," *IEEE Trans. Ind. Electron.*, vol. 61, no. 4, pp. 1–1, 2013.

[34] S. G. Johansson, G. Asplund, E. Jansson, and R. Roberto, "Power System Stability Benefits with VSC DC-Transmission Systems," in *CIGRE Conference*, 2004, pp. 1–8.

[35] V. Sood, F. Ieee, H. Patel, and S. M. Ieee, "Comparison between Direct and Vector control Strategy for VSC-HVDC system in EMTP-RV," in *Power Electronics, Drives and Energy Systems (PEDES)*, 2010, pp. 1–6.

[36] L. Herman, I. Papic, and B. Blazic, "A Proportional-Resonant Current Controller for Selective Harmonic Compensation in a Hybrid Active Power Filter," *IEEE Trans. Power Deliv.*, vol. 29, no. 5, pp. 2055–2065, 2014.

[37] N. Bianchi and M. Dai Pre, "Active power filter control using neural network technologies," in *IEE Proceedings-Electric Power Applications*, 2003, vol. 150, no. 2, pp. 139–145.

[38] A. Dekka, R. Ghaffari, B. Venkatech, and B. Wu, "A Survey on Energy Storage Technologies in

Power Systems," *IEEE Electr. Power Energy Conf.*, 2015.

[39]   A. A. A. Radwan and Y. A. R. I. Mohamed, "Bidirectional Power Management in Hybrid AC-DC Islanded Microgrid System," in *IEEE PES General Meeting, Conference & Exposition*, 2014, pp. 1–5.

[40]   L. Zhang, L. Harnefors, and H. P. Nee, "Power-synchronization control of grid-connected voltage-source converters," *IEEE Trans. Power Syst.*, vol. 25, no. 2, pp. 809–820, 2010.

[41]   A. Ge, J. Wan, Z. Niu, and L. Bin, "Research on current feed forward decoupling control for energy feedback and grid-connected device," in *Power Electronics Systems and Applications*, 2011, pp. 1–6.

[42]   M. Mirjana and A. Goran, "Decoupling Current Control and Maximum Power Point Control in Small Power Network with Photovoltaic Source," in *IEEE PES Power Systems Conference and Exposition*, 2006.

[43]   S. D'Arco, J. A. Suul, and O. B. Fosso, "Small-signal modeling and parametric sensitivity of a virtual synchronous machine in islanded operation," *Electr. Power Energy Syst.*, vol. 72, pp. 3–15, 2015.

[44]   A. Manoloiu, H. A. Pereira, R. Teodorescu, M. Bongiorno, M. Eremia, and S. R. Silva, "Comparison of PI and PR current controllers applied on two-level VSC-HVDC transmission system," in *2015 IEEE Eindhoven PowerTech*, 2015, vol. 2, pp. 1–5.

[45]   J. M. Guerrero, J. Matas, L. G. De Vicuña, M. Castilla, and J. Miret, "Wireless-control strategy for parallel operation of distributed-generation inverters," *IEEE Trans. Ind. Electron.*, vol. 53, no. 5, pp. 1461–1470, 2006.

[46]   S. D. Arco, J. A. Suul, and O. B. Fosso, "Automatic Tuning of Cascaded Controllers for Power Converters Using Eigenvalue Parametric Sensitivities," *IEEE Trans. Ind. Appl.*, vol. 51, no. 2, pp. 1743–1753, 2015.

[47]   "IEEE Standard for Interconnecting Distributed Resources with Electric Power Systems," *IEEE Standard 1547*, no. July, pp. 1–27, 2003.

[48]   L. Zhang, H. P. Nee, and L. Harnefors, "Analysis of stability limitations of a VSC-HVDC link using power-synchronization control," *IEEE Trans. Power Syst.*, vol. 26, no. 3, pp. 1326–1337, 2011.

[49]   G. Eirea and S. R. Sanders, "Adaptive output current feedforward control in VR applications," *PESC Rec. - IEEE Annu. Power Electron. Spec. Conf.*, vol. 23, no. 4, pp. 9–14, 2007.

[50]   F. Luo, Y. M. Lai, K. H. Loo, C. K. Tse, and X. Ruan, "A generalized droop-control scheme for

decentralized control of inverter-interfaced microgrids," in *Proceedings - IEEE International Symposium on Circuits and Systems*, 2013, pp. 1320–1323.

[51]   C. Li, P. Zhan, J. Wen, M. Yao, N. Li, and W. J. Lee, "Offshore wind farm integration and frequency support control utilizing hybrid multiterminal HVDC transmission," in *in Industry Applications Society Annual Meeting*, 2013, pp. 1–9.

[52]   Anand;Sandeep and F. G., "Reduced-Order Model and Stability Analysis of Low-Voltage DC Microgrid," *IEEE Trans. Ind. Electron.*, vol. 60, no. 11, pp. 5040–5049, 2013.

[53]   F. Katiraei, M. R. Iravani, and P.W. Lehn, "Small-signal dynamic model of a micro-grid including conventional and electronically interfaced distributed resources," *IET Gener. Transm. Distrib.*, vol. 1, no. 3, pp. 369–378, 2007.

[54]   A. Mohamed, V. Salehi, and O. Mohammed, "Real-Time Energy Management Algorithm for Mitigation of Pulse Loads in Hybrid Microgrids," *IEEE Trans. Smart Grid*, vol. 3, no. 4, pp. 1911–1922, 2012.

[55]   Y. Chen, R. Hesse, D. Turschner, and H. P. Beck, "Investigation of the virtual synchronous machine in the island mode," in *IEEE PES Innovative Smart Grid Technologies Conference Europe*, 2012, pp. 1–6.

[56]   H. Bevrani, T. Ise, and Y. Miura, "Virtual synchronous generators: A survey and new perspectives," *Int. J. Electr. Power Energy Syst.*, vol. 54, no. 1, pp. 244–254, Jan. 2014.

[57]   T. Shintai, Y. Miura, and T. Ise, "Oscillation damping of a distributed generator using a virtual synchronous generator," *IEEE Trans. Power Deliv.*, vol. 29, no. 2, pp. 668–676, 2014.

[58]   M. P. N. Van Wesenbeeck, S. W. H. De Haan, P. Varela, and K. Visscher, "Grid tied converter with virtual kinetic storage," in *IEEE Bucharest PowerTech Conference*, 2009, no. 1, pp. 1–7.

[59]   V. Van Thong, A. Woyte, M. Albu, M. Van Hest, J. Bozelie, J. Diaz, T. Loix, D. Stanculescu, and K. Visscher, "Virtual synchronous generator: Laboratory scale results and field demonstration," in *IEEE Bucharest PowerTech Conference*, 2009, pp. 1–6.

[60]   M. Torres and L. a C. Lopes, "Virtual synchronous generator control in autonomous wind-diesel power systems," in *IEEE Electrical Power and Energy Conference*, 2009, no. 1, pp. 1–6.

[61]   H. Alsiraji Alrajhi and R. El-Shatshat, "Comprehensive Assessment of Virtual Synchronous Machine Based Voltage Source Converter Controllers," *IET Gener. Transm. Distrib.*, 2017.

[62]   J. Alipoor, Y. Miura, and T. Ise, "Power System Stabilization Using Virtual Synchronous Generator With Alternating Moment of Inertia," *IEEE J. Emerg. Sel. Top. POWER Electron.*, vol. 3, no. 2, pp. 451–458, 2015.

[63] H. P. Beck and R. Hesse, "Virtual synchronous machine," in *9th International Conference on Electrical Power Quality and Utilisation, EPQU*, 2007, pp. 1–6.

[64] Y. Chen, R. Hesse, D. Turschner, and H. Beck, "Dynamic Properties of the Virtual Synchronous Machine (VISMA)," in *Proc. ICREPQ*, 2011, pp. 1–5.

[65] R. Hesse, D. Turschner, and H. Beck, "Micro grid stabilization using the Virtual Synchronous Machine (VISMA)," in *International Conference on Renewable Energies and Power Quality*, 2009, pp. 1–6.

[66] Q. C. Zhong and G. Weiss, "Synchronverters: Inverters that mimic synchronous generators," *IEEE Trans. Ind. Electron.*, vol. 58, no. 4, pp. 1259–1267, 2011.

[67] E. Brown and George Weiss, "Using synchronverters for power grid stabilization," in *Convention of Electrical and Electronics Engineers in Israel*, 2014, pp. 1–5.

[68] S. Dong, Y. Chi, and Y. Li, "Active voltage feedback control for hybrid multiterminal HVDC system adopting improved synchronverters," *IEEE Trans. Power Deliv.*, vol. 31, no. 2, pp. 445–455, 2016.

[69] S. D. Arco and J. A. Suul, "Virtual Synchronous Machines – Classification of Implementations and Analysis of Equivalence to Droop Controllers for Microgrids," in *PowerTech*, 2013, pp. 1–7.

[70] J. O. Tande, "On Inertial Dynamics of Virtual-Synchronous-Controlled DFIG-Based Wind Turbines," *IEEE Trans. ENERGY Convers.*, vol. 30, no. 4, pp. 1691–1702, 2015.

[71] S. Wang, J. Hu, and X. Yuan, "Virtual Synchronous Control for Grid-Connected DFIG-Based Wind Turbines," *IEEE J. Emerg. Sel. Top. Power Electron.*, vol. 3, no. 4, pp. 932–944, 2015.

[72] S. D. Arco and J. A. Suul, "Equivalence of Virtual Synchronous Machines and Frequency-Droops for Converter-Based MicroGrids," *IEEE Trans. Smart Grid*, vol. 5, no. 1, pp. 394–395, 2014.

[73] S. D. Arco, J. Are, and O. B. Fosso, "A Virtual Synchronous Machine implementation for distributed control of power converters in SmartGrids," *Electr. Power Syst. Res.*, vol. 122, pp. 180–197, 2015.

[74] N. Soni and S. Doolla, "Inertia Design Methods for Islanded Microgrids having Static and Rotating Energy Sources," *IEEE Trans. Ind. Appl.*, vol. PP, no. 99, pp. 1–10, 2016.

[75] M. Yu, A. J. Roscoe, C. D. Booth, A. Dy, and R. Ierna, "Use of an Inertia-less Virtual Synchronous Machine within Future Power Networks with High Penetrations of Converters," in *Power Systems Computation Conference (PSCC)*, 2016, pp. 1–7.

[76] J. A. Suul, S. D. Arco, and G. Guidi, "Virtual Synchronous Machine-Based Control of a Single-Phase Bi-Directional Battery Charger for Providing Vehicle-to-Grid Services," *IEEE Trans. Ind.*

Appl., vol. 52, no. 4, pp. 3234–3244, 2016.

[77] M. Guan, W. Pan, J. Zhang, Q. Hao, J. Cheng, and X. Zheng, "Synchronous Generator Emulation Control Strategy for Voltage Source Converter (VSC) Stations," *IEEE Trans. Power Syst.*, vol. 30, no. 6, pp. 3093–3101, 2015.

[78] A. H. Etemadi and R. Iravani, "Supplementary mechanisms for smooth transition between control modes in a microgrid," *Electr. Power Syst. Res.*, vol. 142, pp. 249–257, 2017.

[79] J. Machowski, J. W. Bialek, and J. R. Bumby, *POWER SYSTEM DYNAMICS Stability and Control*, Second Edi. Wiley, 2008.

[80] N. Mohan, T. Undeland, and W. Robbins, *Power Electronics: Converters, Applications, and Design*, 3rd ed. John Wiley & Sons, Inc, 2013.

[81] T. Hoevenaars, P. Eng, K. Ledoux, W. Little, and Y. Rd, "Interpreting IEEE Std 519 and Meeting its Harmonic Limits in VFD Applications," in *Proceedings of the IEEE Industry Applications Society 50th Annual Petroleum and Chemical Industry Conference*, 2003, pp. 1–6.

[82] J. C. Das, *Power system analysis: short-circuit load flow and harmonics*, vol. 22. CRC Press, 2002.

[83] P. Pillay and M. Manyage, "Definitions of voltage unbalance," *IEEE Power Eng. Rev.*, vol. 22, no. 11, pp. 49–50, 2002.

[84] M. a Hannan, A. Mohamed, and A. Hussain, "Dynamic Phasor Modeling and EMT Simulation of USSC," in *Proceedings of the World Congress on Engineering and Computer Science*, 2009, vol. I, pp. 1–7.

[85] H. A. Alsiraji, R. ElShatsha, and A. A. Radwan, "A Novel Control Strategy for the Interlinking Converter in Hybrid Microgrid," in *Proc. IEEE PES General Meeting*, 2017, pp. 1–5.

[86] H. Alrajhi Alsiraji, A. A. Radwan, and R. El-Shatshat, "Modelling and Analysis of a Synchronous Machine-Emulated Active Intertying Converter in Hybrid AC/DC Microgrids," *IET Gener. Transm. Distrib.*, 2018.

[87] I. Serban and C. Marinescu, "Control strategy of three-phase battery energy storage systems for frequency support in microgrids and with uninterrupted supply of local loads," *IEEE Trans. Power Electron.*, vol. 29, no. 9, pp. 5010–5020, 2014.

[88] F. Teng and G. Strbac, "Assessment of the Role and Value of Frequency Response Support from Wind Plants," *IEEE Trans. Sustain. Energy*, vol. 7, no. 2, pp. 586–595, 2016.

[89] A. A. A. Radwan and Y. A. I. Mohamed, "Assessment and Mitigation of Interaction Dynamics in Hybrid AC / DC Distribution Generation Systems," *IEEE Trans. Smart Grid*, vol. 3, no. 3, pp. 1382–1393, 2012.

[90]   C. Cho, J. H. Jeon, J. Y. Kim, S. Kwon, K. Park, and S. Kim, "Active synchronizing control of a microgrid," *IEEE Trans. Power Electron.*, vol. 26, no. 12, pp. 3707–3719, 2011.

[91]   J. Driesen, T. Green, T. Van Craenenbroeck, and R. Belmans, "The development of power quality markets," *2002 IEEE Power Eng. Soc. Winter Meet. Conf. Proc. (Cat. No.02CH37309)*, vol. 1, no. c, pp. 262–267, 2002.

[92]   H. Alrajhi Alsiraji, A. A. Radwan, and R. El-Shatshat, "Modeling and Analysis of a Synchronous Machine-Emulated Active Intertying Converter in Hybrid AC/DC Microgrids," *IET Gener. Transm. Distrib.*, 2018.

[93]   Y. Xia, Y. Peng, P. Yang, M. Yu, and W. Wei, "Distributed Coordination Control for Multiple Bidirectional Power Converters in a Hybrid AC/DC Microgrid," *IEEE Trans. Power Electron.*, vol. PP, no. 99, pp. 1–10, 2016.

[94]   C. Wan, M. Huang, C. K. Tse, S. C. Wong, and X. Ruan, "Nonlinear behavior and instability in a three-phase boost rectifier connected to a nonideal power grid with an interacting load," *IEEE Trans. Power Electron.*, vol. 28, no. 7, pp. 3255–3265, 2013.

[95]   X. Zhuang, L. Rui, Z. Hui, X. Dianguo, and C. H. Zhang, "Control of Parallel Multiple Converters for Direct-Drive Permanent-MagnetWind Power Generation Systems," *IEEE Trans. POWER Electron.*, vol. 27, no. 3, pp. 1259–1270, 2012.

[96]   M. Narimani and G. Moschopoulos, "Improved method for paralleling reduced switch VSI modules: Harmonic content and circulating current," *IEEE Trans. Power Electron.*, vol. 29, no. 7, pp. 3308–3317, 2014.

[97]   R. Teixeira Pinto, P. Bauer, S. F. Rodrigues, E. J. Wiggelinkhuizen, J. Pierik, and B. Ferreira, "A novel distributed direct-voltage control strategy for grid integration of offshore wind energy systems through MTDC network," *IEEE Trans. Ind. Electron.*, vol. 60, no. 6, pp. 2429–2441, 2013.

[98]   H. Bevrani, T. Ise, and Y. Miura, "Virtual synchronous generators: A survey and new perspectives," *Int. J. Electr. Power Energy Syst.*, vol. 54, pp. 244–254, 2014.

[99]   M. Hamzeh, A. Ghazanfari, H. Mokhtari, and H. Karimi, "Integrating hybrid power source into an Islanded MV microgrid using CHB multilevel inverter under unbalanced and nonlinear load conditions," *IEEE Trans. Energy Convers.*, vol. 28, no. 3, pp. 643–651, 2013.

[100] U. Borup, P. N. Enjeti, and F. Blaabjerg, "A new space-vector-based control method for UPS systems powering nonlinear and unbalanced loads," *IEEE Trans. Ind. Appl.*, vol. 37, no. 6, pp. 1864–1870, 2001.

[101] M. Hamzeh, S. Emamian, H. Karimi, and J. Mahseredjian, "Robust Control of an Islanded

Microgrid Under Unbalanced and Nonlinear Load Conditions," *IEEE J. Emerg. Sel. Top. Power Electron.*, vol. 4, no. 2, pp. 512–520, 2016.

[102] M. B. Delghavi and A. Yazdani, "Islanded-Mode Control of Electronically Coupled Distributed-Resource Units Under Unbalanced and Nonlinear Load Conditions," *IEEE Trans. POWER Deliv.*, vol. 26, no. 2, pp. 661–673, 2011.

[103] U. Borup, F. Blaabjerg, and P. N. Enjeti, "Sharing of nonlinear load in parallel-connected three-phase converters," *IEEE Trans. Ind. Appl.*, vol. 37, no. 6, pp. 1817–1823, 2001.

[104] B. Wei, J. M. Guerrero, J. C. Vásquez, and X.-Q. Guo, "A Circulating-Current Suppression Method for Parallel Connected Voltage Source Inverters (VSI) with Common DC and AC Buses," *IEEE Trans. Ind. Appl.*, vol. PP, no. 99, pp. 1–11, 2016.

[105] S. D'Arco and J. A. Suul, "Equivalence of Virtual Synchronous Machines and Frequency-Droops for Converter-Based MicroGrids," *IEEE Trans. Smart Grid*, vol. 5, no. 1, pp. 394–395, 2014.

[106] E. F. Fuchs and M. A. S. Masoum, *Power quality in power systems and electrical machines*, 1st ed. Academic Press/Elsevier, 2008.

[107] R. C. Dugan, S. McGranaghan, Mark F. Santoso, and H. W. Beaty, *Electrical Power System Quality*, 2nd ed. Tata McGraw-Hill Education, 2012.

[108] T. Kataoka, Y. Fuse, D. Nakajima, and S. Nishikata, "A three-phase voltage-type PWM rectifier with the function of an active power filter," in *2000 Eighth International Conference on Power Electronics and Variable Speed Drives (IEE Conf. Publ. No. 475)*, 2000, pp. 1–6.

[109] B. Bennett, "Unbalanced voltage supply The damaging effects on three phase induction motors and rectifiers," *ABB Power Conditioning – Electrification Products Division*, Napier, New Zealand, pp. 1–5, 2017.

[110] M. B. Delghavi and A. Yazdani, "Islanded-mode control of electronically coupled distributed-resource units under unbalanced and nonlinear load conditions," *IEEE Trans. Power Deliv.*, vol. 26, no. 2, pp. 661–673, 2011.

[111] L. Arachchige, "Determination of Requirements for Smooth Operating Mode Transition and Development of a Fast Islanding Detection Technique for Microgrids," University of Manitoba, PhD thesis, 2012.

[112] M. Amin, A. Ardal, and M. Molinas, "Self-synchronisation of Wind Farm in MMC-based HVDC System: A Stability Investigation," *IEEE Trans. Energy Convers.*, vol. 32, no. 2, pp. 458–470, 2017.

[113] C. A. C. M, "Power/energy: Automated power distribution: Increasingly diverse and complex

power operation and distribution systems will mean a larger role for microprocessor and communications technologies," *IEEE Spectr.*, vol. 19, no. 4, pp. 55–60, 1982.

[114]   J. S. Siva Prasad and G. Narayanan, "Minimization of grid current distortion in parallel-connected converters through carrier interleaving," *IEEE Trans. Ind. Electron.*, vol. 61, no. 1, pp. 76–91, 2014.

[115]   S. Augustine, M. K. Mishra, and N. Lakshminarasamma, "Adaptive droop control strategy for load sharing and circulating current minimization in low-voltage standalone DC microgrid," *IEEE Trans. Sustain. Energy*, vol. 6, no. 1, pp. 132–141, 2015.

[116]   Z. Ye, P. K. Jain, and P. C. Sen, "Circulating current minimization in high-frequency AC power distribution architecture with multiple inverter modules operated in parallel," *IEEE Trans. Ind. Electron.*, vol. 54, no. 5, pp. 2673–2687, 2007.

[117]   L. Yi-Hung and C. Hung Chi, "Simplified PWM With Switching Constraint Method to Prevent Circulating Currents for Paralleled Bidirectional AC/DC Converters in Grid-Tied System Using Graphic Analysis," *Ind. Electron. IEEE Trans.*, vol. 62, no. 7, pp. 4573–4586, 2015.

Appendix A

Small Signal Model of AC/DC Converter

LCL Power Circuit:

$$\frac{dil_d}{dt} = -\frac{Rf}{Lf}.il_d + w.il_q + \frac{1}{Lf}vi_d - \frac{1}{Lf}vo_d$$

$$\frac{dil_q}{dt} = -\frac{Rf}{Lf}.il_q - w.il_d + \frac{1}{Lf}vi_q - \frac{1}{Lf}vo_q$$

$$\frac{dvo_d}{dt} = w.vo_q + \frac{1}{Cf}il_d - \frac{1}{Cf}io_d$$

$$\frac{dvo_q}{dt} = -w.vo_d + \frac{1}{Cf}il_q - \frac{1}{Cf}io_q$$

$$\frac{dio_d}{dt} = \frac{1}{Lc}vo_d - \frac{1}{Lc}vb_d - \frac{Rc}{Lc}.io_d + w.io_q$$

$$\frac{dio_q}{dt} = \frac{1}{Lc}vo_q - \frac{1}{Lc}vb_q - \frac{Rc}{Lc}.io_q - w.io_d$$
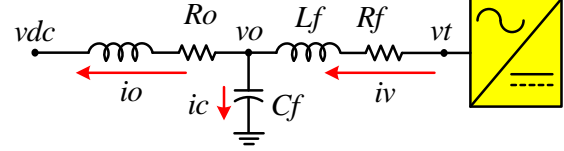
AC/DC Converter

$$
\begin{bmatrix} \dot{il}_d \\ \dot{il}_q \\ \dot{vo}_d \\ \dot{vo}_q \\ \dot{io}_d \\ \dot{io}_q \end{bmatrix} =
\begin{bmatrix}
-R_f/L_f & w & -1/L_f & 0 & 0 & 0 \\
-w & -R_f/L_f & 0 & -1/L_f & 0 & 0 \\
1/C_f & 0 & 0 & w & -1/CL_f & 0 \\
0 & 1/C_f & -w & 0 & 0 & -1/CL_f \\
0 & 0 & 1/L_f & 0 & -R_o/L_o & w \\
0 & 0 & 0 & 1/CL_f & -w & -R_o/L_o
\end{bmatrix}
\begin{bmatrix} il_d \\ il_q \\ vo_d \\ vo_q \\ io_d \\ io_q \end{bmatrix} +
\begin{bmatrix}
1/Lf & 0 \\
0 & 1/Lf \\
0 & 0 \\
0 & 0 \\
0 & 0 \\
0 & 0
\end{bmatrix}
\begin{bmatrix} \Delta vi_d \\ \Delta vi_q \end{bmatrix}
$$

$$
+ \begin{bmatrix}
0 & 0 \\
0 & 0 \\
0 & 0 \\
0 & 0 \\
-1/Lf & 0 \\
0 & -1/Lf
\end{bmatrix}
\begin{bmatrix} \Delta vb_d \\ \Delta vb_q \end{bmatrix} +
\begin{bmatrix}
il_q \\
-il_d \\
vo_q \\
-vo_d \\
io_q \\
-io_d
\end{bmatrix} [\Delta w]
$$

$$[\dot{x}_{LCL}] = [A_{LCL}][\Delta x_p] + [B1_{LCL}]\begin{bmatrix} \Delta vi_d \\ \Delta vi_q \end{bmatrix} + [B2_{LCL}][\Delta w]$$

Voltage Controller:

$$il_d^* = H(io_d) - w_nC_f\big(vo_q\big) + K_{pv}(vo_d^* - vo_d) + \frac{K_{iv}}{s}(vo_d^* - vo_d)$$

$$il_q^* = H\big(io_q\big) + w_nC_f(vo_d) + K_{pv}\big(vo_q^* - vo_q\big) + \frac{K_{iv}}{s}\big(vo_q^* - vo_q\big)$$

$$\vartheta_{vd} = \frac{1}{s}(vo_d^* - vo_d)$$

$$\vartheta_{vq} = \frac{1}{s}\big(vo_q^* - vo_q\big)$$

$$il_d^* = H(io_d) - w_nC_f\big(vo_q\big) + K_{pv}(vo_d^* - vo_d) + K_{iv}\vartheta_{vd}$$

$$il_q^* = H\big(io_q\big) + w_nC_f(vo_d) + K_{pv}\big(vo_q^* - vo_q\big) + K_{iv}\vartheta_{vq}$$

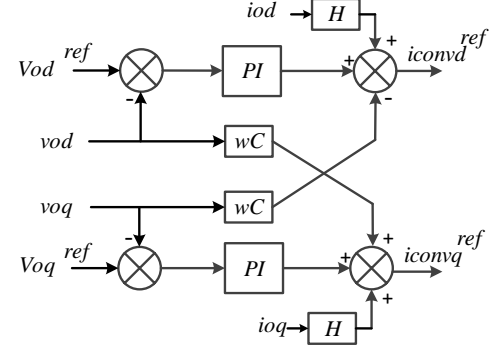$$\begin{bmatrix} \Delta\dot\vartheta_{vd} \\ \Delta\dot\vartheta_{vq} \end{bmatrix} = \begin{bmatrix} 0 & 0 \\ 0 & 0 \end{bmatrix}\begin{bmatrix} \Delta\vartheta_{vd} \\ \Delta\vartheta_{vq} \end{bmatrix} + \begin{bmatrix} K_{iv} & 0 \\ 0 & K_{iv} \end{bmatrix}\begin{bmatrix} \Delta vo_d^* \\ \Delta vo_q^* \end{bmatrix} + \begin{bmatrix} -K_{iv} & 0 \\ 0 & -K_{iv} \end{bmatrix}\begin{bmatrix} \Delta vo_d \\ \Delta vo_q \end{bmatrix}$$

$$\begin{bmatrix} \Delta il_d^* \\ \Delta il_q^* \end{bmatrix} = \begin{bmatrix} 1 & 0 \\ 0 & 1 \end{bmatrix}\begin{bmatrix} \Delta\vartheta_{vd} \\ \Delta\vartheta_{vq} \end{bmatrix} + \begin{bmatrix} K_{pv} & 0 \\ 0 & K_{pv} \end{bmatrix}\begin{bmatrix} \Delta vo_d^* \\ \Delta vo_q^* \end{bmatrix} + \begin{bmatrix} 0 & 0 & H & 0 & -K_{pv} & -wCf \\ 0 & 0 & 0 & H & wCf & -K_{pv} \end{bmatrix}[\Delta x_p]$$

$$[\dot\vartheta_v] = [0][\Delta\vartheta_v] + [Bv_1][\Delta vo^*] + [Bv_2][\Delta x_{p1}]$$

$$[\Delta il^*] = [Cv][\Delta\vartheta_v] + [Dv_1][\Delta vo^*] + [Dv_2][\Delta x_{p1}]$$

Current Controller:

$$vi_d^* = vo_d - w_nL_f\big(il_q\big) + K_{pc}(il_d^* - il_d) + \frac{K_{ic}}{s}(il_d^* - il_d)$$

$$vi_q^* = vo_q + w_nL_f(il_d) + K_{pc}\big(il_q^* - il_q\big) + \frac{K_{ic}}{s}\big(il_q^* - il_q\big)$$

$$\gamma_{cd} = \frac{1}{s}\big(il_q^* - il_q\big)$$

$$\gamma_{cq} = \frac{1}{s}\big(il_q^* - il_q\big)$$

$$vi_d^* = -w_nL_f\big(il_q\big) + K_{pc}(il_d^* - il_d) + K_{ic}\gamma_{vd} + vo_d$$

$$vi_q^* = +w_nL_f(il_d) + K_{pc}\big(il_q^* - il_q\big) + K_{ic}\gamma_{vq} + vo_q$$

$$\begin{bmatrix} \Delta\dot\vartheta_{vd} \\ \Delta\dot\vartheta_{vq} \end{bmatrix} = \begin{bmatrix} 0 & 0 \\ 0 & 0 \end{bmatrix}\begin{bmatrix} \Delta\gamma_{cd} \\ \Delta\gamma_{vq} \end{bmatrix} + \begin{bmatrix} K_{ic} & 0 \\ 0 & K_{ic} \end{bmatrix}\begin{bmatrix} \Delta vo_d^* \\ \Delta vo_q^* \end{bmatrix} + \begin{bmatrix} -K_{ic} & 0 \\ 0 & -K_{ic} \end{bmatrix}\begin{bmatrix} \Delta vo_d \\ \Delta vo_q \end{bmatrix}$$

$$\begin{bmatrix} \Delta il_d^* \\ \Delta il_q^* \end{bmatrix} = \begin{bmatrix} 1 & 0 \\ 0 & 1 \end{bmatrix}\begin{bmatrix} \Delta\gamma_{cd} \\ \Delta\gamma_{vq} \end{bmatrix} + \begin{bmatrix} K_{pc} & 0 \\ 0 & K_{pc} \end{bmatrix}\begin{bmatrix} \Delta vo_d^* \\ \Delta vo_q^* \end{bmatrix} + \begin{bmatrix} -K_{pc} & -wL_f & 0 & 0 & 1 & 0 \\ wL_f & -K_{pc} & 0 & 0 & 0 & 1 \end{bmatrix}[\Delta x_p]$$

$$[\dot\vartheta_c] = [0][\Delta\vartheta_c] + [Bc_1][\Delta vo^*] + [Bc_2][\Delta x_{p1}]$$

$$[\Delta il^*] = [Cc][\Delta\vartheta_v] + [Dc_1][\Delta vo^*] + [Dc_2][\Delta x_{p1}]$$
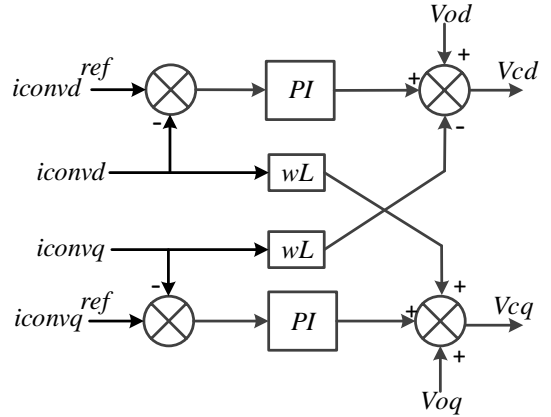
Power Controller:

$$\dot{P} = \left(\frac{\omega_c}{s + \omega_c}\right)\left((vo_d . io_d) + (vo_q . io_q)\right)$$

$$\dot{Q} = \left(\frac{\omega_c}{s + \omega_c}\right)\left((vo_d . io_q) - (vo_q . io_d)\right)$$

$$\omega^* = \omega_n - m_p P \quad \Rightarrow \quad \Delta\omega^* = -m_p \Delta P$$

$$V^* = V_n - n_q Q \quad \Rightarrow \quad \Delta V^* = -n_q \Delta Q$$

$$\theta = \frac{1}{s} w^* = \delta$$

$$\dot{\delta} = (\omega^* - \omega_{com}) \quad \Rightarrow \quad \left(\omega_n - m_p P - \omega_{com}\right) \quad \Rightarrow \quad \Delta\delta = -m_p \Delta P - \Delta\omega_{com}$$

$$\dot{P} = \left(\frac{3}{2}\right)\left(\omega_c\left((vo_d . io_d) + (vo_q . io_q) - P\right)\right) \quad \Rightarrow$$

$$\Delta\dot{P} = \left(\frac{3}{2}\right)(\omega_c \Delta vo_d . io_d) + (\omega_c \Delta vo_d . io_d) + (\omega_c vo_q . \Delta io_q) + (\omega_c vo_q . \Delta io_q)$$

$$\dot{Q} = \left(\frac{3}{2}\right)\left(\omega_c\left((vo_d . io_q) - (vo_q . io_d) - Q\right)\right) \quad \Rightarrow$$

$$\Delta\dot{Q} = \left(\frac{3}{2}\right)(\omega_c \Delta vo_d . io_q) - (\omega_c \Delta vo_q . io_d) + (\omega_c vo_d . \Delta io_q) - (\omega_c vo_q . \Delta io_d)$$

$$\begin{bmatrix} \Delta\dot{\delta} \\ \Delta\dot{P} \\ \Delta\dot{\theta} \end{bmatrix} = \begin{bmatrix} -\omega_c & 0 & 0 \\ 0 & -\omega_c & 0 \\ -m_p & 0 & 0 \end{bmatrix} \begin{bmatrix} \Delta\delta \\ \Delta P \\ \Delta\theta \end{bmatrix} + \frac{3}{2}\begin{bmatrix} 0 & 0 & 0 & 0 & 0 & 0 \\ 0 & 0 & \omega_c . io_d & \omega_c . io_q & \omega_c vo_d & \omega_c vo_q \\ 0 & 0 & \omega_c . io_q & -\omega_c . io_d & -\omega_c vo_q & \omega_c vo_d \end{bmatrix} \begin{bmatrix} \Delta il_d \\ \Delta il_q \\ \Delta vo_d \\ \Delta vo_q \\ \Delta io_d \\ \Delta io_q \end{bmatrix}$$

$$+ \begin{bmatrix} -1 \\ 0 \\ 0 \end{bmatrix}[\Delta\omega_{com}]$$

$$\begin{bmatrix} \Delta\omega \\ \Delta vo_d \\ \Delta vo_q \end{bmatrix} = \begin{bmatrix} 0 & -m_p & 0 \\ 0 & 0 & -n_q \\ 0 & 0 & 0 \end{bmatrix} \begin{bmatrix} \Delta\delta \\ \Delta P \\ \Delta\theta \end{bmatrix}$$

$$[\Delta\dot{x}_d] = [A_d][\Delta x_d] + [B_d][\Delta x_{p1}] + [B_{dcom}][\Delta\omega_{com}]$$

$$[\Delta y_d] = [\Delta C_d][\Delta x_d]$$

$$\Delta x_{inv} = [\Delta\delta \quad \Delta P \quad \Delta Q \quad \Delta\vartheta v_d \quad \Delta\vartheta v_q \quad \Delta\gamma i_d \quad \Delta\gamma i_q \quad \Delta il_d \quad \Delta il_q \quad \Delta vo_d \quad \Delta vo_q \quad \Delta io_d \quad \Delta io_q]$$

$$\begin{bmatrix} \Delta\delta \\ \Delta P \\ \Delta Q \end{bmatrix} = [A_p]\begin{bmatrix} \Delta\delta \\ \Delta P \\ \Delta Q \end{bmatrix} + [B_p]\begin{bmatrix} \Delta il_d \\ \Delta il_q \\ \Delta vo_d \\ \Delta vo_q \\ \Delta io_d \\ \Delta io_q \end{bmatrix} + [B_{pcom}][\Delta\omega_{com}]$$

$$\begin{bmatrix} \Delta\vartheta v_d \\ \Delta\vartheta v_q \end{bmatrix} = [0]\begin{bmatrix} \Delta\vartheta v_d \\ \Delta\vartheta v_q \end{bmatrix} + [Bv_1]\begin{bmatrix} \Delta vo_d^* \\ \Delta vo_q^* \end{bmatrix} + [Bv_2]\begin{bmatrix} \Delta il_d \\ \Delta il_q \\ \Delta vo_d \\ \Delta vo_q \\ \Delta io_d \\ \Delta io_q \end{bmatrix}$$

$$\begin{bmatrix} \Delta\gamma i_d \\ \Delta\gamma i_q \end{bmatrix} = [0]\begin{bmatrix} \Delta\gamma i_d \\ \Delta\gamma i_q \end{bmatrix} + [Bc_1]\begin{bmatrix} \Delta il_d^* \\ \Delta il_q^* \end{bmatrix} + [Bc_2]\begin{bmatrix} \Delta il_d \\ \Delta il_q \\ \Delta vo_d \\ \Delta vo_q \\ \Delta io_d \\ \Delta io_q \end{bmatrix}$$

$$\begin{bmatrix} \Delta il_d \\ \Delta il_q \\ \Delta vo_d \\ \Delta vo_q \\ \Delta io_d \\ \Delta io_q \end{bmatrix} = [ALCL]\begi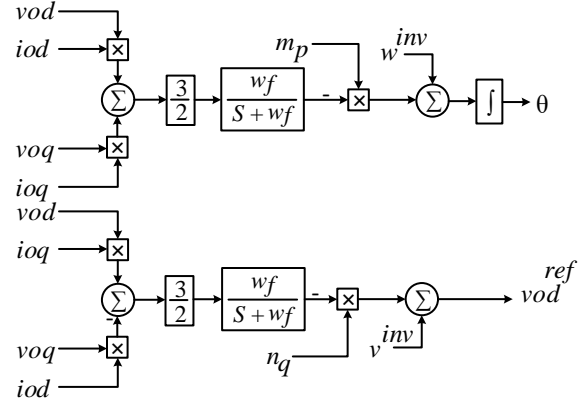n{bmatrix} \Delta il_d \\ \Delta il_q \\ \Delta vo_d \\ \Delta vo_q \\ \Delta io_d \\ \Delta io_q \end{bmatrix} + [BLCL_1]\begin{bmatrix} \Delta vi_d^* \\ \Delta vi_q^* \end{bmatrix} + [BLCL_2]\begin{bmatrix} \Delta vb_d \\ \Delta vb_q \end{bmatrix} + [BLCL_3][\Delta\omega]$$

$$\begin{bmatrix} \Delta\omega \\ \Delta vo_d \\ \Delta vo_q \end{bmatrix} = \begin{matrix} [Cp_w] \\ [Cp_v] \end{matrix}\begin{bmatrix} \Delta\delta \\ \Delta P \\ \Delta Q \end{bmatrix}$$

$$\begin{bmatrix} \Delta il_d^* \\ \Delta il_q^* \end{bmatrix} = [cv]\begin{bmatrix} \Delta\vartheta v_d \\ \Delta\vartheta v_q \end{bmatrix} + [Dv1]\begin{bmatrix} \Delta vo_d^* \\ \Delta vo_q^* \end{bmatrix} + [Dv2]\begin{bmatrix} \Delta il_d \\ \Delta il_q \\ \Delta vo_d \\ \Delta vo_q \\ \Delta io_d \\ \Delta io_q \end{bmatrix}$$

$$\begin{bmatrix} \Delta vi_d^* \\ \Delta vi_q^* \end{bmatrix} = [cc]\begin{bmatrix} \Delta\gamma i_d \\ \Delta\gamma i_q \end{bmatrix} + [Dc1]\begin{bmatrix} \Delta il_d^* \\ \Delta il_q^* \end{bmatrix} + [Dc2]\begin{bmatrix} \Delta il_d \\ \Delta il_q \\ \Delta vo_d \\ \Delta vo_q \\ \Delta io_d \\ \Delta io_q \end{bmatrix}$$

$$\begin{bmatrix} \Delta io_d \\ \Delta io_q \end{bmatrix} = \begin{bmatrix} \cos(\delta) & -\sin(\delta) \\ \sin(\delta) & \cos(\delta) \end{bmatrix} \begin{bmatrix} \Delta io_d \\ \Delta io_q \end{bmatrix} + \begin{bmatrix} -io_d \sin(\delta) - io_q \cos(\delta) \\ io_d \cos(\delta) - io_q \sin(\delta) \end{bmatrix} [\Delta \delta]$$

$$\underbrace{\phantom{\begin{bmatrix} \cos(\delta) & -\sin(\delta) \\ \sin(\delta) & \cos(\delta) \end{bmatrix}}}_{T_S} \qquad \underbrace{\phantom{\begin{bmatrix} -io_d \sin(\delta) \\ io_d \cos(\delta) \end{bmatrix}}}_{T_C}$$

$$\begin{bmatrix} \Delta vb_d \\ \Delta vb_q \end{bmatrix} = inv \begin{bmatrix} \cos(\delta) & -\sin(\delta) \\ \sin(\delta) & \cos(\delta) \end{bmatrix} \begin{bmatrix} \Delta vb_d \\ \Delta vb_q \end{bmatrix} + \begin{bmatrix} -vb_D \sin(\delta) + vb_Q \cos(\delta) \\ -vb_D \cos(\delta) - vb_Q \sin(\delta) \end{bmatrix} [\Delta \delta]$$

$$\begin{bmatrix} \Delta \delta \\ \Delta P \\ \Delta Q \end{bmatrix} = [A_p] \begin{bmatrix} \Delta \delta \\ \Delta P \\ \Delta Q \end{bmatrix} + [B_p] \begin{bmatrix} \Delta il_d \\ \Delta il_q \\ \Delta vo_d \\ \Delta vo_q \\ \Delta io_d \\ \Delta io_q \end{bmatrix} + [B_{pcom}][\Delta \omega_{com}]$$

$$\begin{bmatrix} \Delta \vartheta v_d \\ \Delta \vartheta v_q \end{bmatrix} = [0] \begin{bmatrix} \Delta \vartheta v_d \\ \Delta \vartheta v_q \end{bmatrix} + [Bv_1] \begin{bmatrix} \Delta vo_d^* \\ \Delta vo_q^* \end{bmatrix} + [Bv_2] \begin{bmatrix} \Delta il_d \\ \Delta il_q \\ \Delta vo_d \\ \Delta vo_q \\ \Delta io_d \\ \Delta io_q \end{bmatrix}$$

$$\begin{bmatrix} [\Delta \omega] \\ \begin{bmatrix} \Delta vo_d^* \\ \Delta vo_q^* \end{bmatrix} \end{bmatrix} = \begin{matrix} [Cp_w] \\ [Cp_v] \end{matrix} \begin{bmatrix} \Delta \delta \\ \Delta P \\ \Delta Q \end{bmatrix}$$

$$\begin{bmatrix} \Delta \vartheta v_d \\ \Delta \vartheta v_q \end{bmatrix} = [0] \begin{bmatrix} \Delta \vartheta v_d \\ \Delta \vartheta v_q \end{bmatrix} + [Bv_1] \left[[Cp_v] \begin{bmatrix} \Delta P \\ \Delta Q \end{bmatrix} \right] + [Bv_2] \begin{bmatrix} \Delta il_d \\ \Delta il_q \\ \Delta vo_d \\ \Delta vo_q \\ \Delta io_d \\ \Delta io_q \end{bmatrix}$$

$$\begin{bmatrix} \Delta \omega \\ \Delta vo_d^* \\ \Delta vo_q^* \end{bmatrix} = \begin{matrix} [Cp_w] \\ [Cp_v] \end{matrix} \begin{bmatrix} \Delta \delta \\ \Delta P \\ \Delta Q \end{bmatrix} \qquad \begin{bmatrix} \Delta il_d^* \\ \Delta il_q^* \end{bmatrix} = [cv] \begin{bmatrix} \Delta \vartheta v_d \\ \Delta \vartheta v_q \end{bmatrix} + [Dv1] \begin{bmatrix} \Delta vo_d^* \\ \Delta vo_q^* \end{bmatrix} + [Dv2] \begin{bmatrix} \Delta il_d \\ \Delta il_q \\ \Delta vo_d \\ \Delta vo_q \\ \Delta io_d \\ \Delta io_q \end{bmatrix}$$
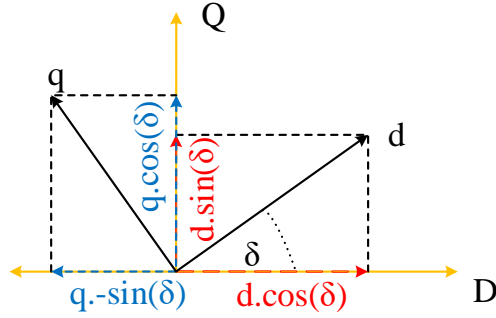
125

$$\begin{bmatrix} \Delta\gamma i_d \\ \Delta\gamma i_q \end{bmatrix} = [0]\begin{bmatrix} \Delta\gamma i_d \\ \Delta\gamma i_q \end{bmatrix} + [\text{Bc}_1]\left[[cv]\begin{bmatrix} \Delta\vartheta v_d \\ \Delta\vartheta v_q \end{bmatrix} + [Dv1]\left[[Cp_v]\begin{bmatrix} \Delta P \\ \Delta Q \end{bmatrix} \right] + [Dv2]\begin{bmatrix} \Delta il_d \\ \Delta il_q \\ \Delta vo_d \\ \Delta vo_q \\ \Delta io_d \\ \Delta io_q \end{bmatrix} \right] + [\text{Bc}_2]\begin{bmatrix} \Delta il_d \\ \Delta il_q \\ \Delta vo_d \\ \Delta vo_q \\ \Delta io_d \\ \Delta io_q \end{bmatrix}$$

$$\begin{bmatrix} \Delta vi_d^* \\ \Delta vi_q^* \end{bmatrix} = [cc]\begin{bmatrix} \Delta\gamma i_d \\ \Delta\gamma i_q \end{bmatrix} + [Dc1]\begin{bmatrix} \Delta il_d^* \\ \Delta il_q^* \end{bmatrix} + [Dc2]\begin{bmatrix} \Delta il_d \\ \Delta il_q \\ \Delta vo_d \\ \Delta vo_q \\ \Delta io_d \\ \Delta io_q \end{bmatrix}$$

$$\begin{bmatrix} \Delta il_d^* \\ \Delta il_q^* \end{bmatrix} = [cv]\begin{bmatrix} \Delta\vartheta v_d \\ \Delta\vartheta v_q \end{bmatrix} + [Dv1]\left[[Cp_v]\begin{bmatrix} \Delta P \\ \Delta Q \end{bmatrix} \right] + [Dv2]\begin{bmatrix} \Delta il_d \\ \Delta il_q \\ \Delta vo_d \\ \Delta vo_q \\ \Delta io_d \\ \Delta io_q \end{bmatrix}$$

$$\begin{bmatrix} \Delta vi_d^* \\ \Delta vi_q^* \end{bmatrix} = [cc]\begin{bmatrix} \Delta\gamma i_d \\ \Delta\gamma i_q \end{bmatrix} + [Dc1]\left[[cv]\begin{bmatrix} \Delta\vartheta v_d \\ \Delta\vartheta v_q \end{bmatrix} + [Dv1]\left[[Cp_v]\begin{bmatrix} \Delta P \\ \Delta Q \end{bmatrix} \right] + [Dv2]\begin{bmatrix} \Delta il_d \\ \Delta il_q \\ \Delta vo_d \\ \Delta vo_q \\ \Delta io_d \\ \Delta io_q \end{bmatrix} \right] + [Dc2]\begin{bmatrix} \Delta il_d \\ \Delta il_q \\ \Delta vo_d \\ \Delta vo_q \\ \Delta io_d \\ \Delta io_q \end{bmatrix}$$

$$\begin{bmatrix} \Delta il_d \\ \Delta il_q \\ \Delta vo_d \\ \Delta vo_q \\ \Delta io_d \\ \Delta io_q \end{bmatrix} = [ALCL] \begin{bmatrix} \Delta il_d \\ \Delta il_q \\ \Delta vo_d \\ \Delta vo_q \\ \Delta io_d \\ \Delta io_q \end{bmatrix} + [BLCL_1] \left[[cc] \begin{bmatrix} \Delta \gamma i_d \\ \Delta \gamma i_q \end{bmatrix} + [Dc1] \left[[cv] \begin{bmatrix} \Delta \vartheta v_d \\ \Delta \vartheta v_q \end{bmatrix} + [Dv1] \left[[Cp_v] \begin{bmatrix} \Delta P \\ \Delta Q \end{bmatrix} \right] + [Dv2] \begin{bmatrix} \Delta il_d \\ \Delta il_q \\ \Delta vo_d \\ \Delta vo_q \\ \Delta io_d \\ \Delta io_q \end{bmatrix} \right] + [Dc2] \begin{bmatrix} \Delta il_d \\ \Delta il_q \\ \Delta vo_d \\ \Delta vo_q \\ \Delta io_d \\ \Delta io_q \end{bmatrix} \right]$$

$$+ [BLCL_2] \left[\underbrace{inv \begin{bmatrix} \cos(\delta) & -\sin(\delta) \\ \sin(\delta) & \cos(\delta) \end{bmatrix}}_{T_s} \begin{bmatrix} \Delta vb_d \\ \Delta vb_q \end{bmatrix} + \underbrace{\begin{bmatrix} -vb_D \sin(\delta) + vb_Q \cos(\delta) \\ -vb_D \cos(\delta) - vb_Q \sin(\delta) \end{bmatrix}}_{T_v^{-1}} [\Delta \delta] \right] + [BLCL_3] \big[[Cp_w][\Delta \delta] \big]$$

$$A_{inv} = \begin{bmatrix} (A_p)_{3\times3} & ((0)_{2\times2}) & (0)_{2\times2} & (B_p)_{3\times6} \\ (Bv_1 * Cp_v)_{2\times3} & ((0)_{2\times2}) & (0)_{2\times2} & (Bv_2)_{3\times6} \\ (Bc_1 * Dv_1 * Cp_v)_{2\times3} & (Bc_1 * Cv_1)_{2\times2} & (0)_{2\times2} & (Bc_1 * Dv_2 * Bc_2)_{2\times6} \\ \left(\begin{matrix} (BLCL_1 * Dc_1 * Dv_1 * Cpv) + \\ BLCL_2 * \\ \left(\begin{bmatrix} T_v^{-1} & (0)_{3\times2} \\ (0)_{4\times1} & (0)_{3\times2} \end{bmatrix} \right) + (BLCL_3 * Cpw) \end{matrix} \right)_{6\times3} & (BLCL_1 * DC_1 * Cv)_{6\times2} & (BLCL_1 * Cc)_{6\times2} & \left(\begin{matrix} ALCL + BLCL_1 * Dc_1 * Dv_2 \\ BLCL_1 * Dc_2 \end{matrix} \right)_{6\times6} \end{bmatrix}$$

$$B_{inv} = \begin{bmatrix} ((0)_{3\times2}) \\ ((0)_{2\times2}) \\ ((0)_{2\times2}) \\ \left(BLCL_2 * \begin{bmatrix} (0)_{4\times2} \\ T_s^{-1} \end{bmatrix} \right)_{6\times2} \end{bmatrix} \begin{bmatrix} \Delta vb_d \\ \Delta vb_q \end{bmatrix}$$

$$B_{inv} = \begin{bmatrix} [B_{pcom}] \\ (0)_{2\times1} \\ (0)_{2\times1} \\ (0)_{6\times1} \end{bmatrix} [\Delta \delta]$$

$$C_{inv_w} = \begin{cases} [(Cp_w)_{1\times3} \quad (0)_{1\times10}][\Delta \delta] & \text{if } Inverter\ index = 1 \\ [(0)_{1\times13}] \quad [\Delta \delta] & \text{if } Inverter\ index \neq 1 \end{cases}$$

$$C_{inv_c} = [(T_C)_{2\times1} \quad (0)_{2\times10} \quad (T_S)_{2\times2}][\Delta x_{inv}]$$

127

Appendix B

Small Signal Model of DC/DC Converter
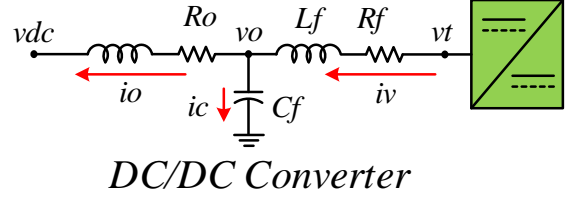
Small signal model of DC/DC converter:

$$\frac{div}{dt} = \frac{1}{Lf}(\dot{v}t) - \frac{1}{Lf}(\dot{v}o) - \frac{Rf}{Lf}.(\imath v)$$

$$\frac{dio}{dt} = \frac{1}{Lo}(\dot{v}o) - \frac{1}{Lo}(\dot{v}dc) - \frac{Ro}{Lo}.(\imath o)$$

$$\frac{dvo}{dt} = \frac{1}{Cf}(\imath v) - \frac{1}{Cf}(\imath o)$$

DC/DC Converter

$$\begin{bmatrix} \dot{\imath v} \\ \dot{\imath o} \\ \dot{v o} \end{bmatrix} = \begin{bmatrix} -\dfrac{R_f}{L_f} & 0 & -\dfrac{1}{L_f} \\ 0 & -\dfrac{R_o}{L_o} & -\dfrac{1}{L_o} \\ \dfrac{1}{C_f} & -\dfrac{1}{C_f} & 0 \end{bmatrix} \begin{bmatrix} \Delta iv \\ \Delta io \\ \Delta vo \end{bmatrix} + \begin{bmatrix} \dfrac{1}{L_f} \\ 0 \\ 0 \end{bmatrix} [\Delta \dot{v}t] + \begin{bmatrix} 0 \\ -\dfrac{1}{L_o} \\ 0 \end{bmatrix} [\Delta \dot{v}dc]$$

Voltage and Current Controller:

$$[\dot{x}_p] = [A_p][\Delta x_p] + [B1_p][\Delta \dot{v}t] + [B2_p][\Delta vdc]$$

$$iv' = (\dot{v}o - vdc)Kp_v + (\dot{v}o - vdc)\frac{Ki_v}{s} + H(\imath o)$$

$$\vartheta_v = (\dot{v}o - vdc)\frac{Ki_v}{s}$$

$$[iv'] = [1][\Delta \vartheta_v] + [Kp_v][\Delta \dot{v}o] + [-Kp_v][\Delta vdc] + [H][\Delta \imath o]$$

$$[\dot{\vartheta}_v] = [0][\Delta \vartheta_v] + [Ki_v][\Delta \dot{v}o] + [-Ki_v][\Delta \dot{v}dc]$$

$$\dot{v}t = (\imath v - iv)Kp_c + (\imath v - iv)\frac{Ki_c}{s}$$

$$\vartheta_c = (\imath v - iv)\frac{Ki_c}{s}$$

$$[\dot{v}t] = [1][\Delta \vartheta_c] + [Kp_c][\Delta \imath v] + [-Kp_c][\Delta iv]$$

$$[\dot{\vartheta}_c] = [0][\Delta \vartheta_v] + [Kp_v][\Delta \dot{v}o] + [-Kp_v][\Delta \dot{v}dc]$$

DC Power Controller

$$P\dot{d}c = \left(\frac{w}{s+w}\right)(io - vo)$$

$$[P\dot{d}c] = [w.vo][\Delta io] + [w.io][\Delta vo] + [-w][\Delta Pdc]$$

$$\dot{v}o = vo - m_{dc}P_{dc}$$

$$[\Delta \dot{v}o] = [-m_{dc}][\Delta P_{dc}]$$

Overall small signal model of DC/DC converter

$$[\dot{x}_p] = [A_p][\Delta x_p] + [B1_p][\Delta \dot{v}t] + [B2_p][\Delta v\dot{d}c]$$

$$[iv'] = [1][\Delta\vartheta_v] + [Kp_v][\Delta \dot{v}o] + [-Kp_v][\Delta v\dot{d}c] + [H][\Delta\iota\dot{o}]$$

$$[\dot{\vartheta}_v] = [0][\Delta\vartheta_v] + [Ki_v][\Delta \dot{v}o] + [-Ki_v][\Delta v\dot{d}c]$$
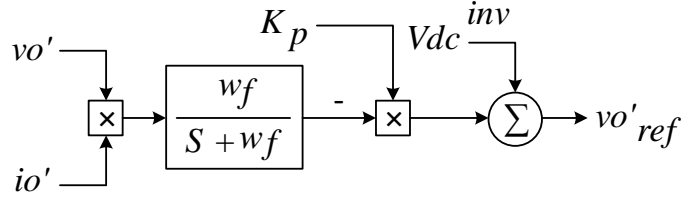
$$[\dot{v}t] = [1][\Delta\vartheta_c] + [Kp_c][\Delta\iota\dot{v}] + [-Kp_c][\Delta iv]$$

$$[\dot{\vartheta}_c] = [0][\Delta\vartheta_v] + [Ki_c][\Delta\iota\dot{v}] + [-Ki_c][\Delta iv]$$

$$[P\dot{d}c] = [w.vo][\Delta io] + [w.io][\Delta vo] + [-w][\Delta Pdc]$$

$$[\Delta \dot{v}o] = [-m_{dc}][\Delta P_{dc}]$$

Re-arrangement:

$$[iv'] = [1][\Delta\vartheta_v] + [Kp_v][-m_{dc}][\Delta P_{dc}] + [-Kp_v][\Delta v\dot{d}c] + [H][\Delta\iota\dot{o}]$$

$$[\dot{v}t] = [1][\Delta\vartheta_c] + [Kp_c]\Big[[1][\Delta\vartheta_v] + [Kp_v][-m_{dc}][\Delta P_{dc}] + [-Kp_v][\Delta v\dot{d}c] + [H][\Delta\iota\dot{o}]\Big] + [-Kp_c][\Delta iv]$$

State space model then:

$$[\dot{x}_p] = [A_p][\Delta x_p] + [B1_p][1][\Delta\vartheta_c] + [Kp_c][B1_p][1][\Delta\vartheta_v] + [Kp_c][B1_p][Kp_v][-m_{dc}][\Delta P_{dc}]$$
$$+ \{[Kp_c][B1_p][-Kp_v][\Delta v\dot{d}c]\} + [Kp_c][B1_p][H][\Delta\iota\dot{o}] + [B1_p][-Kp_c][\Delta iv]$$
$$+ \{[B2_p][\Delta v\dot{d}c]\}$$

$$[P\dot{d}c] = [w.vo][\Delta io] + [w.io][\Delta vo] + [-w][\Delta Pdc]$$

$$[\dot{\vartheta}_v] = [0][\Delta\vartheta_v] + [Ki_v][-m_{dc}][\Delta P_{dc}] + \{[-Ki_v][\Delta v\dot{d}c]\}$$

$$[\dot{\vartheta}_c] = [0][\Delta\vartheta_v] + [Ki_c][1][\Delta\vartheta_v] + [Ki_c][Kp_v][-m_{dc}][\Delta P_{dc}] + \{[Ki_c][-Kp_v][\Delta v\dot{d}c]\} + [Ki_c][H][\Delta\iota\dot{o}]$$
$$+ [-Ki_c][\Delta iv]$$

$$Ap_{dc} = \begin{bmatrix} \left(Ap + \begin{bmatrix} ([B1_p]*[-Kp_c]) \begin{bmatrix} 0 & 0 \\ 0 & 0 \\ 0 & 0 \end{bmatrix} \end{bmatrix} \\ + \begin{bmatrix} \begin{bmatrix} 0 \\ 0 \\ 0 \end{bmatrix} ([Kp_c]*[B1_p]*[H]) \begin{bmatrix} 0 \\ 0 \\ 0 \end{bmatrix} \end{bmatrix} \right)_{3\times3} & ([Kp_c][B1_p][Kp_v][-m_{dc}])_{3\times1} & ([Kp_c][B1_p][1])_{3\times1} & (B1_p)_{3\times1} \\ (0 \ [w.vo] \ [w.io])_{1\times3} & (-w)_{1\times1} & (0)_{1\times1} & (0)_{1\times1} \\ \left(\begin{bmatrix} 0 & 0 & 0 \end{bmatrix} \\ +[-Ki_c \ ([Ki_c]*[H]) \ 0] \right)_{2\times3} & \left(\begin{bmatrix} [Ki_v][-m_{dc}] \\ [Ki_c][Kp_v][-m_{dc}] \end{bmatrix} \right)_{2\times1} & \left(\begin{bmatrix} 0 \\ [Ki_c] \end{bmatrix} \right)_{2\times1} & (0)_{2\times1} \end{bmatrix} \begin{bmatrix} \Delta iv \\ \Delta io \\ \Delta vo \\ \Delta P_{dc} \\ \vartheta_v \\ \vartheta_c \end{bmatrix}$$

$$Bp_{dc} = \begin{bmatrix} \left(\begin{matrix} [Kp_c]*[B1_p]*[-Kp_v] \\ +[B2_p] \end{matrix} \right)_{3\times1} \\ (0)_{1\times1} \\ ([-Ki_v])_{1\times1} \\ ([Ki_c][-Kp_v])_{1\times1} \end{bmatrix} [\Delta V_{dc}]$$

In order to implement the state space model for the entire DC microgrid, the DC loads must be included in the system matrix. Therefore, the A matrix of inverter # 1 and #3 will be changed, while converter #2 remain to the previous state space model.

$$[\dot{X}_P] = \begin{bmatrix} Ap_{dc1} & (0)_{6\times6} & (0)_{6\times6} \\ (0)_{6\times6} & Ap_{dc2} & (0)_{6\times6} \\ (0)_{6\times6} & (0)_{6\times6} & Ap_{dc3} \end{bmatrix} [\Delta X_P]$$

$$+ \begin{bmatrix} Bp_{dc1} \\ Bp_{dc2} \\ Bp_{dc3} \end{bmatrix} \begin{bmatrix} \Delta Vdc1 \\ \Delta Vdc2 \\ \Delta Vdc3 \end{bmatrix}$$

$\because V_{dc1} = i_{load1} * R_{load1}$

$\quad V_{dc3} = i_{load3} * R_{load3}$

$\therefore i_{load1} = (i_{o1} + i_{line1})$

$\quad i_{load3} = (i_{o3} + i_{line3})$


Thus:

$$[\dot{X}_P] = \begin{bmatrix} Ap_{dc1} & (0)_{6\times6} & (0)_{6\times6} \\ (0)_{6\times6} & Ap_{dc2} & (0)_{6\times6} \\ (0)_{6\times6} & (0)_{6\times6} & Ap_{dc3} \end{bmatrix} [\Delta X_P] + \begin{bmatrix} Bp_{dc1} \\ Bp_{dc2} \\ Bp_{dc3} \end{bmatrix} \begin{bmatrix} (\Delta i_{o1} + \Delta i_{line1}) * R_{load1} \\ \Delta Vdc2 \\ (\Delta i_{o3} + \Delta i_{line2}) * R_{load3} \end{bmatrix}$$

It is clear that includeing the DC loads shows some elements are related to the state matrix. Therefore, these elements must be considered in the state matrix as illustrated below:

$$[\dot{X}_P] = \left(\begin{bmatrix} Ap_{dc1} & (0)_{6\times6} & (0)_{6\times6} \\ (0)_{6\times6} & Ap_{dc2} & (0)_{6\times6} \\ (0)_{6\times6} & (0)_{6\times6} & Ap_{dc3} \end{bmatrix} [\Delta X_P] + \begin{bmatrix} Bp_{dc1} \\ Bp_{dc3} \end{bmatrix} \begin{bmatrix} R_{load1} \\ R_{load3} \end{bmatrix} \begin{bmatrix} \Delta i_{o1} \\ \Delta i_{o3} \end{bmatrix} \right) + \begin{bmatrix} Bp_{dc1} \\ Bp_{dc3} \end{bmatrix} \begin{bmatrix} R_{load1} \\ R_{load3} \end{bmatrix} \begin{bmatrix} \Delta i_{line1} \\ \Delta i_{line2} \end{bmatrix}$$

$$+ [Bp_{dc2}][\Delta Vdc2]$$

$$\because Bp_{dc1} = \begin{bmatrix} \left(\begin{matrix} ([Kp_c]*[B1_p]) \\ *[-Kp_v] \\ +[B2_p] \end{matrix} \right)_{3\times1} \\ (0)_{1\times1} \\ ([-Ki_v])_{1\times1} \\ ([Ki_c][-Kp_v])_{1\times1} \end{bmatrix} [R_{load1}][\Delta i_{o1}] \implies Bp_{dc1} = \begin{bmatrix} \left(\begin{matrix} [Kp_c]*[B1_p]* \\ [-Kp_v]*[R_{load1}] \\ +[B2_p]*[R_{load1}] \end{matrix} \right)_{3\times1} \\ (0)_{1\times1} \\ ([-Ki_v]*[R_{load1}])_{1\times1} \\ ([Ki_c][-Kp_v]*[R_{load1}])_{1\times1} \end{bmatrix} [\Delta i_{o1}]$$
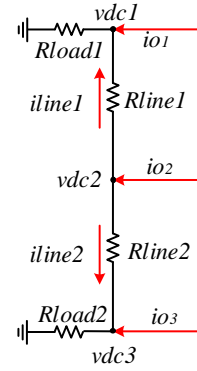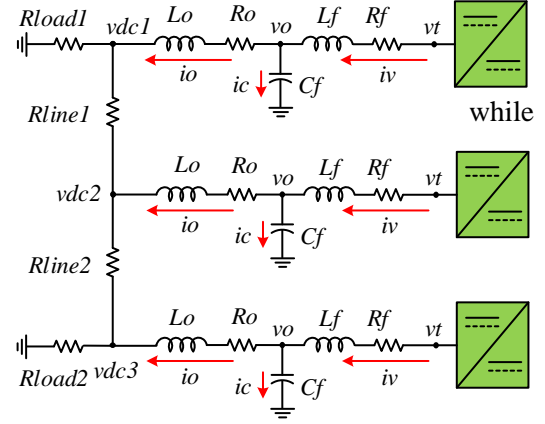
Therefore: the $(Ap_{dc(i)})$ becomes as written below including the load and lines resistances:

$Ap_{dc(i)}$

$$= \begin{bmatrix} \begin{pmatrix} Ap_{(i)} + \begin{bmatrix} ([B1_{p(i)}][-Kp_{c(i)}]) \begin{bmatrix} 0 & 0 \\ 0 & 0 \\ 0 & 0 \end{bmatrix} \end{bmatrix} \\ + \begin{bmatrix} 0 \\ 0 \\ 0 \end{bmatrix} ([Kp_{c(i)}][B1_{p(i)}] * [H_i]) \begin{bmatrix} 0 \\ 0 \\ 0 \end{bmatrix} \\ + \begin{bmatrix} 0 \\ 0 \\ 0 \end{bmatrix} \left(\begin{bmatrix} \begin{pmatrix} \frac{[Kp_{c(i)}][B1_{p(i)}][-Kp_{v(i)}][R_{load(i)}]}{+[B2_{p(i)}][R_{load(i)}]} \end{pmatrix}_{3\times1} \\ (0)_{1\times1} \\ ([-Ki_{v(i)}][R_{load(i)}])_{1\times1} \\ ([Ki_{c(i)}][-Kp_{v(i)}][R_{load(i)}])_{1\times1} \end{bmatrix} \right) \begin{bmatrix} 0 \\ 0 \\ 0 \end{bmatrix} \\ (0 \ [w_i.vo_i] \ [w_i.io_i])_{1\times3} \\ \begin{pmatrix} [0 \ 0 \ 0] \\ + [-Ki_{c(i)}] \ ([Ki_{c(i)}][H_{(i)}]) \ 0] \end{pmatrix}_{2\times3} \end{pmatrix}_{3\times3} & \begin{pmatrix} [Kp_{c(i)}][B1_{p(i)}] \\ \times [Kp_{v(i)}][-m_{dc(i)}] \end{pmatrix}_{3\times1} & \begin{pmatrix} [Kp_{c(i)}][1] \\ \times [B1_{p(i)}] \end{pmatrix}_{3\times1} & (B1_{p(i)})_{3\times1} \\ (-w_i)_{1\times1} & (0)_{1\times1} & (0)_{1\times1} \\ \left(\begin{bmatrix} [Ki_{v(i)}][-m_{dc(i)}] \\ \begin{pmatrix} [Ki_{c(i)}][Kp_{v(i)}] \\ \times [-m_{dc(i)}] \end{pmatrix} \end{bmatrix} \right)_{2\times1} & \left(\begin{bmatrix} 0 \\ [Ki_{c(i)}] \end{bmatrix} \right)_{2\times1} & (0)_{2\times1} \end{bmatrix} \begin{bmatrix} \Delta iv_i \\ \Delta io_i \\ \Delta vo_i \\ \Delta Pdc_i \\ \vartheta_{v_i} \\ \vartheta_{c_i} \end{bmatrix}$$

The input matrixes then can be written as:

$$Bp_{dc(i)} = \begin{bmatrix} \begin{pmatrix} [Kp_{c(i)}] * [B1_{p(i)}] * [-Kp_{v(i)}] * [R_{load(i)}] \\ + [B2_{p(i)}] * [R_{load(i)}] \end{pmatrix}_{3\times1} \\ (0)_{1\times1} \\ ([-Ki_{v(i)}] * [R_{load(i)}])_{1\times1} \\ ([Ki_{c(i)}][-Kp_{v(i)}] * [R_{load(i)}])_{1\times1} \end{bmatrix} [\Delta i_{line(i)}]$$

132

Appendix C

Small signal model of IC

Power Circuit of IC equations:

$$\frac{di_d}{dt} = \frac{1}{L_f}vt_d - \frac{1}{L_f}vo_d - \frac{R_f}{L_f}i_d + wi_q$$

$$\frac{di_q}{dt} = \frac{1}{L_f}vt_q - \frac{1}{L_f}vo_q - \frac{R_f}{L_f}i_q - wi_d$$

$$\frac{dvo_d}{dt} = \frac{1}{C_f}io_d - \frac{1}{C_f}i_d + wv_q$$

$$\frac{dvo_q}{dt} = \frac{1}{C_f}io_q - \frac{1}{C_f}i_q - wv_d$$

$$\frac{dv_{dc}}{dt} = \frac{1}{C_{dc}}io_{dc} - \frac{1}{C_f}i$$

$$\therefore vt_d + vt_q = m_d v_{dc} + m_q v_{dc}$$

$$\therefore i_d + i_q = \frac{3}{2}m_d v_{dc} + \frac{3}{2}m_q v_{dc}$$
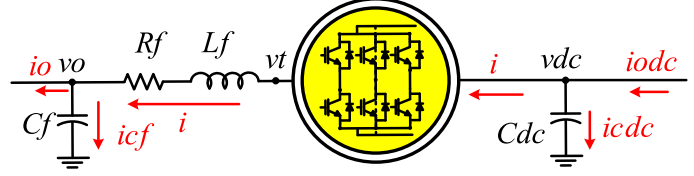
1. Power Circuit model:

$$\Delta \dot{I}_d = -\frac{1}{L_f}\Delta v_d + \frac{m_d}{L_f}\Delta v_{dc} + \frac{v_{dc}}{L_f}\Delta m_d - \frac{R_f}{L_f}\Delta i_d + w.\Delta i_q + i_q.\Delta\omega \tag{1}$$

$$\Delta \dot{I}_q = -\frac{1}{L_f}\Delta v_q + \frac{m_q}{L_f}\Delta v_{dc} + \frac{v_{dc}}{L_f}\Delta m_q - \frac{R_f}{L_f}\Delta i_q - w.\Delta i_d - i_d\Delta\omega \tag{2}$$

$$\Delta \dot{v}_d = -\frac{1}{C_f}\Delta io_d + \frac{1}{C_f}\Delta i_d + w^o.\Delta v_q + v_q^o.\Delta w \tag{3}$$

$$\Delta \dot{v}_q = -\frac{1}{C_f}\Delta io_q + \frac{1}{C_f}\Delta i_q - w^o.\Delta v_d - v_d^o \cdot \Delta w \tag{4}$$

$$\Delta \dot{v}_{dc} = \left(-\frac{1.5m_d}{C_{dc}}\Delta i_d - \frac{1.5i_d}{C_{dc}}\Delta m_d - \frac{1.5m_q}{C_{dc}}\Delta i_q - \frac{1.5i_q}{C_{dc}}\Delta m_q\right) + \frac{1}{C_{dc}}\Delta iodc \tag{5}$$

$$
\begin{bmatrix} \Delta \dot{i}_d \\ \Delta \dot{i}_q \\ \Delta \dot{v}_d \\ \Delta \dot{v}_q \\ \Delta \dot{v}_{dc} \end{bmatrix}_{[\Delta \dot{x}_p]} = \underbrace{\begin{bmatrix} -\dfrac{R_f}{L_f} & w & -\dfrac{1}{L_f} & 0 & \dfrac{m_d}{L_f} \\ -w & -\dfrac{R_f}{L_f} & 0 & -\dfrac{1}{L_f} & \dfrac{m_q}{L_f} \\ \dfrac{1}{C_f} & 0 & 0 & w & 0 \\ 0 & \dfrac{1}{C_f} & -w & 0 & 0 \\ -\dfrac{1.5 m_d^o}{C_{dc}} & -\dfrac{1.5 m_q^o}{C_{dc}} & 0 & 0 & 0 \end{bmatrix}}_{[Ap]} \begin{bmatrix} \Delta i_d \\ \Delta i_q \\ \Delta v_d \\ \Delta v_q \\ \Delta v_{dc} \end{bmatrix} + \underbrace{\begin{bmatrix} -\dfrac{v_{dc}}{L_f} & 0 \\ 0 & -\dfrac{v_{dc}}{L_f} \\ 0 & 0 \\ 0 & 0 \\ -\dfrac{1.5 I_d^o}{C_{dc}} & -\dfrac{1.5 I_q^o}{C_{dc}} \end{bmatrix}}_{[Bp1]} \underbrace{\begin{bmatrix} \Delta m_d \\ \Delta m_q \end{bmatrix}}_{[\Delta m_{dq}]}
$$

$$
+ \underbrace{\begin{bmatrix} i_q \\ -i_d \\ v_q \\ -v_d \\ 0 \end{bmatrix}}_{[Bp2]} [\Delta \omega] + \underbrace{\begin{bmatrix} 0 & 0 \\ 0 & 0 \\ -\dfrac{1}{C_f} & 0 \\ 0 & -\dfrac{1}{C_f} \\ 0 & 0 \end{bmatrix}}_{[Bp3]} \begin{bmatrix} \Delta io_d \\ \Delta io_q \end{bmatrix} + \underbrace{\begin{bmatrix} 0 \\ 0 \\ 0 \\ 0 \\ -\dfrac{1}{C_{dc}} \end{bmatrix}}_{[Bp4]} [\Delta iodc]
$$

$$
\color{red}{[\Delta \dot{x}_p] = [Ap]_{5\times5}[\Delta x_p] + [Bp1]_{5\times2}[\Delta m_{dq}] + [Bp2]_{5\times1}[\Delta \omega] + [Bp3]_{5\times2}[\Delta io_{dq}]}
$$
$$
\color{red}{+ [Bp4]_{5\times1}[\Delta iodc]}
$$

2. Current Controller model:

$$
\Delta m_d = \frac{k_{pc}}{v_{dc}}\left(\Delta i_q^* - \Delta i_q\right) + \frac{k_{ic}}{v_{dc}}\Delta \theta_{id} + \frac{1}{v_{dc}}\Delta v_d^c - \frac{w L_f}{v_{dc}}\Delta I_q^c - \frac{i_q L_f}{v_{dc}}\Delta w - \frac{m_d}{v_{dc}}\Delta v_{dc} \tag{8}
$$

$$
\Delta m_q = \frac{k_{pc}}{v_{dc}}\left(\Delta i_q^* - \Delta i_q\right) + \frac{k_{ic}}{v_{dc}}\Delta \theta_{iq} + \frac{1}{v_{dc}}\Delta v_q^c + \frac{w L_f}{v_{dc}}\Delta I_d^c + \frac{i_d L_f}{v_{dc}}\Delta w - \frac{m_q}{v_{dc}}\Delta v_{dc} \tag{9}
$$

$$
\Delta \dot{\theta}_{id} = \Delta i_d^* - \Delta i_d \tag{10}
$$

$$
\Delta \dot{\theta}_{iq} = \Delta i_q^* - \Delta i_q \tag{11}
$$

$$
\begin{bmatrix} \Delta \dot{\theta}_{id} \\ \Delta \dot{\theta}_{iq} \end{bmatrix} = \begin{bmatrix} 0 & 0 \\ 0 & 0 \end{bmatrix}\begin{bmatrix} \Delta \theta_{id} \\ \Delta \theta_{iq} \end{bmatrix} + \underbrace{\begin{bmatrix} 1 & 0 \\ 0 & 1 \end{bmatrix}}_{B1i}\begin{bmatrix} \Delta i_d^* \\ \Delta i_q^* \end{bmatrix} + \underbrace{\begin{bmatrix} -1 & 0 \\ 0 & -1 \end{bmatrix}}_{B2i}\color{cyan}{\begin{bmatrix} \Delta i_d \\ \Delta i_q \end{bmatrix}}
$$

134

$$\begin{bmatrix}\Delta m_d \\ \Delta m_Q\end{bmatrix} = \underbrace{\begin{bmatrix}\dfrac{k_{ic}}{v_{dc}} & 0 \\ 0 & \dfrac{k_{ic}}{v_{dc}}\end{bmatrix}}_{Ci}\begin{bmatrix}\Delta\theta_{id} \\ \Delta\theta_{iq}\end{bmatrix} + \underbrace{\begin{bmatrix}\dfrac{k_{pc}}{v_{dc}} & 0 \\ 0 & \dfrac{k_{pc}}{v_{dc}}\end{bmatrix}}_{Di1}\begin{bmatrix}\Delta i_d^* \\ \Delta i_q^*\end{bmatrix} + \underbrace{\begin{bmatrix}-\dfrac{k_{pc}}{v_{dc}} & -\dfrac{wL_f}{v_{dc}} \\ \dfrac{wL_f}{v_{dc}} & -\dfrac{k_{pc}}{v_{dc}}\end{bmatrix}}_{Di2}\begin{bmatrix}\Delta i_d \\ \Delta i_q\end{bmatrix} + \underbrace{\begin{bmatrix}\dfrac{1}{v_{dc}} & 0 \\ 0 & \dfrac{1}{v_{dc}}\end{bmatrix}}_{D13}\begin{bmatrix}\Delta v_d \\ \Delta v_q\end{bmatrix}$$

$$+ \underbrace{\begin{bmatrix}-\dfrac{L_f i_q}{v_{dc}} \\ \dfrac{L_f i_d}{v_{dc}}\end{bmatrix}}_{Di4}[\Delta w] + \underbrace{\begin{bmatrix}-\dfrac{m_d}{v_{dc}} \\ -\dfrac{m_q}{v_{dc}}\end{bmatrix}}_{Di5}[\Delta v_{dc}]$$

$$[\Delta\dot{\theta}_{\iota dq}] = [Bi1][\Delta i_{dq}^*] + [Bi2][\Delta i_{dq}] \qquad\qquad\text{(b)}$$

$$[\Delta m_{dq}^o] = [Ci][\Delta\theta_{idq}] + [Di1][\Delta i_{dq}^*] + [Di2][\Delta i_{dq}] + [Di3][\Delta v_{dq}] + [Di4][\Delta w] + [Di5][\Delta v_{dc}] \qquad\text{(c)}$$

3. Voltage Controller model:

$$\Delta I_d^* = k_{pv}(\Delta v_d^* - \Delta v_d^c) + k_{iv}\Delta\theta_{vd} + H\Delta Io_d^c - w^o C_f \Delta v_q^c - C_f v_q^o \Delta w \qquad\qquad\text{(6)}$$

$$\Delta I_q^* = k_{pv}(\Delta v_q^* - \Delta v_q^c) + k_{iv}\Delta\theta_{vq} + H\Delta Io_q^c + w^o C_f \Delta v_d^c + C_f v_d^o \Delta w \qquad\qquad\text{(7)}$$

$$\Delta\dot{\theta}_{vd} = \Delta v_d^* - \Delta v_d^c \qquad\qquad\text{(10)}$$

$$\Delta\dot{\theta}_{vq} = \Delta v_q^* - \Delta v_q^c \qquad\qquad\text{(11)}$$

$$\begin{bmatrix}\Delta I_d^* \\ \Delta I_q^*\end{bmatrix} = \underbrace{\begin{bmatrix}k_{iv} & 0 \\ 0 & k_{iv}\end{bmatrix}}_{Cv}\begin{bmatrix}\Delta\theta_{vd} \\ \Delta\theta_{vq}\end{bmatrix} + \underbrace{\begin{bmatrix}k_{pv} & 0 \\ 0 & k_{pv}\end{bmatrix}}_{Dv1}\begin{bmatrix}\Delta v_d^* \\ \Delta v_q^*\end{bmatrix} + \underbrace{\begin{bmatrix}-k_{pv} & -wC_f \\ wC_f & -k_{pv}\end{bmatrix}}_{Dv2}\begin{bmatrix}\Delta v_d^c \\ \Delta v_q^c\end{bmatrix} + \underbrace{\begin{bmatrix}-C_f v_q^o \\ C_f v_d^o\end{bmatrix}}_{Dv3}[\Delta w]$$

$$+ \underbrace{\begin{bmatrix}H & 0 \\ 0 & H\end{bmatrix}}_{Dv4}\begin{bmatrix}\Delta Io_d^c \\ \Delta Io_q^c\end{bmatrix}$$

$$\begin{bmatrix}\Delta\dot{\theta}_{vd} \\ \Delta\dot{\theta}_{vq}\end{bmatrix} = \begin{bmatrix}0 & 0 \\ 0 & 0\end{bmatrix}\begin{bmatrix}\Delta\theta_{vd} \\ \Delta\theta_{vq}\end{bmatrix} + \underbrace{\begin{bmatrix}1 & 0 \\ 0 & 1\end{bmatrix}}_{B1v}\begin{bmatrix}\Delta v_d^* \\ \Delta v_q^*\end{bmatrix} + \underbrace{\begin{bmatrix}-1 & 0 \\ 0 & -1\end{bmatrix}}_{B2v}\begin{bmatrix}\Delta v_d^c \\ \Delta v_q^c\end{bmatrix}$$

$$[\Delta I_{dq}^*] = [Cv][\Delta\theta_{vdq}] + [Dv1][\Delta v_{dq}^*] + [Dv2][\Delta v_{dq}] + [Dv3][\Delta w] + [Dv4][\Delta io_{dq}] \qquad\text{(d)}$$

$$[\Delta\dot{\theta}_{vdq}] = [Bv1][\Delta v_{dq}^*] + [Bv2][\Delta v_{dq}] \qquad\qquad\text{(e)}$$

4. Virtual impedances model:

$$\Delta v_d^* = \Delta V_{ref} - R_v\Delta io_d + wL_v\Delta io_q + L_v io_q \Delta w$$

$$\Delta v_q^* = 0 \qquad - R_v\Delta io_q - wL_v\Delta io_d - L_v io_d \Delta w$$

$$\begin{bmatrix}\Delta v_d^* \\ \Delta v_q^*\end{bmatrix} = \underbrace{\begin{bmatrix}-R_v & w^o L_v \\ -w^o L_v & -R_v\end{bmatrix}}_{Dvr1}\begin{bmatrix}\Delta io_d \\ \Delta io_q\end{bmatrix} + \underbrace{\begin{bmatrix}+io_q L_v \\ -io_d L_v\end{bmatrix}}_{Dvr2}[\Delta w]$$

$$[\Delta v_{dq}^*] = [Dvr1][\Delta io_{dq}] + [Dvr2][\Delta w] \qquad\qquad\text{(f)}$$

135

5. Swing equation model:

$$\frac{dw}{dt} = \frac{P_{ref}}{2J} - \frac{P_{IC}}{2J} - \frac{K_d * w_{VSM}}{2J} + \frac{K_d * w_g^*}{2J}$$

$$\Delta \dot{w} = \frac{\Delta P_{ref}}{2J} - \frac{1.5io_d}{2J}\Delta v_d^o - \frac{1.5io_q}{2J}\Delta v_q^o - \frac{1.5v_d}{2J}\Delta io_d - \frac{1.5v_q}{2J}\Delta io_q - \frac{K_d}{2J}\Delta w_{VSM} + \frac{K_d}{2J}\Delta w_g^*$$

$$\frac{d\theta_{vsm}}{dt} = w_{VSM}$$

$$\Delta \dot{\theta}_{vsm} = \Delta w_{VSM}$$

$$\begin{bmatrix}\Delta \dot{w}_{VSM} \\ \Delta \dot{\theta}_{vsm}\end{bmatrix} = \underbrace{\begin{bmatrix}-\dfrac{K_d}{2J} & 0 \\ 1 & 0\end{bmatrix}}_{A_s}\begin{bmatrix}\Delta w_{VSM} \\ \Delta \theta_{vsm}\end{bmatrix} + \underbrace{\begin{bmatrix}-\dfrac{1.5v_d}{2J} & -\dfrac{1.5v_q}{2J} \\ 0 & 0\end{bmatrix}}_{B_s1}\begin{bmatrix}\Delta io_d^c \\ \Delta io_q^c\end{bmatrix} + \underbrace{\begin{bmatrix}-\dfrac{1.5io_d}{2J} & -\dfrac{1.5io_q}{2J} \\ 0 & 0\end{bmatrix}}_{B_s2}\begin{bmatrix}\Delta v_d^c \\ \Delta v_q^c\end{bmatrix}$$

$$+ \underbrace{\begin{bmatrix}\dfrac{K_d}{2J} \\ 0\end{bmatrix}}_{B_s3}[\Delta w_g]$$

$$\begin{bmatrix}\Delta \dot{w} \\ \Delta \dot{\theta}_{vsm}\end{bmatrix} = [A_s]\begin{bmatrix}\Delta w_{VSM} \\ \Delta \theta_{vsm}\end{bmatrix} + [B_s1][\Delta io_{dq}] + [B_s2][\Delta v_{dq}] + [B_s3][\Delta w_g] \qquad (g)$$

$$[\Delta \dot{x}_p] = [Ap]_{5\times5}[\Delta x_p] + [Bp1]_{5\times2}[\Delta m_{dq}] + [Bp2]_{5\times1}[\Delta \omega] + [Bp3]_{5\times2}[\Delta io_{dq}]$$
$$+ [Bp4]_{5\times1}[\Delta iodc]$$

$$[\Delta \dot{\theta}_{idq}] = [Bi1][\Delta i_{dq}^*] + [Bi2][\Delta i_{dq}]$$
$$[\Delta m_{dq}] = [Ci][\Delta \theta_{idq}] + [Di1][\Delta i_{dq}^*] + [Di2][\Delta i_{dq}] + [Di3][\Delta v_{dq}] + [Di4][\Delta w] + [Di5][\Delta v_{dc}]$$
$$[\Delta I_{dq}^*] = [Cv][\Delta \theta_{vdq}] + [Dv1][\Delta v_{dq}^*] + [Dv2][\Delta v_{dq}] + [Dv3][\Delta w] + [Dv4][\Delta io_{dq}]$$
$$[\Delta \dot{\theta}_{vdq}] = [Bv1][\Delta v_{dq}^*] + [Bv2][\Delta v_{dq}]$$
$$[\Delta v_{dq}^*] = [Dvr1][\Delta io_{dq}] + [Dvr2][\Delta w]$$
$$\begin{bmatrix}\Delta \dot{w} \\ \Delta \dot{\theta}_{vsm}\end{bmatrix} = [A_s]\begin{bmatrix}\Delta w_{VSM} \\ \Delta \theta_{vsm}\end{bmatrix} + [B_s1][\Delta io_{dq}] + [B_s2][\Delta v_{dq}] + [B_s3][\Delta w_g]$$

2

$$[\Delta \dot{\theta}_{idq}] = [Bi1][\Delta i_{dq}^*] + [Bi2][\Delta i_{dq}]$$
$$[\Delta i_{dq}^*] = [Cv][\Delta \theta_{vdq}] + [Dv1][\Delta v_{dq}^*] + [Dv2][\Delta v_{dq}] + [Dv3][\Delta w] + [Dv4][\Delta io_{dq}]$$

$$[\Delta v_{dq}^*] = [Dvr1][\Delta io_{dq}] + [Dvr2][\Delta w]$$

$$[\Delta \dot{\theta}_{idq}] = [Bi1]\Big[[Cv][\Delta \theta_{vdq}] + [Dv1]\big[[Dvr1][\Delta io_{dq}] + [Dvr2][\Delta w]\big] + [Dv2][\Delta v_{dq}]$$

$$+ [Dv3][\Delta w] + [Dv4][\Delta io_{dq}]\Big] + [Bi2][\Delta i_{dq}]$$

136

$$[\Delta\dot{\theta}_{\iota dq}] = [Bi1][Cv][\Delta\theta_{vdq}] + [Bi1][Dv1][Dvr1][\Delta io_{dq}] + [Bi1][Dv1][Dvr2][\Delta w]$$

$$+ [Bi1][Dv2][\Delta v_{dq}] + [Bi1][Dv3][\Delta w] + [Bi1][Dv4][\Delta io_{dq}] + [Bi2][\Delta i_{dq}]$$

	$[\Delta\dot{\theta}_{vdq}]$	$[\Delta\dot{w} \quad \Delta\theta_{vsm}]$	$[\Delta x_p] = [\Delta I_{dq} \quad \Delta v_{dq} \quad \Delta v_{dc}]^T$	$[\Delta\dot{\theta}_{\iota dq}]$
$[\Delta\dot{\theta}_{\iota dq}]$	$[Bi1][Cv]$	$[Bi1][Dv1][Dvr2]$	$[Bi2] \quad [Bi1][Dv2] \quad 0$	0

3

$$[\Delta\dot{\theta}_{vdq}] = [Bv1][\Delta v^*_{dq}] + [Bv2][\Delta v_{dq}]$$
$$[\Delta v^*_{dq}] = [Dvr1][\Delta io_{dq}] + [Dvr2][\Delta w]$$

$$[\Delta\dot{\theta}_{vdq}] = [Bv1]\big[[Dvr1][\Delta io_{dq}] + [Dvr2][\Delta w]\big] + [Bv2][\Delta v_{dq}]$$

$$[\Delta\dot{\theta}_{vdq}] = [Bv1][Dvr1][\Delta io_{dq}] + [Bv1][Dvr2][\Delta w] + [Bv2][\Delta v_{dq}]$$

	$[\Delta\dot{\theta}_{vdq}]$	$[\Delta\dot{w} \quad \Delta\theta_{vsm}]$	$[\Delta x_p] = [\Delta I_{dq} \quad \Delta v_{dq} \quad \Delta v_{dc}]^T$	$[\Delta\dot{\theta}_{\iota dq}]$
$[\Delta\dot{\theta}_{vdq}]$	0	$[Bv1][Dvr2]$	$0 \quad [Bv2] \quad 0$	0

4

$$\begin{bmatrix} \Delta\dot{w} \\ \Delta\dot{\theta}_{vsm} \end{bmatrix} = [A_s]\begin{bmatrix} \Delta w_{VSM} \\ \Delta\theta_{vsm} \end{bmatrix} + [B_s1][\Delta io_{dq}] + [B_s2][\Delta v_{dq}] + [B_s3][\Delta w_g]$$

	$[\Delta\dot{\theta}_{vdq}]$	$[\Delta\dot{w} \quad \Delta\theta_{vsm}]$	$[\Delta x_p] = [\Delta I_{dq} \quad \Delta v_{dq} \quad \Delta v_{dc}]^T$	$[\Delta\dot{\theta}_{\iota dq}]$
$[\Delta\dot{\theta}_{vdq}]$	0	$[A_s]$	$0 \quad [B_s2] \quad 0$	0

1

$$[\Delta\dot{x}_p] = [Ap][\Delta x_p] + [Bp1][\Delta m_{dq}] + [Bp2][\Delta\omega] + [Bp3][\Delta io_{dq}] + [Bp4][\Delta iodc]$$

$$[\Delta m_{dq}] = [Ci][\Delta\theta_{idq}] + [Di1][\Delta i^*_{dq}] + [Di2][\Delta i_{dq}] + [Di3][\Delta v_{dq}] + [Di4][\Delta w] + [Di5][\Delta v_{dc}]$$

$$[\Delta i^*_{dq}] = [Cv][\Delta\theta_{vdq}] + [Dv1][\Delta v^*_{dq}] + [Dv2][\Delta v_{dq}] + [Dv3][\Delta w] + [Dv4][\Delta io_{dq}]$$

$$[\Delta v^*_{dq}] = [Dvr1][\Delta io_{dq}] + [Dvr2][\Delta w]$$

$$\big[\Delta \dot{x}_p\big] = [Ap]\big[\Delta x_p\big]$$

$$+ [Bp1]\Big[[Ci]\big[\Delta\theta_{idq}\big]$$

$$+ [Di1]\Big[[Cv]\big[\Delta\theta_{vdq}\big] + [Dv1]\Big[[Dvr1]\big[\Delta io_{dq}\big] + [Dvr2][\Delta w]\Big] + [Dv2]\big[\Delta v_{dq}\big]$$

$$+ [Dv3][\Delta w] + [Dv4]\big[\Delta io_{dq}\big]\Big] + [Di2]\big[\Delta i_{dq}\big] + [Di3]\big[\Delta v_{dq}\big] + [Di4][\Delta w]$$

$$+ [Di5][\Delta v_{dc}]\Big] + [Bp2][\Delta\omega] + [Bp3]\big[\Delta io_{dq}\big] + [Bp4][\Delta iodc]$$

$$\big[\Delta \dot{x}_p\big] = [Ap]\big[\Delta x_p\big] + [Bp1][Ci]\big[\Delta\theta_{idq}\big] + [Bp1][Di1][Cv]\big[\Delta\theta_{vdq}\big]$$

$$+ [Bp1][Di1][Dv1][Dvr1]\big[\Delta io_{dq}\big] + [Bp1][Di1][Dv1][Dvr2][\Delta w]$$

$$+ [Bp1][Di1][Dv2]\big[\Delta v_{dq}\big] + [Bp1][Di1][Dv3][\Delta w] + [Bp1][Di1][Dv4]\big[\Delta io_{dq}\big]$$

$$+ [Bp1][Di2]\big[\Delta i_{dq}\big] + [Bp1][Di3]\big[\Delta v_{dq}\big] + [Bp1][Di4][\Delta w]$$

$$+ [Bp1][Di5][\Delta v_{dc}] + [Bp2][\Delta\omega] + [Bp3]\big[\Delta io_{dq}\big] + [Bp4][\Delta iodc]$$

$$\big[\Delta \dot{x}_p\big] = [Ap]\big[\Delta x_p\big] + [Bp1][Ci]\big[\Delta\theta_{idq}\big] + [Bp1][Di1][Cv]\big[\Delta\theta_{vdq}\big]$$

$$+ [Bp1][Di1][Dv1][Dvr1]\big[\Delta io_{dq}\big] + [Bp1][Di1][Dv1][Dvr2][\Delta w]$$

$$+ [Bp1][Di1][Dv2]\big[\Delta v_{dq}\big] + [Bp1][Di1][Dv3][\Delta w] + [Bp1][Di1][Dv4]\big[\Delta io_{dq}\big]$$

$$+ [Bp1][Di2]\big[\Delta i_{dq}\big] + [Bp1][Di3]\big[\Delta v_{dq}\big] + [Bp1][Di4][\Delta w]$$

$$+ [Bp1][Di5][\Delta v_{dc}] + [Bp2][\Delta\omega] + [Bp3]\big[\Delta io_{dq}\big] + [Bp4][\Delta iodc]$$

	$\big[\Delta\dot{\theta}_{vdq}\big]$	$[\Delta\dot{w} \quad \Delta\theta_{vsm}]$	$\big[\Delta x_p\big]$ $= [\Delta I_{dq} \quad \Delta v_{dq} \quad \Delta v_{dc}]^T$	$\big[\Delta\dot{\theta}_{idq}\big]$
$\begin{bmatrix}\Delta i_{dq}\\ \Delta v_{dq}\\ \Delta v_{dc}\end{bmatrix}$	$[Bp1][Di1][Cv]$	$[Bp1][Di1][Dv1][Dvr2]$ $+ [Bp2]$	$[Ap]$ $+ \big([Bp1][Di2]\big[\Delta i_{dq}\big]$ $+ [Bp1][Di1][Dv2]\big[\Delta v_{dq}\big]$ $+ 0\big)$	$[Bp1][Ci]$

138

$$\begin{bmatrix} \Delta \dot{X}_p \\ \Delta \dot{\theta i}_{dq} \\ \Delta \dot{\theta v}_{dq} \\ \Delta \dot{w} \end{bmatrix} = \begin{bmatrix} \begin{pmatrix} Ap + \\ [Bp1Di2 \quad Bp1Di1Dv2 \quad 0] \end{pmatrix} & Bp1Ci & Bp1Di1Cv & \begin{pmatrix} Bp1Di1Dv1Dvr2 \\ +Bp2 \end{pmatrix} \\ (Bi2 \quad Bi1Dv2 \quad 0) & 0 & Bi1Cv & Bi1Dv1Dvr2 \\ (0 \quad Bv2 \quad 0) & 0 & 0 & Bv1Dvr2 \\ (0 \quad Bs2 \quad 0) & 0 & 0 & As \end{bmatrix} \begin{bmatrix} \Delta X_p \\ \Delta \theta i_{dq} \\ \Delta \theta v_{dq} \\ \Delta w \end{bmatrix}$$

$$+ \begin{bmatrix} \begin{pmatrix} (Bp1Di1Dv1Cvr) \\ +(Bp1Di1Dv3) \\ +Bp2 \end{pmatrix} \\ \begin{pmatrix} (Bi1Dv1Cvr) \\ +(Bi1Dv3) \end{pmatrix} \\ Bv1 * Cvr \\ Bs2 \end{bmatrix} [\Delta io_{dq}]$$